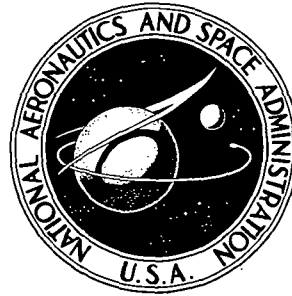NASA CONTRACTOR
REPORT

NASA CR-2342

NASA CR-2342

NOISE CHARACTERISTICS OF JET FLAP TYPE EXHAUST FLOWS

by G. O. Schrecker and J. R. Maus

NATIONAL AERCNAUTICS AND SPACE ADMINISTRATION • WASHINGTON, D. C. • FEBRUARY 1974

1. Report No. NASA CR-2342	2. Government Accession No.	3. Recipient's Catalog No.
4. Title and Subtitle NOISE CHARACTERISTICS OF JET FLAP TYPE EXHAUST FLOWS		5. Report Date February, 1974
		6. Performing Organization Code
7. Author(s) G. O. Schrecker and J. R. Maus		8. Performing Organization Report No.
9. Performing Organization Name and Address The University of Tennessee Space Institute Tullahoma, Tennessee		10. Work Unit No. 501-04-01-01
		11. Contract or Grant No. NGR 43-001-075
12. Sponsoring Agency Name and Address National Aeronautics and Space Administration Washington, DC 20546		13. Type of Report and Period Covered Contractor Report
		14. Sponsoring Agency Code

15. Supplementary Notes

This is a final report.

16. Abstract

An experimental investigation of the aerodynamic noise and flow field characteristics of internal-flow jet-augmented flap configurations (abbreviated by the term "jet flap" throughout the study) is presented. The first part is a parametric study of the influence of the Mach number (subsonic range only), the slot nozzle aspect ratio and the flap length on the overall radiated sound power and the spectral composition of the jet noise, as measured in a reverberation chamber. In the second part, mean and fluctuating velocity profiles, spectra of the fluctuating velocity and space correlograms were measured in the flow field of jet flaps by means of hot-wire anemometry. Using an expression derived by Lilley, an attempt was made to estimate the overall sound power radiated by the free mixing region that originates at the orifice of the slot nozzle (primary mixing region) relative to the overall sound power generated by the free mixing region that originates at the trailing edge of the flap (secondary mixing region). It is concluded that at least as much noise is generated in the secondary mixing region as in the primary mixing region. Furthermore, the noise generation of the primary mixing region appears to be unaffected by the presence of a flap.

17. Key Words (Suggested by Author(s)) Noise, STOL, Upper Surface Blowing, Turbulence, Jet Exhaust Surface Interaction	18. Distribution Statement Unclassified - Unlimited		
19. Security Classif. (of this report) Unclassified	20. Security Classif. (of this page) Unclassified	21. No. of Pages 135	22. Price* Domestic, $4.50 Foreign, $7.00

Page Intentionally Left Blank

FOREWORD

This report represents the results of the work done
at The University of Tennessee Space Institute for Langley
Research Center under NASA Grant NGR 43-001-075. The report
was excerpted from the doctoral dissertation of the first
author, and the work was carried out under the direction of Dr.
H. D. Gruschka, principal investigator of the grant.

iii

Page Intentionally Left Blank

TABLE OF CONTENTS

LIST OF FIGURES

NOMENCLATURE

a	Speed of sound
b	Width of the mixing region (in x_2-direction)
b_a	Width of the mixing region between $0.1 \bar{U}_{1\ max}$ $0.9 \bar{U}_{1\ max}$
b_b	Width of the mixing region at $0.5 I_{1\ max}$
d	Nozzle diameter
f	Frequency
f (r)	Longitudinal velocity correlation coefficient
f_c	Center frequency
f_p	Peak frequency of the power density spectra of the noise
f_p*	Peak frequency of the power density spectra of the fluctuating velocities
Δf	Bandwidth
Δf_3	Width of the power density spectra 3 dB below the peak frequency
G	Power spectral density
$g (x_2)$	Lateral velocity correlation coefficient
h	Height of slot nozzles
I_1	Turbulence intensity in x_1-direction = $100\ u_1/\bar{U}_{1\ max}$ per cent
I	Acoustic Source Intensity
L_p	Overall radiated sound power level = $10 \log_{10} P/P_o$
L_{x_1}	Longitudinal scale of turbulence, as defined in Appendix D

L_{x_2} Lateral Scale of turbulence, as defined in
             Appendix D

ℓ_c Core length

ℓ_F Flap length

M   Mach number

P   Overall radiated sound power

P_o Reference sound power $= 10^{-12}$ watt

p   Pressure

Re   Reynolds number

S   Area

Str   Strouhal number

t   Time

U   Nozzle exit velocity

$\bar{U}_i$ Mean velocity, velocity in x_i-direction

u_i Instantaneous velocity in x_i-direction

$\hat{u}_i$ Root-mean square of the fluctuating velocity in
             x_i-direction

u_n Outward normal velocity component

V   Volume

dV, ΔV Volume element

w   nozzle width

w_F Width of the wetted area of the flap (in x_2-direction)

x_i Space coordinates, $i = 1, 2, 3$

Greek

δ	Boundary layer thickness
δ_c	Non-dimensional core length $= \ell_c/h$
δ_F	Non-dimensional flap length $= \ell_F/h$
η_a	Non-dimensional width of the mixing region $= \dfrac{b_a}{h}$ (for circular nozzles, d is used instead of h)
η_b	Non-dimensional width of the mixing region $= \dfrac{b_b}{h}$ (for circular nozzles, d is used instead of h)
Λ	Nozzle aspect ratio $= w/h$
λ	Wavelength
μ	Dynamic viscosity
ρ	Density of the acoustic medium
$\bar{\rho}$	Mean density in the jet
$\bar{\tau}_{12}$	Mean lateral shear $= \partial \bar{U}_1/\partial x_2$
$\bar{\tau}_{12}$	Non-dimensional lateral shear $= \dfrac{h}{U_e} \dfrac{\partial \bar{U}_1}{\partial x_2}$ (for circular nozzles, d is used instead of h)

Subscripts

e	Represents the value of a quantity in the nozzle exit
F	Represents flap
max	Represents maximum
o	Represents the values of the surrounding medium at rest
p	Represents peak
pr	Represents primary
R	Represents reference
sec	Respresents secondary

CHAPTER I

INTRODUCTION

Unnoticed by the general public, aircraft propulsion system design, particularly the turbine engine design, has undergone a major change during the last fifteen years. The principle of "thrust regardless of noise" has been gradually replaced by "noise conscious" design principles. The noise reduction achieved, in spite of large increases in thrust, has been respectable. Siddon (1)[1] demonstrated the achievements by two impressive graphs which are reproduced here (Figures 1 and 2).
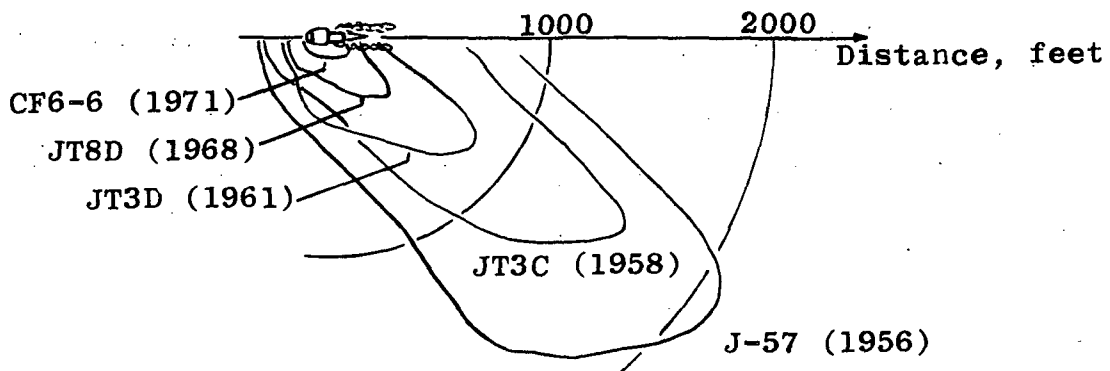
Figure 1. Footprints of Turbine Engines at Equivalent Distances for 110 dB Contours.

Source: Siddon, T. E. "Jet Noise Research - Progress and Prognosis," Inter-Noise 72 Proceedings, International Conference on Noise Control Engineering, Washington, D.C. October 1972.

---

[1]Numbers in parentheses refer to similarly numbered references in the bibliography.
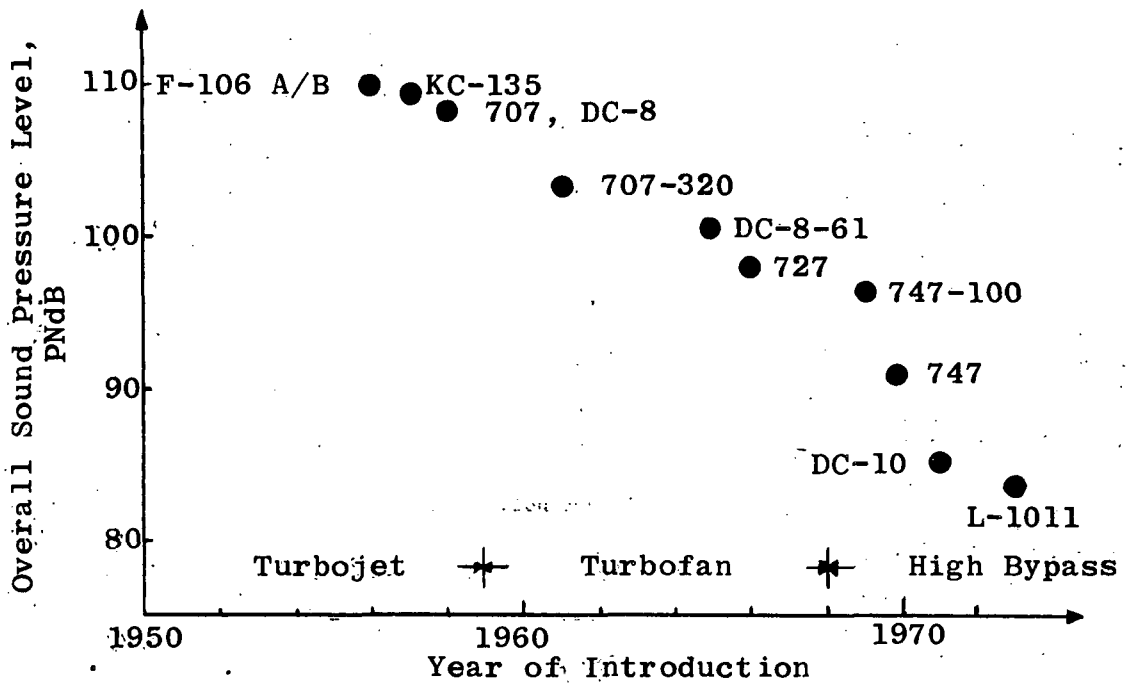
Figure 2. Flyover Aircraft Noise (1000 Feet Altitude).

Source: Siddon, T. E. "Jet Noise Research – Progress and Prognosis," Inter-Noise 72 Proceedings, International Conference on Noise Control Engineering, Washington, D. C. October 1972.

However, the reductions are not yet sufficient for large STOL[2] aircraft to operate from airfields near city centers. The need for high lift devices adds additional noise sources which may radiate a considerable amount of acoustic power. Dorsch et al. (2) conducted acoustic tests with models of high lift devices such as blown flap, augmentor wing and

---

[2]Short Take-Off and Landing (STOL).

2

jet flap[3] which are currently developed for STOL aircraft.
The noise data of the blown flap and the augmentor wing were
extrapolated to represent full scale STOL airplane flap
systems. Dorsch <u>et al.</u> concluded that both systems will have
serious noise problems. With an engine such as the NASA[4]
Quiet Engine (3) the high lift devices may be even the major
contribution to the aircraft noise.

The noise data in Reference (2) for the jet flap were
not extrapolated to full scale. Comparison of the model re-
sults, however, showed that the jet flap was the quietest of
the three configurations. This result together with the fact
that it is a simple device (as opposed to the jet-augmented
flap) makes it a promising propulsion system component for
STOL aircraft.

Some fifteen years ago interest in the jet flap was
originated by promising aerodynamic as well as acoustical
features. Aerodynamically the high energy jet emerging from
a slot on the upper surface of the wing, blowing tangen-
tially to this surface, will result in a higher lift coeffi-
cient due to an increase in circulation and acceleration of
the boundary layer. The higher lift coefficient would result

---

[3]Following (2) the term "Jet flap" will subsequently
be used for jets emerging from a rectangular slot nozzle over
a flap attached to the nozzle (Figure 3). In the literature
this configuration is also known as an "internal-flow jet-
augmented flap configuration" (4) or, more simply, jet-aug-
mented flap (5).

[4]National Aeronautics and Space Administration (NASA).
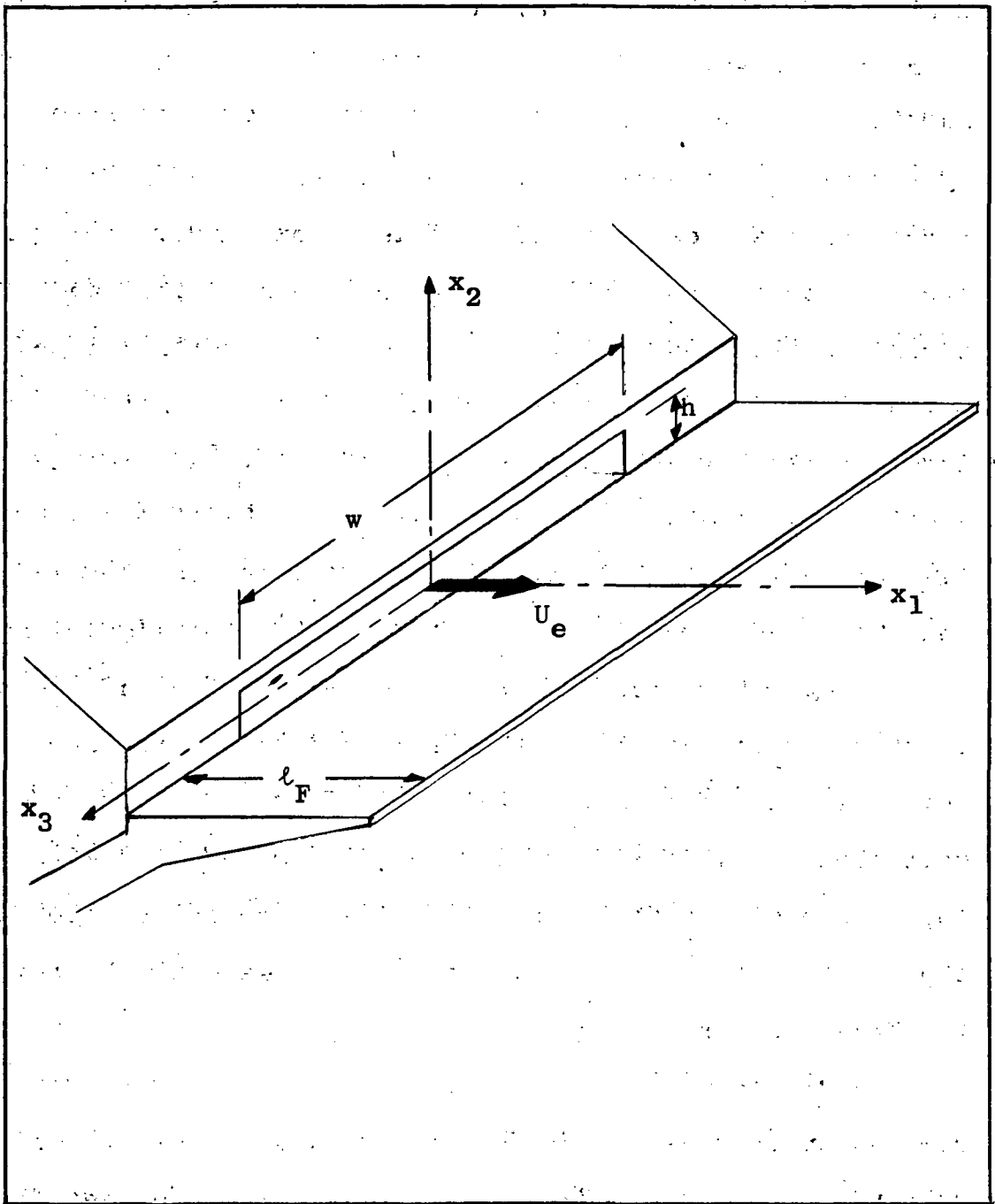
Figure 3. Coordinate System of the Jet Flap.

in a decrease of the landing and take-off distance, which is a necessary step on the way to high-density traffic operation, one of NASA's primary considerations in the research on STOL.

From the acoustic point of view there are several features which suggest the jet flap as a potentially quieter propulsion system component. In 1959 Coles (5) showed both experimentally and analytically that the total sound power output of a slot nozzle of high aspect ratio[5] is half, or 3 dB less, of the output of a circular nozzle having the same exit area and exit velocity. This analysis was based on similarities of fundamental mixing-zone structure between the slot nozzle and the circular nozzle. Moreover a change in geometry from circular to rectangular shifts the spectrum of the noise to higher frequencies and thus shorter wavelength due to the change of characteristic length (diameter and slot height respectively). A flap, acting as a sound shield, is effective for wavelengths small compared to the dimension of the flap. Thus part of the jet aircraft exhaust noise could be reflected away from the ground.

Early acoustic tests with jet flaps, however, revealed some unexpected radiation characteristics. Maglieri and Hubbard (4) conducted free-field tests with model jet flaps having an aspect ratio of $\Lambda = 200$ and dimensionless lengths[6] of

---

[5]Aspect ratio = slot width / slot height.

[6]The flap length is made non-dimensional with respect to the slot nozzle height.

20 and 190. For the shorter flap only minor changes in radiation pattern were found but a general increase in noise. For the long flap, however, a considerable noise reduction was observed, especially in the downward or shielded direction. On the other hand an increase in low frequency noise occured. Coles (5) made full-scale free-field tests with a jet flap having an aspect ratio of 100 and a flap length of 20. He reported reductions in overall noise and a beneficial change in the radiation characteristics. Although the two quoted results are in some points somewhat contradictory, both agree on the potential of the jet flap as a quieter jet configuration.

Therefore, one of the goals of this dissertation was to investigate certain aeroacoustic characteristics of jet flaps in more detail. The other goal arose from the necessity to know the location of the main noise sources in order to initiate a jet noise suppression program. This resulted in an effort to estimate the acoustic source strength distribution in the turbulent mixing region originating at the nozzle orifice and in the turbulent mixing region originating at the trailing edge of the flap.[8] Particular attention was directed to the latter mixing region since it was expected that

---

[7]For this mixing region the term "primary mixing region" will be subsequently used.

[8]For this mixing region the term "secondary mixing region" will be subsequently used.

6

this flow region may become an efficient noise source in practical[9] jet flap configurations.

The first part of the investigation was a parametric study on the influence of the slot nozzle aspect ratio, the flap length and the Mach number on the overall sound power output and the spectral composition of the overall radiated noise. The exit area of the nozzles and the flap deflection angle are parameters which were kept constant. Although the problem of jet noise is not limited to subsonic exit velocities, only this range is under consideration here. The acoustic properties of the slot nozzles and the jet flaps are compared with those of the circular reference nozzle which has the same exit area.

The appropriate method of determining the overall sound power and the spectral composition of the noise of a jet is to place the jet into a reverberation chamber and measure the sound pressure level by means of a microphone. Knowing the absorbtion characteristics of the reverberation chamber the overall sound power and its spectral distribution can be calculated. The characteristic feature of a reverberation chamber is the uniformity of the sound energy density everywhere in the chamber except in the near field of the acoustic source and near the walls. Thus the

---

[9]With regard to the necessary integration of the flap into an airplane wing of a STOL airplane, the practical aspects of the jet flap were important for the choice of the flap length. Therefore, when this study was initiated, a maximum flap length of approximately 32 times the slot height was chosen.

7

directivity of the noise source is completely lost. Because the microphone has to be sufficiently far away from the noise source it is impossible to resolve the overall pressure level into sound pressures which are radiated from different parts of the flow field of the jet flap. Therefore, the acoustic tests yield information about the influence of the parameters on the overall sound power and on the spectral distribution, but they cannot give detailed information on the location of the main noise sources.

It appeared that one way of gaining this information was to study those flow field characteristics that are known to be involved in the generation of noise.

The flow fields of a two-dimensional jet and of a two-dimensional jet flap are shown in Figure 4. The flow field produced by a two-dimensional jet emanating into a medium at rest can, in general, be divided into three regions. The initial region (or first regime) extends from the nozzle exit to the point where the potential core disappears. From either side of the edge of the slot (or at the circumferential edge of a circular nozzle) a highly turbulent mixing layer starts to develop that separates the low turbulence potential core from the medium at rest. From certain downstream position which depends on the details of the boundary layer in the nozzle exit, the mean and turbulence velocity profiles of the initial region display similarity. After the turbulent mixing layer has penetrated the potential core sufficiently to

8

Initial region
or
first regime

$0 \leq \dfrac{x_1}{h} < 5$

Transition
region

Region of fully
developed flow

$\dfrac{x_1}{h} > 20 \text{ to } 50$
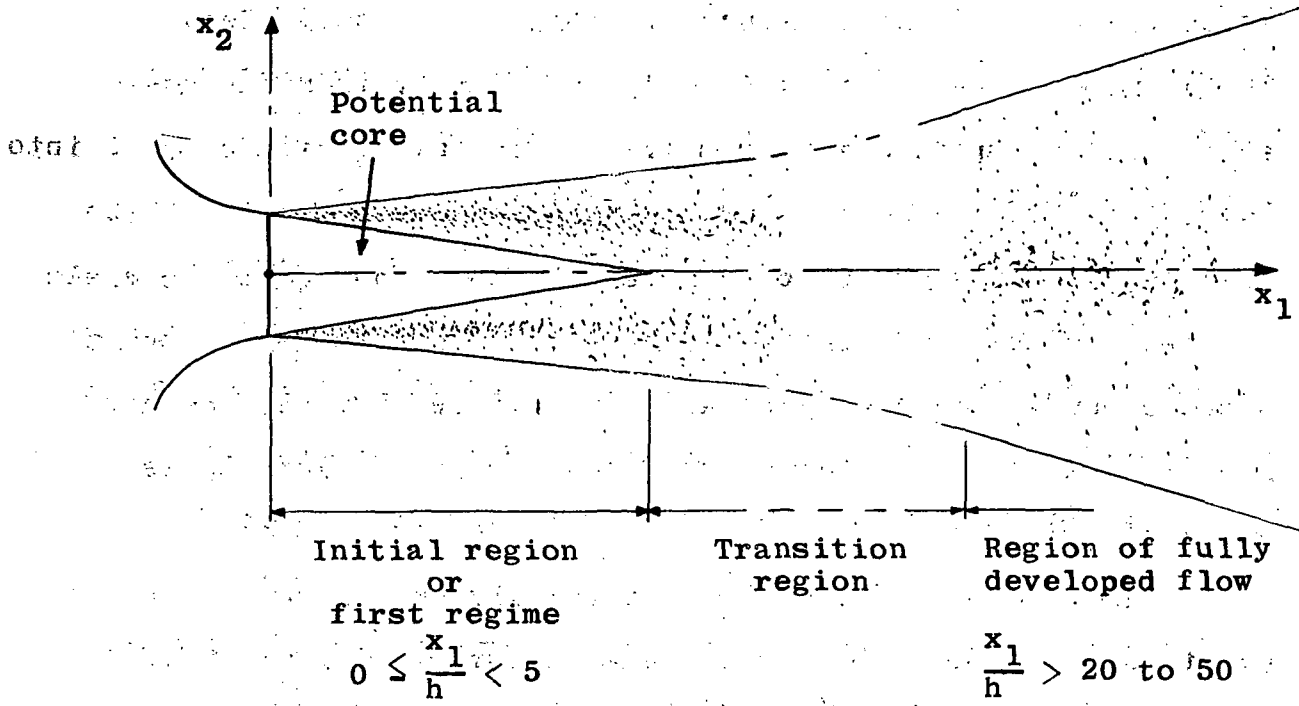
(a) Flow Field of a Two-Dimensional Jet Exhausting
into a Medium at Rest.
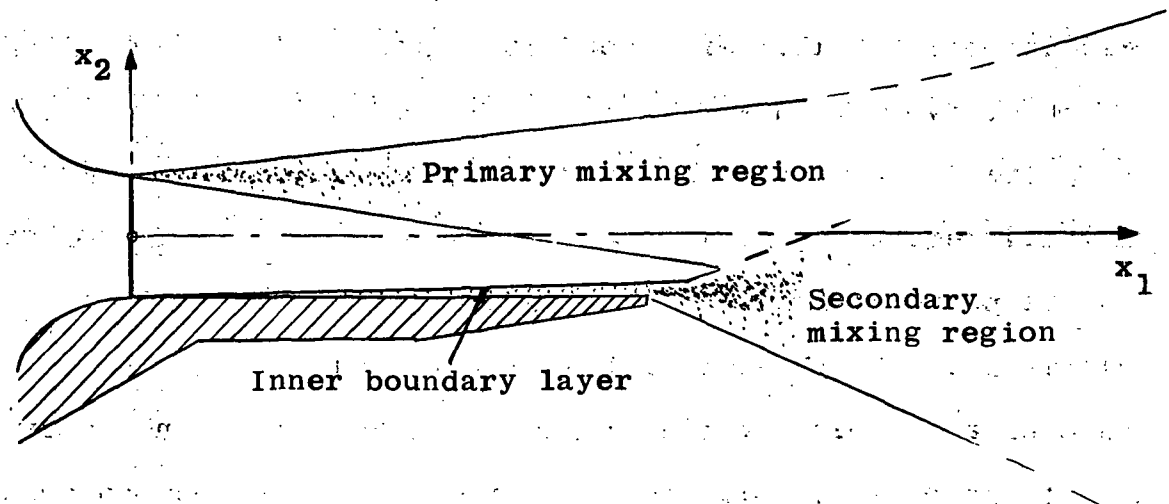
(b) Flow Field of a Two-Dimensional Jet Flap Exhausting
into a Medium at Rest.

Figure 4. Flow Fields of Two-Dimensional Jets and
Jet Flaps.

9

cause its disappearance, the flow field undergoes a transition into the region of fully developed flow which again displays similarity of the mean and turbulence velocity profiles. The intermediate region is often simply called the transition region and is characterized by the lack of any similarity.

The noise producing region of the two-dimensional jet is, in general, the free turbulent flow field as a whole. However, following Lilley (6) the important parts of the turbulent flow field can be specified. Lilley states that

> the central region of the mixing region is mainly responsible for the bulk of the noise emitted, since the distribution of acoustic quadrupole strength across the mixing region is roughly Gaussian, with a half-width less than a quarter of the mixing region breadth.

Furthermore, the greatest contribution to the noise radiated from the initial region is from the interaction between the turbulence and the mean shear (shear-noise), contributing more than 80% of the noise (6). The remaining 20% or less is generated by the turbulence itself (self-noise). In the region of fully developed flow the contributions of shear-noise and self-noise to the radiated sound are approximately equal. Estimates of the sound spectrum suggest that the high frequency sound is generated at the first two to three nozzle heights whereas the bulk of the low frequency noise is originated further downstream up to about six nozzle heights downstream of the nozzle exit. The noise generated further downstream is of low intensity since the quadrupole strength falls off proportional to x_1^{-7}.

The three regions described are also present in the flow field of a jet flap, though only on one side of the potential core. They constitute the primary mixing region. Since the potential core is shielded from mixing on one side by the flap, its length will be increased. The actual length of the core depends primarily on the origin of the secondary mixing region, thus on the flap length, and only secondarily on the inner boundary layer adjacent to the flap.

Both regions generate noise. The inner boundary layer will have high mean shear and may develop high turbulence levels at the outer edge further downstream, but its volume is very small compared to the volume of the primary and secondary mixing regions. To the knowledge of the author nothing was known about the noise generation of the secondary mixing region and this was one of the major subjects of this study.

Based on Lighthill's (7) classical theory on aerodynamic noise Lilley (6) derived approximate equations for the overall sound power output of the shear-noise and the self-noise of a two-dimensional, incompressible turbulent jet. According to these estimates the total sound power of the shear noise depends mainly on the flow properties, turbulence intensity, mean velocity gradient and turbulence scale, whereas the sound power of the self-noise depends mainly on the turbulence intensity and the turbulence scale. These three or two quantities can be combined into an acoustic

source strength term for the shear-noise and the self-noise respectively. Determination of the source strength distribution will yield information on the relative contribution of the two main turbulent mixing regions to the noise generated by a jet flap. The object of the flow measurements was therefore to gain general information on the turbulent flow field of jet flaps and, in particular, to measure those flow quantities related to the acoustic source strength.

This report is arranged into five chapters. Chapter II deals with the acoustic measurements in a reverberation chamber. The results of the overall sound power and frequency spectrum measurements are presented. Chapter III contains the results of the flow field measurements by means of a hot-wire anemometer and Chapter IV presents the estimate of the acoustic source strength distribution in the primary and secondary mixing regions. Finally, Chapter V summarizes the study and presents the conclusions that can be drawn.

ACOUSTIC MEASUREMENTS

I. PREVIOUS EXPERIMENTAL WORK

Some of the noise characteristics of jet flaps have been investigated by several researchers regarding the noise reduction potentials the configuration seems to offer.

One of the earliest tests on jet flaps was performed by Maglieri and Hubbard (4). They conducted free-field measurements with model jet flaps having an aspect ratio of $\Lambda = 200$ and dimensionless flap lengths $\delta_F = 20$, 72 and 190. The exit velocity was that corresponding to an exit Mach number of 0.96. Compared to the pure slot nozzle only minor changes in radiation pattern were found for the shortest flap, but a general increase in noise. For the extremely long flap, $\delta_F = 190$, however, the radiation pattern was substantially changed and below the flap overall-noise reductions of up to 15 dB were measured. On the other hand the noise spectra revealed that a marked increase in low frequency noise occurred.

Coles (5) made full-scale free-field tests with a jet flap having an aspect ratio of 100 and a flap length of 20. The exit velocity of the hot jet was kept constant at 1600 ft/sec, the corresponding Mach number was 0.9. He reported a moderate reduction of sound power over the whole frequency range compared to the pure slot nozzle, except at the low

frequency end of the spectrum. He also calculated the over-
all sound power and obtained a 1.5 dB noise reduction due
to the addition of the flap to the slot nozzle, a very modest
value indeed.

Grosche (8) conducted extensive tests with slot nozzles
whose exhaust jet was shielded by a finite flat plate mounted
parallel to the exit velocity (Figure 5).
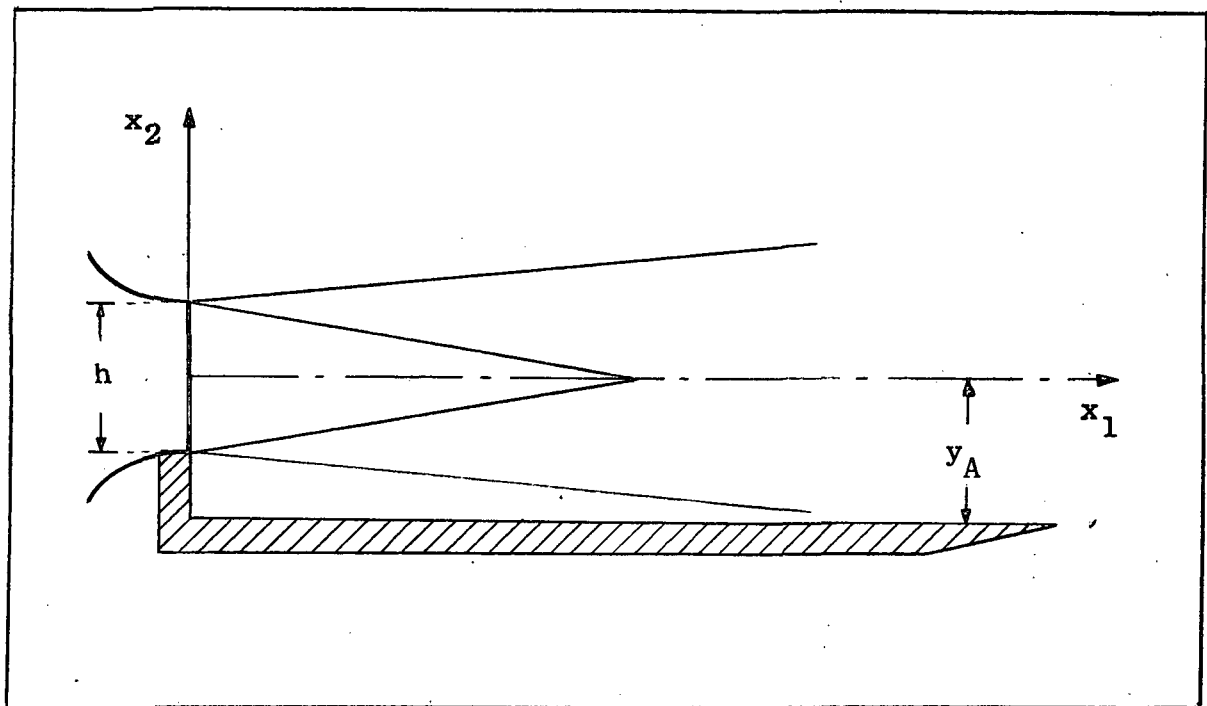
Figure 5. Jet Flap Tested by Grosche.

Source: Grosche, F. R. "Zur Schallerzeugung durch
einen turbulenten Luftstrahl uber einer endlich grossen
ebenen Platte," Mitteilungen aus dem Max-Planck-Institut
fur Stromungsforschung und der Aerodynamischen Versuchs-
anstalt, Selbstverlag Max-Planck-Institut fur Stromungs-
forschung und Aerodynamische Versuchsanstalt, Gottingen,
Nr. 45, 1969.

His primary goal was to study the influence of the parameters y_A aadd ℓ on the acoustic radiation. In the limiting case of $y_A = h/2$ this configuration [10] becomes the jet flap considered in this study. Therefore his results are of interest and will be examined more closely. The model jet flap under consideration had an aspect ratio of 23 and the flap length was variable between $\delta_F = 25$ and 100. The Mach number of the cold air jet was 0.98. Free-field measurements were conducted in the first part of his study. He reported the following conclusions:

1. The flap causes additional noise, mainly in the low frequency range. The radiation is strongest in the plane perpendicular to the jet exit plane (x_1-x_2-plane) and increases in strength with decreasing flap length.

2. If the flap is sufficiently long the radiation field contains less high frequency noise than the field of the pure slot nozzle.

The reasoning for the second conclusion is the following: A flap prevents the mixing of the turbulent plane jet with the ambient air on one side of the jet sheet, especially near the nozzle orifice commonly associated with the source of high frequency noise.

---

[10] The smallest y_A/h attainable with his set-up was $y_A = 0.55$, resulting in a step of 0.1 mm between the nozzle exit and the flap. The effect of this step on the total noise is assumed to be negligible.

In the second part of his study Grosche made an effort to measure the source distribution. Using a spherical reflector, an image of a certain volume of the turbulent flow is obtained outside of the flow. The noise intensity is then measured at the image volume by means of a microphone. One drawback of the method is that the measured noise intensity is, of course, only that radiated to and reflected by the reflector. As a jet flap has a highly directional radiation pattern several measurements have to be performed focusing on the same volume element but from different directions. The measured intensities have then to be superimposed in some suitable way in order to get the source strength of the volume element of turbulence. Dealing with acoustic radiation results in another drawback. Due to diffraction effects caused by the large wavelength the resolution is only satisfactory for high frequency, say 10 KHz. With these restrictions in mind the conclusions are the following:

1. A considerable part of the total acoustic power is radiated by a region at or behind the trailing edge of the flap. Although this observation is valid for all frequencies the largest increase, compared to the pure slot nozzle, occured at the low frequency end of the spectrum.

It may be remarked that for low frequencies the resolution is very poor. This makes it difficult if not impossible to determine the location from which the low frequency noise is emitted.

2. The results support the assumption, that the flow
field near to the nozzle orifice of a jet flap
radiates less high frequency sound than the same
region of a pure slot nozzle.

Grosche measured the influence of the exit velocity on
the intensity and found for the jet flap approximately a
U^5-law. He concluded from this result that the additional
noise of a jet flap is due to dipole radiation from the
trailing edge of the flap. The author noticed, however,
that the peaks of the plotted noise intensity versus x_1 are
located downstream of the trailing edge of the flaps for all
components of the noise spectrum. This implies that strong
noise sources are not only at the trailing edge, but down-
stream of it as well. But these, in the absence of solid
boundaries, would have to be quadrupole sound sources.

Hayden's master thesis (9) confirms the presence of
dipole noise sources along the trailing edge. He showed how
the directivity of a point dipole is changed due to diffrac-
tion of the waves at the trailing edge. Free-field measure-
ments substantiated his calculations. Therefore, it seems to
be well established both theoretically and experimentally
that dipole noise sources are located at the trailing edge.
Powell (10) stated that trailing edge noise will produce
a spectrum whose shape will depend principally on the local
characteristics of the flow there. However, it is expected
to contribute mainly to the lower frequency end of the spec-
trum.

17

So far, only the results of free-field measurements have been reported. Harper (11) and Gruschka (12) made tests on overall sound power and frequency spectra of slot nozzles and jet flaps in a reverberation chamber. Their results will be quoted and compared to those reported in this study.

II. ACOUSTIC TESTS IN A REVERBERATION CHAMBER

The object of the acoustic tests, conducted in a reverberation chamber, is the parametric study on the influence of the slot nozzle aspect ratio, the flap length and the Mach number on the overall radiated sound power and its spectral composition. The test facility in general and its most important parts like the slot nozzles, the flaps, and the stilling chamber as well as the instrumentation and the reverberation room are described in Appendix A.

Overall Sound Power Measurements of
Jet Flaps and Slot Nozzles

Figure 6 gives a general picture of the radiated sound power as a function of the exit Mach number, aspect ratio and flap length. The slot nozzles are generally quieter than the circular nozzle by some 3 dB or more for Mach numbers larger than 0.5 approximately. Adding a flap to the slot nozzle results in an increase of overall sound power over the whole covered Mach number range. For low Mach numbers this increase is substantially larger than for higher subsonic Mach numbers.
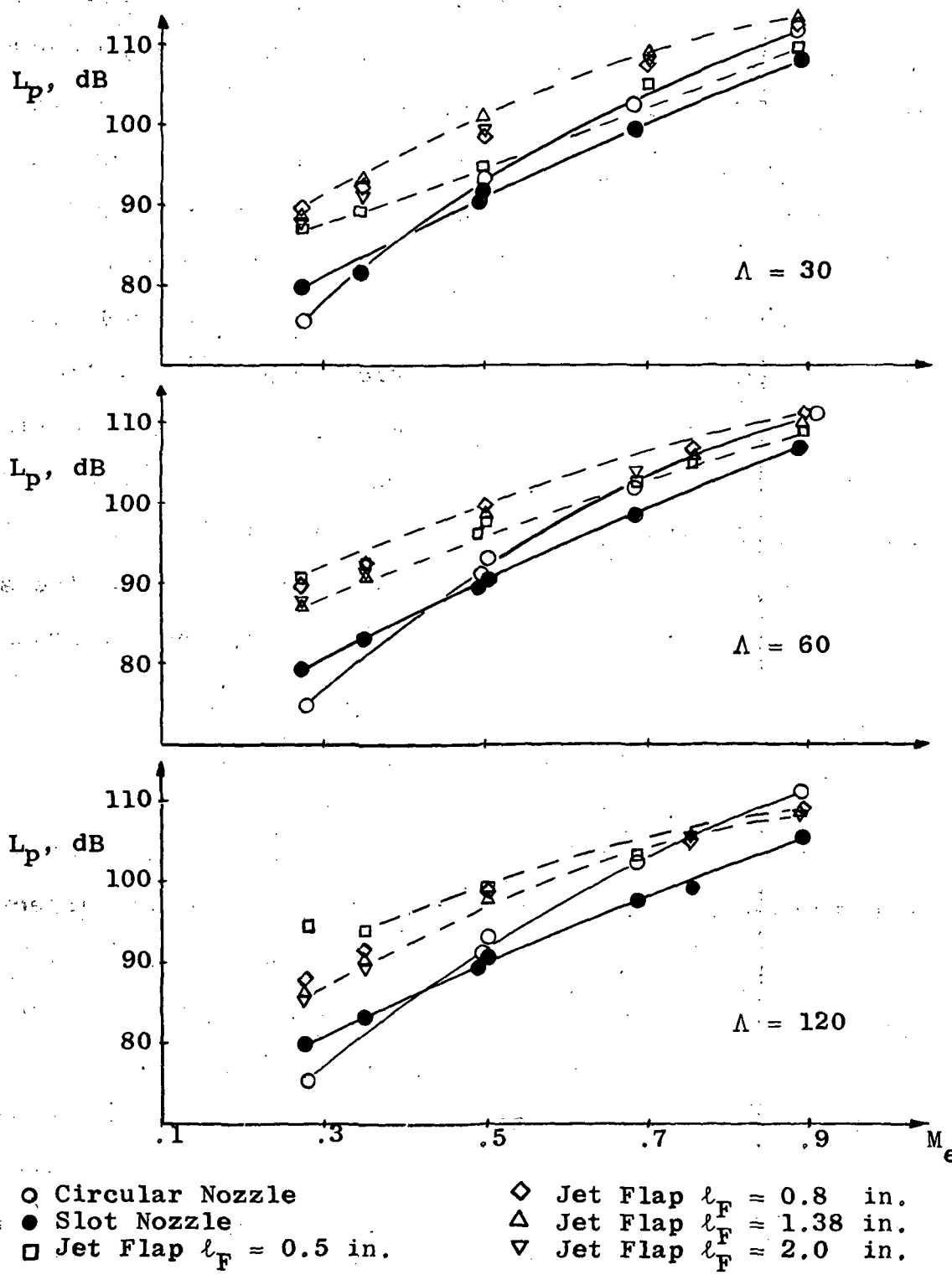
Figure 6: Overall Sound Power Level Versus Mach Number.

19

Figure 7 presents the overall sound power versus the non-dimensional flap length δ_F with the exit Mach number as parameter. For $0 < \delta_F \lesssim 10$ a graph of the sound power versus the dimensional flap length is also presented in Figure 8, since the sound power increases in this range with δ_F and Λ. The rate of increase depends on the Mach number and increases with decreasing Mach number. For $\delta_F > 10$ the sound power remains approximately constant and the influence of the aspect ratio is limited to the highest subsonic Mach number used during the tests. It should be noted that this change in the radiation characteristics occurs at a flap length that equals approximately the maximum potential core length.

Figure 9 is a graph of the overall sound power of the circular reference nozzle and the three slot nozzles versus the exit Mach number plotted in a logarithmic scale. For $M_e > 0.5$ the sound power of the circular nozzle follows very closely Lighthill's U^8-law which is represented by a straight line. The situation is substantially changed for the slot nozzles. At higher subsonic Mach numbers the slot nozzle $\Lambda = 30$ follows the U^8-law, the nozzle $\Lambda = 120$, however, follows a U^7-law, whereas the nozzle $\Lambda = 60$ gives results somewhere in between. For lower Mach numbers the exponent decreases further to approximately 4. For $M_e > 0.5$ the slot nozzles generate less sound than the circular nozzle. This is in agreement with Cole's (5) estimate that the noise
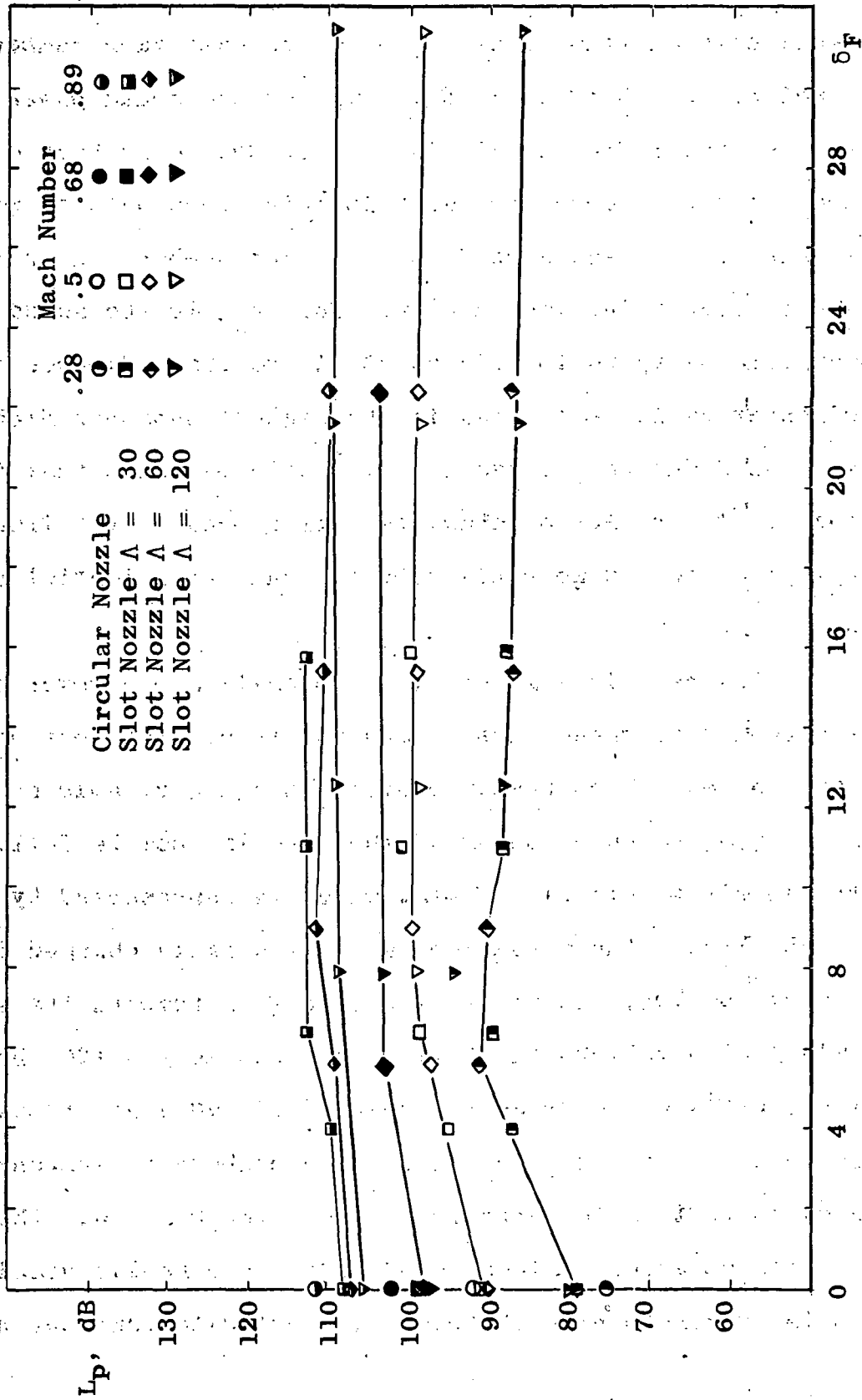
Figure 7. Overall Sound Power Level Versus Dimensionless Flap Length.

21
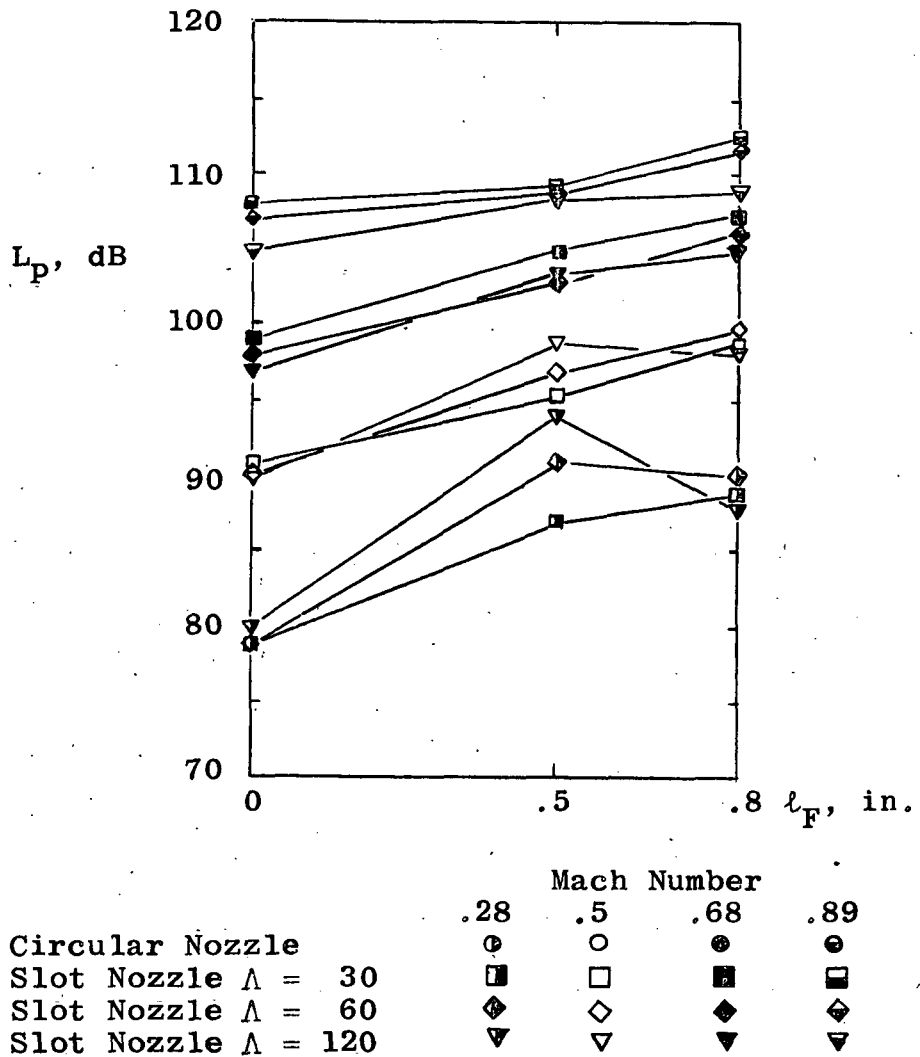
Figure 8. Overall Sound Power Level Versus Flap Length.
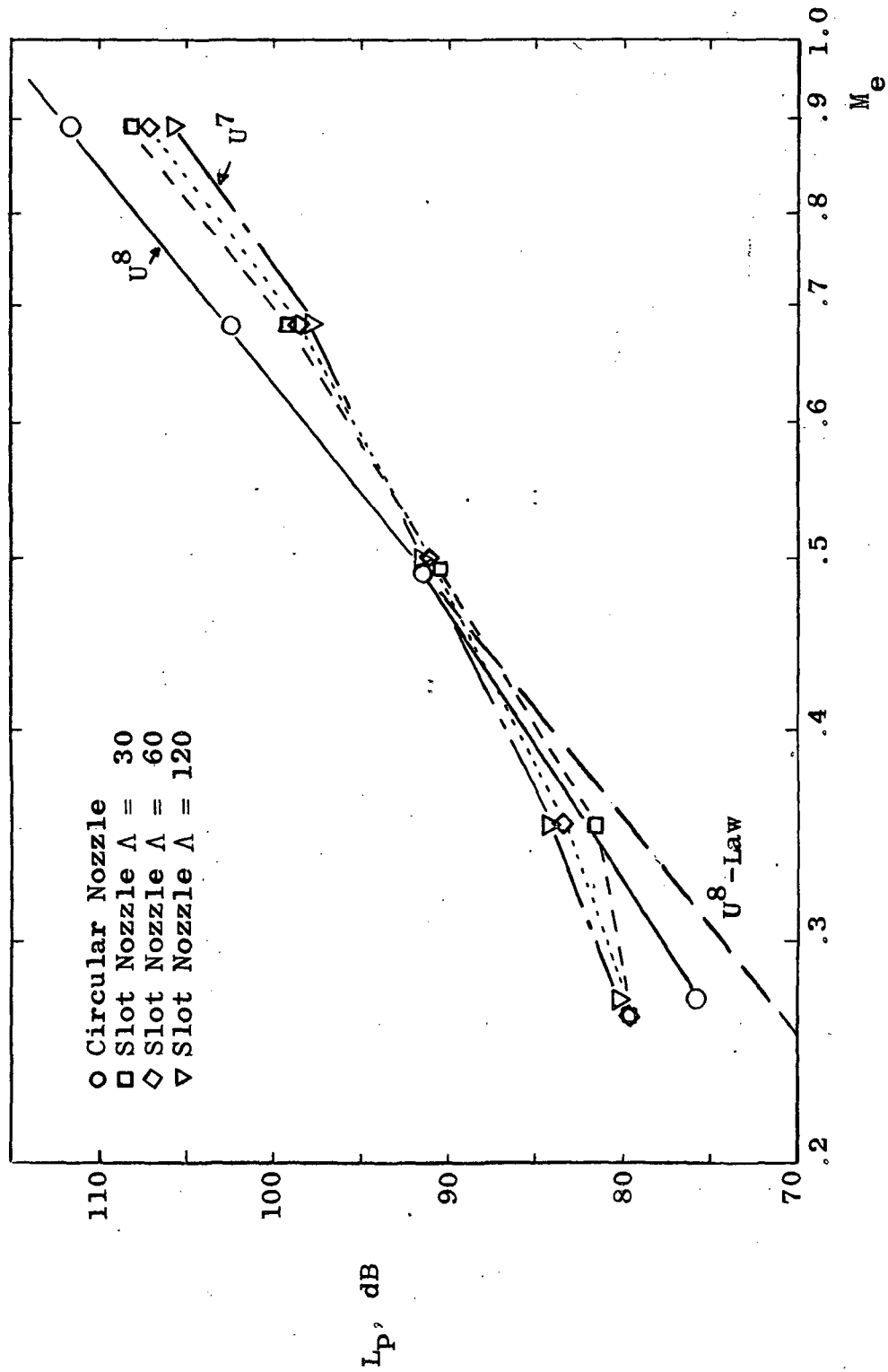
Figure 9. Exit Velocity Power Laws for Circular Nozzle and Slot Nozzles.

23

generation of a slot nozzle with a sufficiently high aspect ratio (in order to neglect the end effects) should be approximately 3 dB less than that of a circular nozzle with the same cross-sectional area and exit velocity.

Figure 10 shows that adding a flap to the slot nozzle increases the radiated sound power. The added flap also changes the exponent in the power law. The jet flap does not follow Lighthill's U^8-law within the Mach number range covered. Even for higher subsonic Mach numbers the exponent is only between 4.6 and 5.7, for lower ones as low as 3.5 to 4.6. The jet flap is noisier than the corresponding slot nozzle regardless of the Mach number, but the differences decrease with increasing Mach number. These observations for $\Lambda = 60$ hold also for the other two slot nozzles, as is evident from Figure 6 (page 19).

For both the slot nozzles and the jet flaps the exponent of the power law seems to depend on the Mach number. Harper (11) and Gruschka (12) report overall sound power measurements of slot nozzles ($\Lambda = 15, 30, 60$) and jet flaps ($\delta_F = 9, 13, 19$) and the corresponding circular reference nozzle. As the measurements were obtained in a reverberation room, they are directly comparable to the results reported here. The sound power of their circular reference nozzle and the circular nozzle used in this study agree very well if the levels are corrected to the same exit area (by plotting them, for example, versus the Lighthill parameter
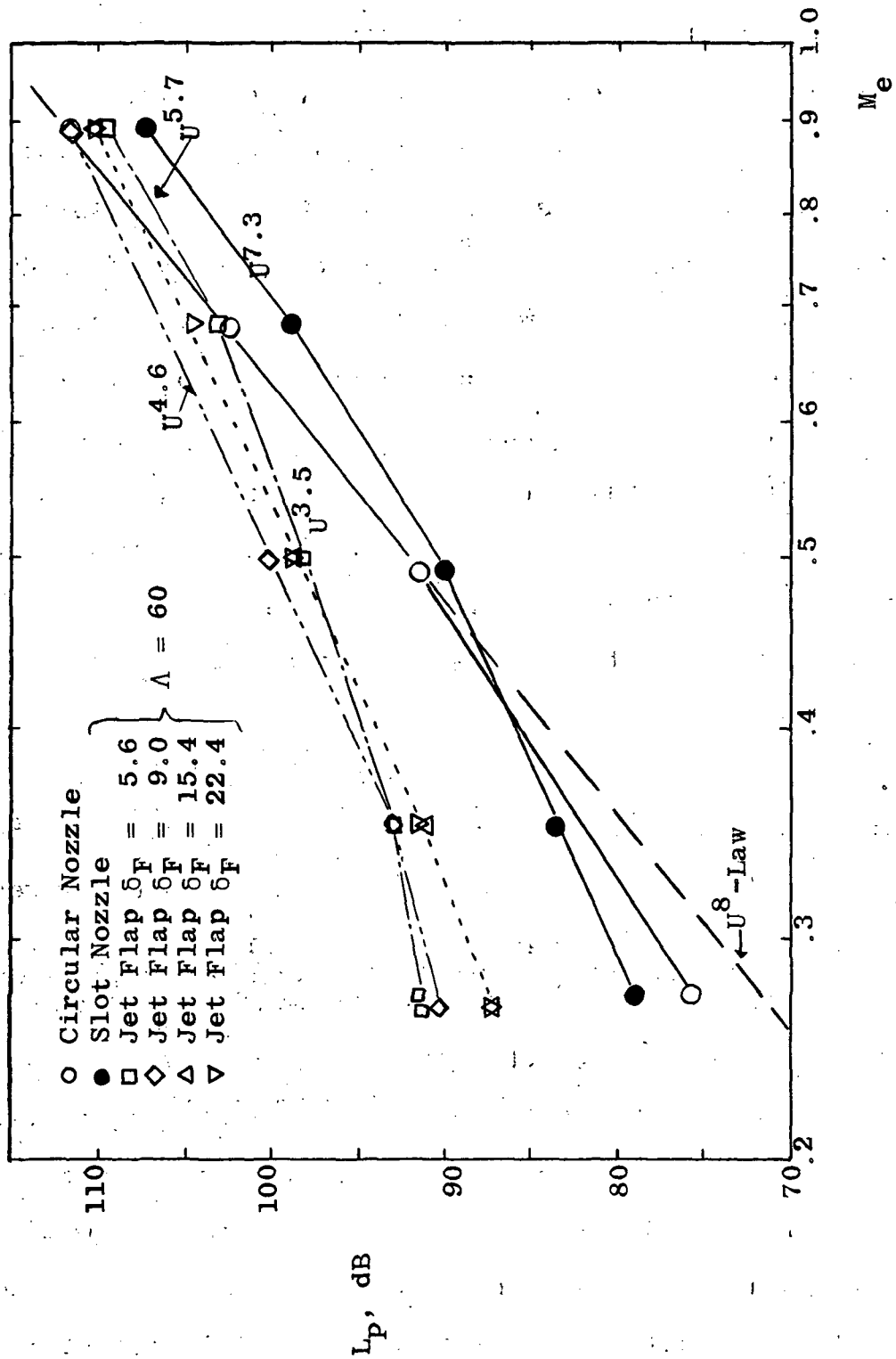
Figure 10. Exit Velocity Power Laws for Jet Flaps with $\Lambda = 60$.

25

$L = \rho_0 A_e a_0^{-5} U_e^8$, as was done in References (12) and (13).
The slopes of the sound power plots reported in (12) also agree
very well with those obtained in this study. This holds for
the slot nozzles as well as for the jet flaps. Only the
sound power is generally lower. It is believed that this
is an effect of the small size of the nozzles and jet flaps
tested. They measured considerable reductions of thrust for
the $\Lambda = 30$ and $\Lambda = 60$ nozzles compared to the circular
nozzle. Therefore, the sound power levels are generally lower
than those obtained in this study.

Power Density Spectra

The power density spectra were calculated from 1/3
octave sound pressure level spectra (Appendix B). Generally
the spectra of the noise are very broad and the maxima are
very flat. It is often difficult to determine the peak fre-
quency without substantial error. Nevertheless, in order to
characterize the power density spectra the peak frequency
will be used here lacking a better parameter.

Figure 11 is a plot of the peak frequency versus Mach
number for the circular nozzle and the three slot nozzles,
Figure 12 shows the bandwidth 3 dB below the peak for the
same nozzles. Comparing these two graphs it is obvious that
high peak frequencies are always associated with large band-
widths, or, in other words, the higher the peak frequency

26
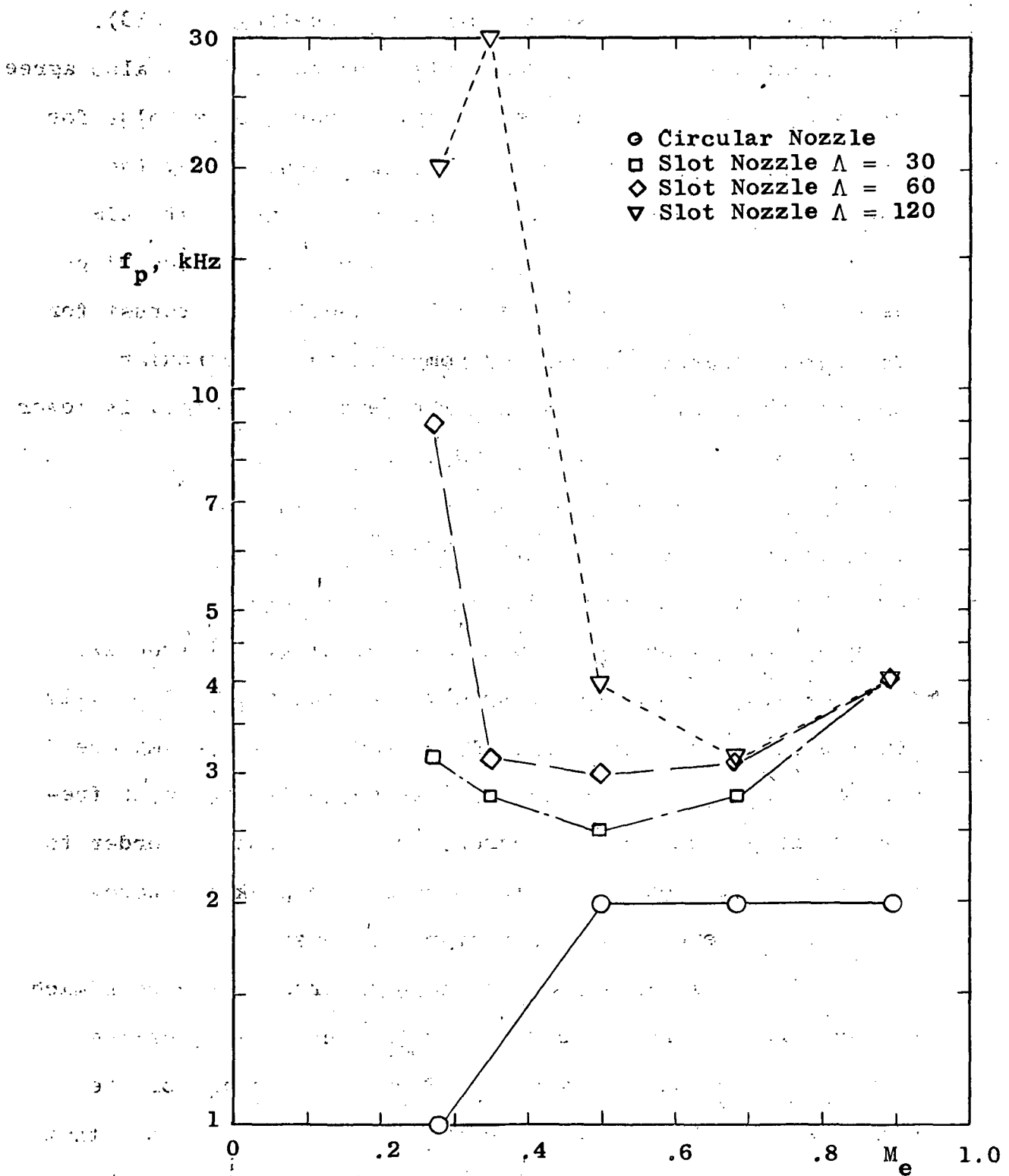
Figure 11. Peak Frequency of Power Density Spectra Versus Mach Number for Circular and Slot Nozzles.
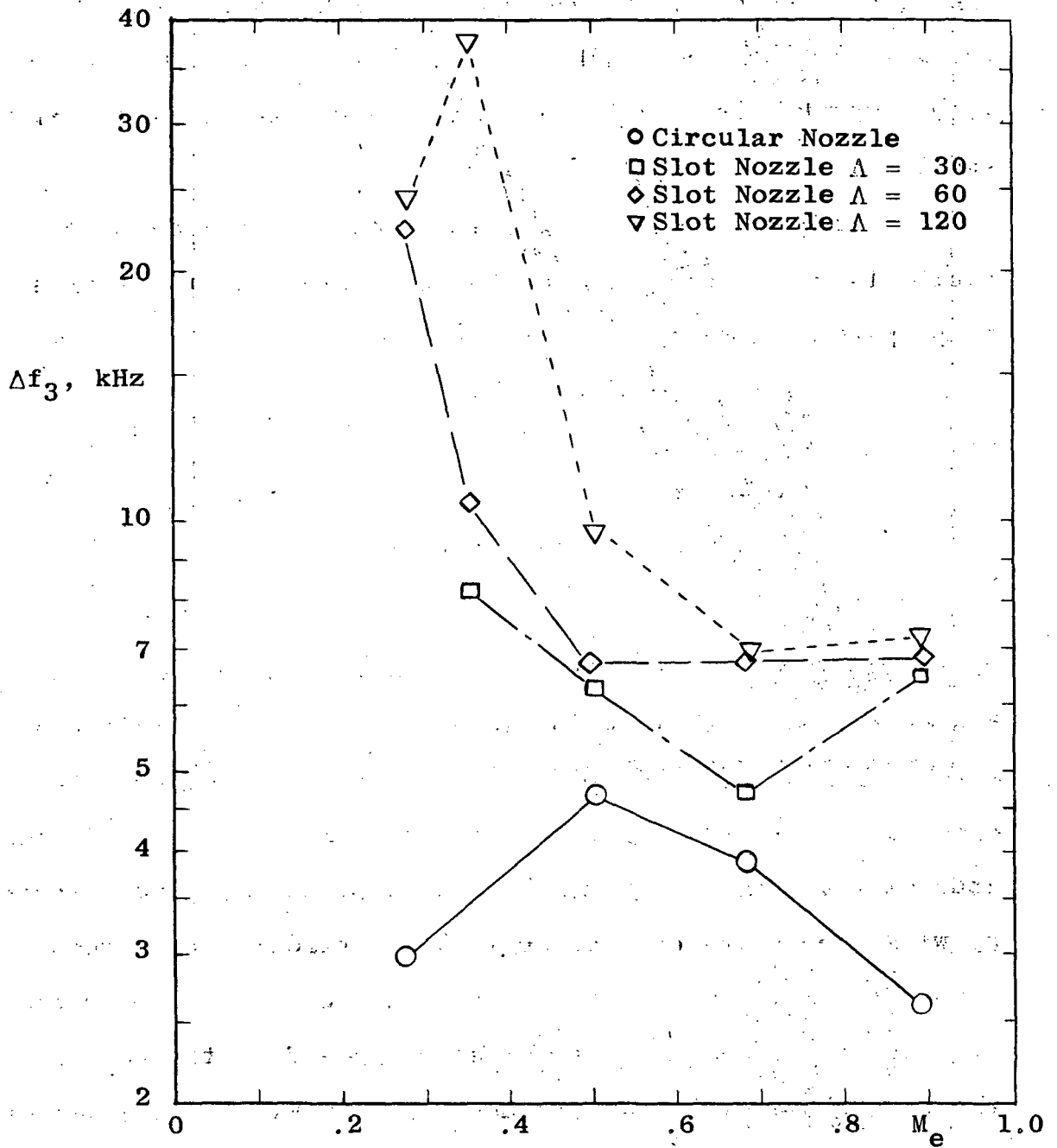
Figure 12.   Width of Power Density Spectra 3 dB Below
Peak Versus Mach Number for Circular Nozzle and Slot Nozzles.

the broader spectrum. This observation holds generally for all tested nozzles. No low peak frequencies associated with large bandwidth or high peak frequencies coupled with small bandwidth were found.

One would expect the peak frequency of a circular nozzle to be proportional to the exit velocity and inversely proportional to the exit diameter

$$f_p \sim U_e/d$$

or

$$Str_p = f_p \times d/U_e = \text{constant}$$

where Str_p is the peak Strouhal number. However, the peak Strouhal number, plotted in Figure 13 versus the exit velocity, shows a different behavior. Lighthill studied data of several researchers and found that the experimental evidence indicates at best a much slower increase of the peak frequency with increasing exit velocity than suggested by a constant Strouhal number. The peak frequencies of the spectra of the slot nozzles were expected to depend on the aspect ratio such that the peak frequency increases with the aspect ratio due to the smaller nozzle heights. Furthermore, as for the circular nozzle, the peak frequency was expected to be proportional to the exit velocity. The influence of the aspect ratio is as expected, though not for the higher subsonic Mach number range. The dependence on the exit velocity is, however, the opposite. In the low Mach number range the
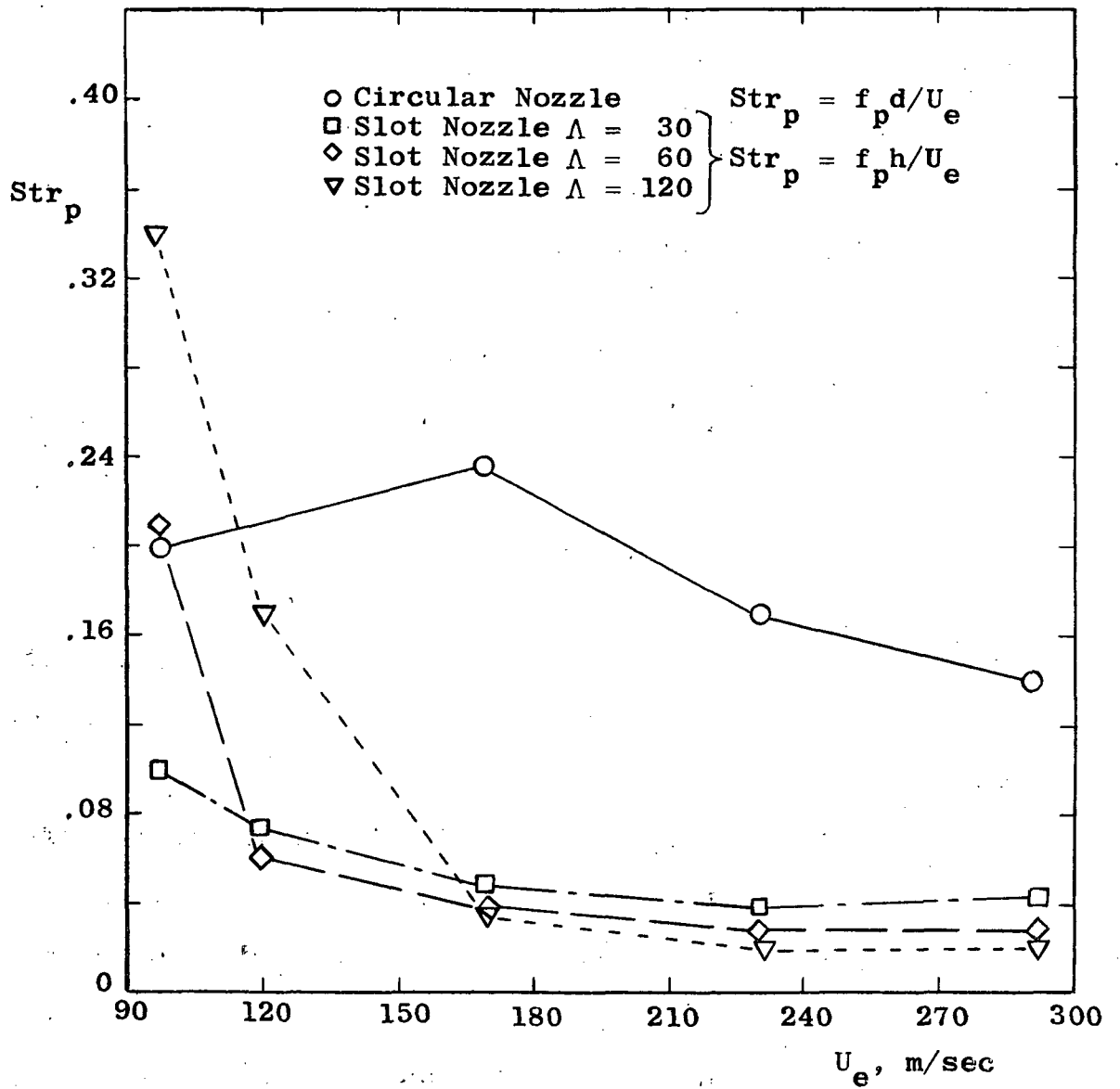
Figure 13. Peak Strouhal Number of Circular Nozzle and Slot Nozzles Versus Nozzle Exit Velocity.

slopes are negative and quite large for $\Lambda = 60$ and $\Lambda = 120$. The peak Strouhal number remains constant only for the higher exit velocities (Figure 13).

For jet flaps the first observation is that the peak frequency does not depend on the exit velocity. Figures 14, 15 and 16 are plots of the peak frequency versus Mach number. Disregarding for the moment jet flaps with $\delta_F < 10$, the graphs display a proportionality of the peak frequency to the exit Mach number and an inverse proportionality on the flap length δ_F. In order to demonstrate the direct proportionality between peak frequency and exit velocity, the Strouhal number was plotted versus the exit velocity for jet flaps with $\Lambda = 60$ and different flap lengths. Figure 17 shows that the Strouhal number remains nearly constant over a wide range of exit velocities. As characteristic length the flap length was chosen, which resulted in a minimum spread of data points.

Jet flaps with $\delta_F < 10$ exhibit somewhat different noise characteristics. Besides some other irregularities the most important seems to be the sudden drop of peak frequencies. First displaying the same proportionality to the exit velocity at low and medium subsonic Mach numbers as jet flaps with $\delta_F > 10$, the behavior is suddenly reversed at higher subsonic Mach numbers, resulting in a decrease of peak frequency with increasing exit velocity. It may be noted again that the jet core extends at a maximum to about ten nozzle heights downstream, if it is completely

31
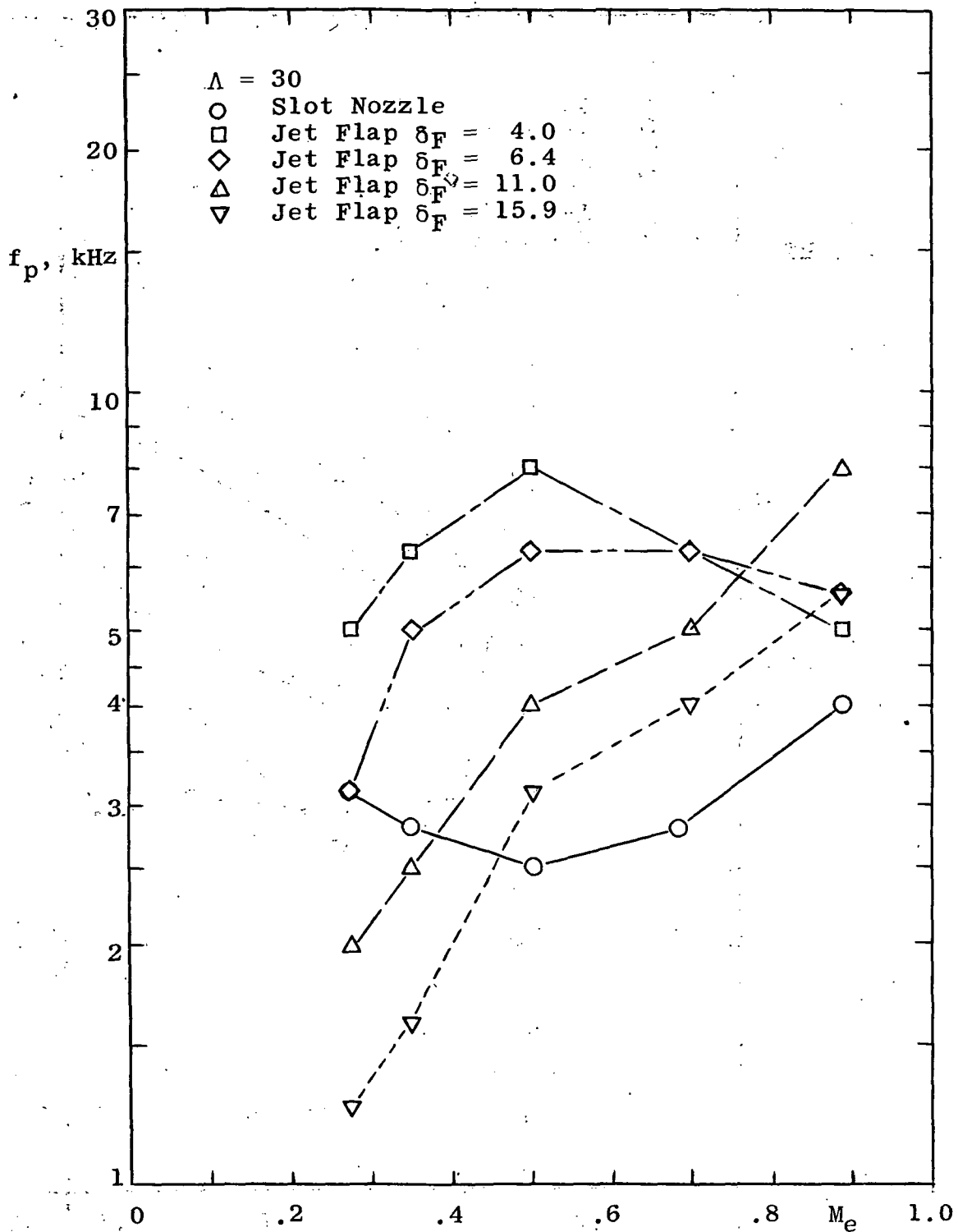
Figure 14. Peak Frequency of Power Density Spectra
for Jet Flaps with Aspect Ratio $\Lambda = 30$ Versus Mach Number.

32
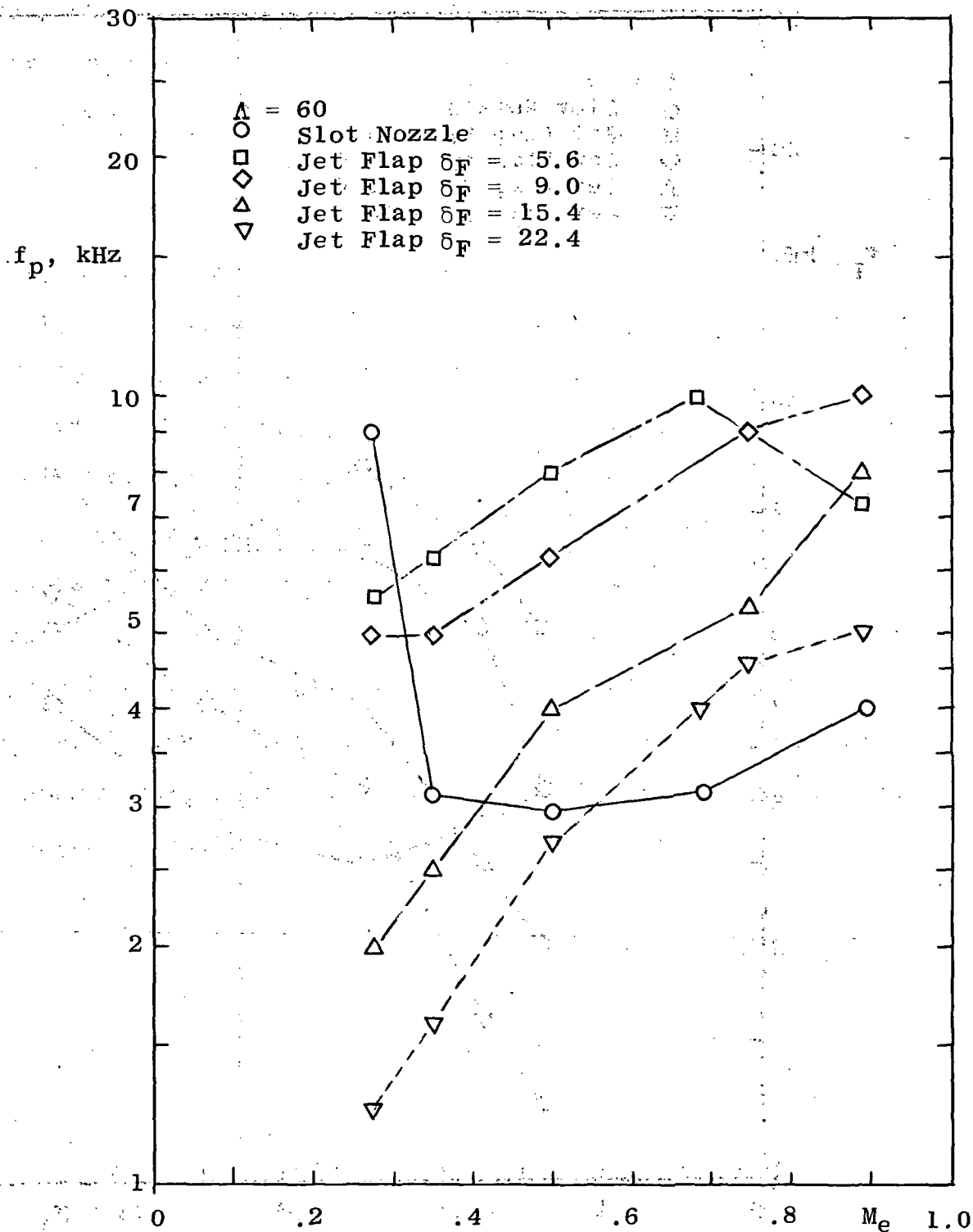
Figure 15. Peak Frequency of Power Density Spectra for Jet Flaps with Aspect Ratio $\Lambda = 60$.
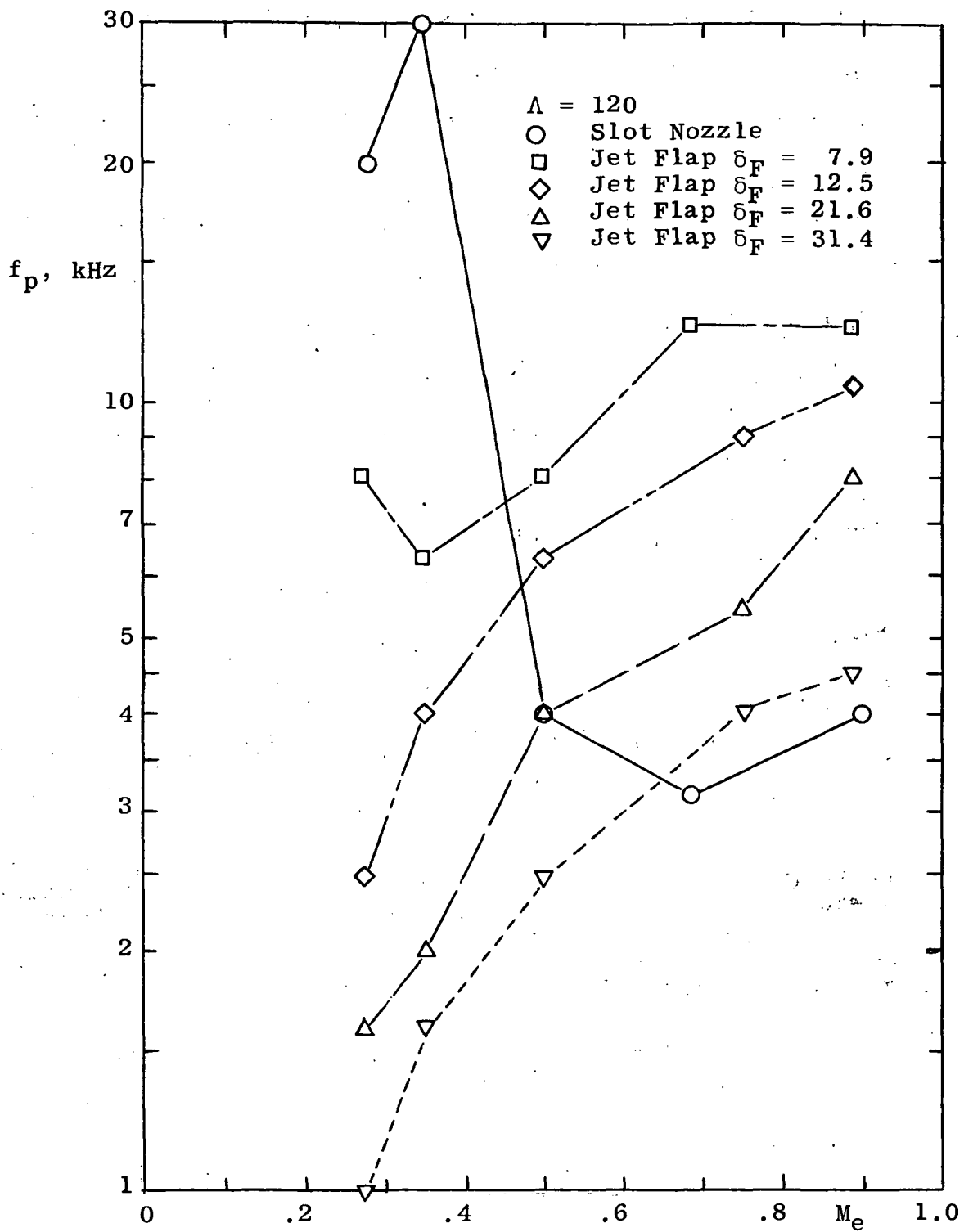
Figure 16. Peak Frequency of Power Density Spectra
for Jet Flaps with Aspect Ratio $\Lambda = 120$.
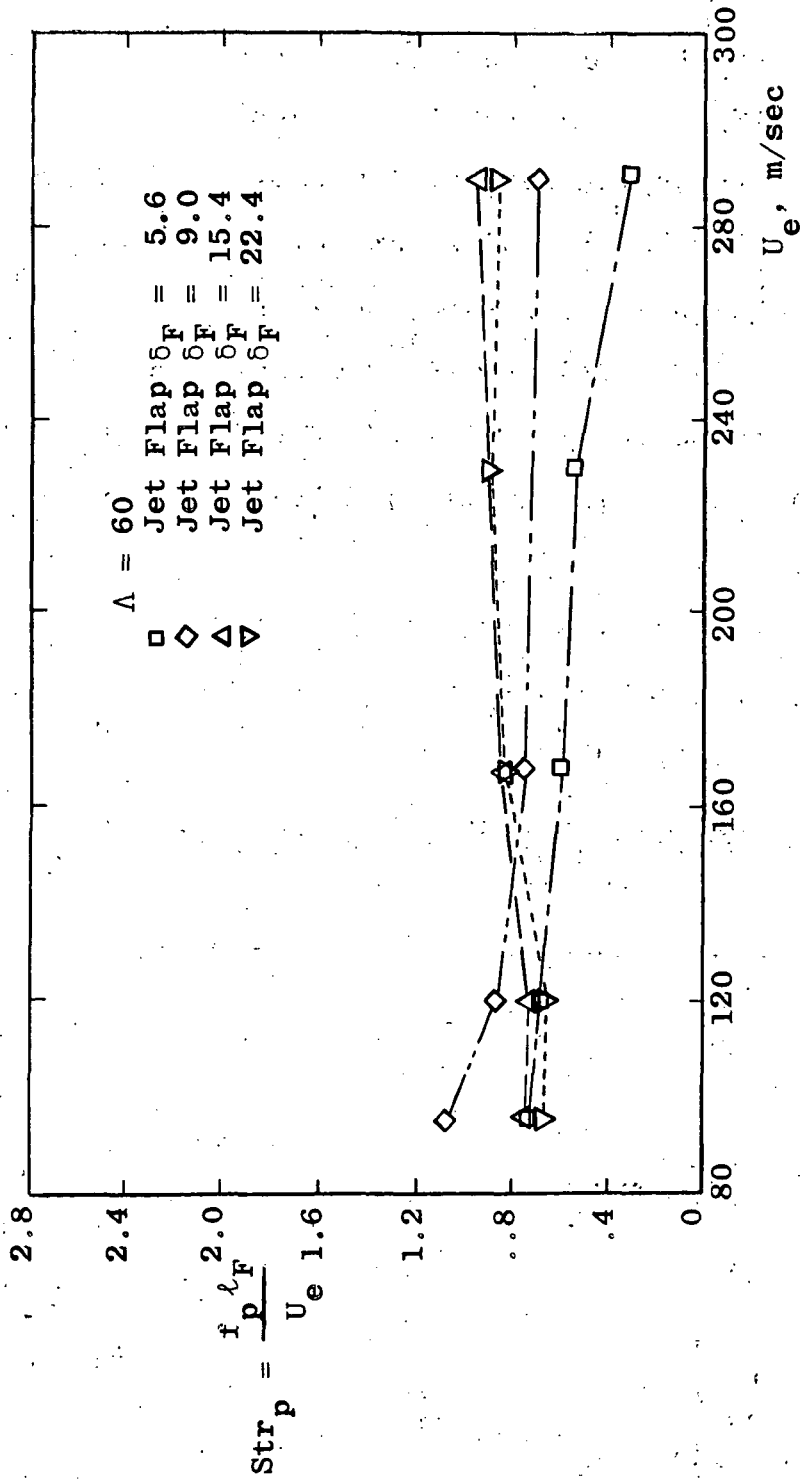
Figure 17. Peak Strouhal Number of Jet Flaps with Aspect Ratio.
$\Lambda = 60$ Versus Nozzle Exit Velocity.

shielded on one side by the flap. For shorter flaps the core
is also shorter but extends over the trailing edge of the
flap.

Figures 18, 19 and 20 present the peak frequency as a
function of the dimensional as well as non-dimensional flap
length with the aspect ratio as a parameter. It should be
noted that the peak frequency is independent of the aspect
ratio of the jet flap for $M_e < 0.9$. This is shown by plot-
ting the peak frequency versus the dimensional flap length
ℓ_F. The scatter of the data by approximately 0.5 KHz is con-
sidered a rather small deviation. If, however, the peak
frequency is plotted versus the non-dimensional flap length
δ_F the graph suggests a dependence on the aspect ratio.
This incorrect impression is caused by using an irrelevent
parameter to non-dimensionalize the influential parameter.

If the aspect ratio has no influence at all it ap-
pears that the peak frequency is just a function of the
ratio of a characteristic speed and the flap length. This
calculated frequency, using the exit velocity as character-
istic speed, is also plotted in Figures 18, 19 and 20. This
ratio is generally too high, especially for the shortest flap,
but represents otherwise approximately the general behavior.

For $M_e = 0.9$, however, where the peak frequency drop
for jets with $\delta_F < 10$ occurs, the aspect ratio has a strong
influence on the peak frequency. If now the flap length,
non-dimensionalized by the nozzle height, is used on the
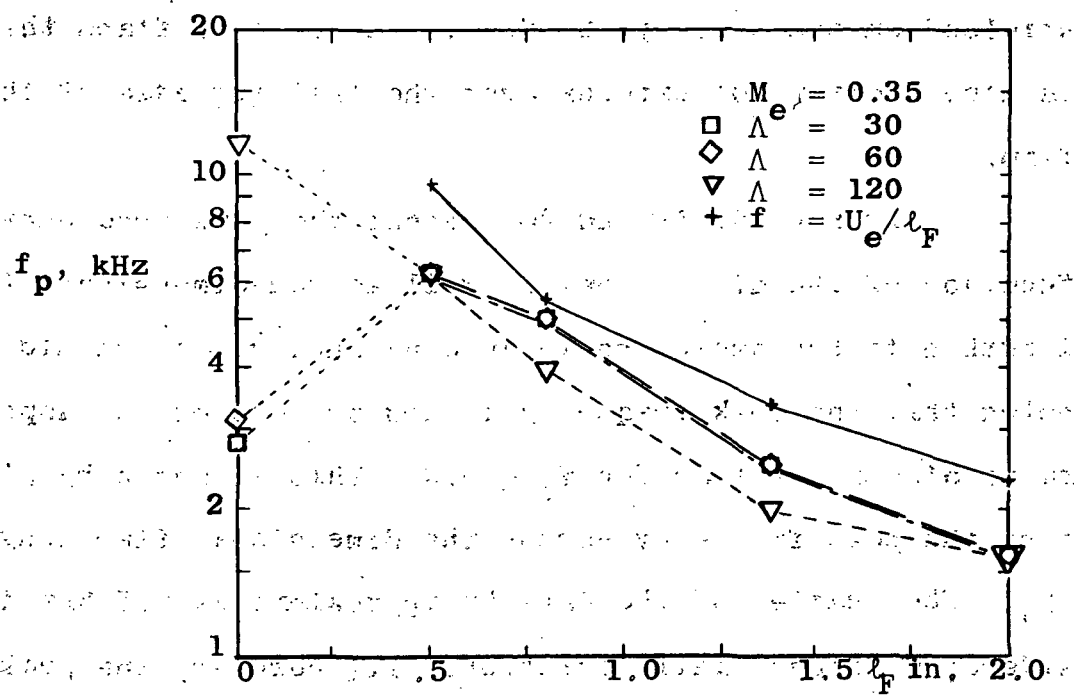
(a) Peak Frequency Versus Dimensional Flap Length.
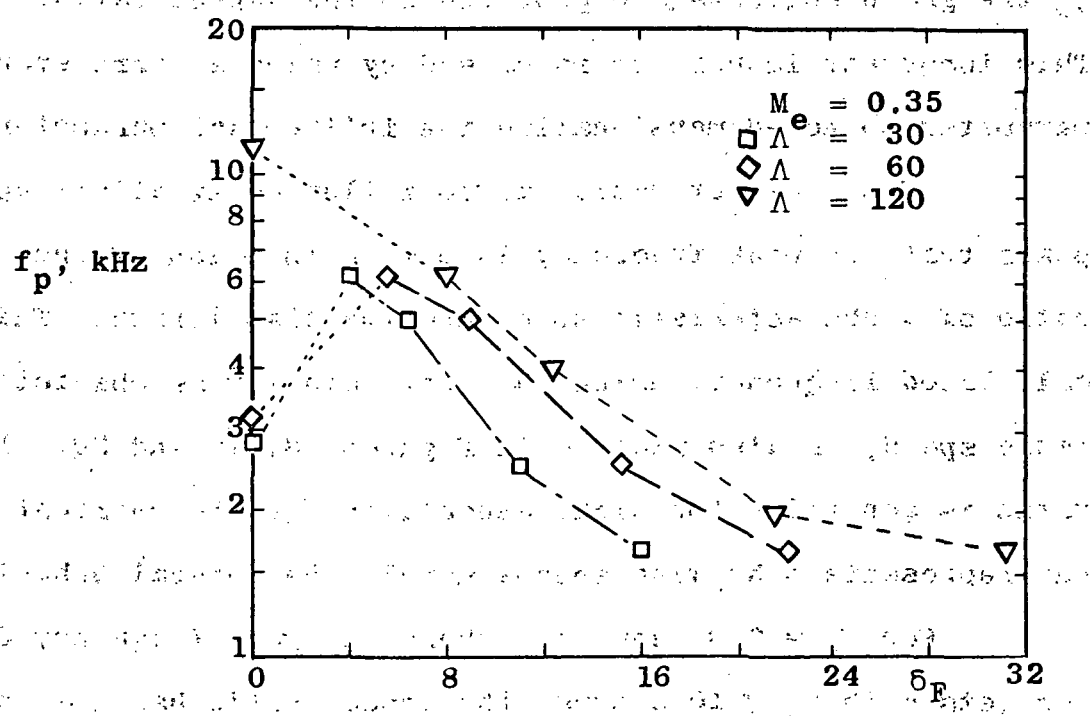
(b) Peak Frequency Versus Dimensionless Flap Length.

Figure 18. Peak Frequency of Power Density Spectra
Versus Flap Length, $M_e = 0.35$.
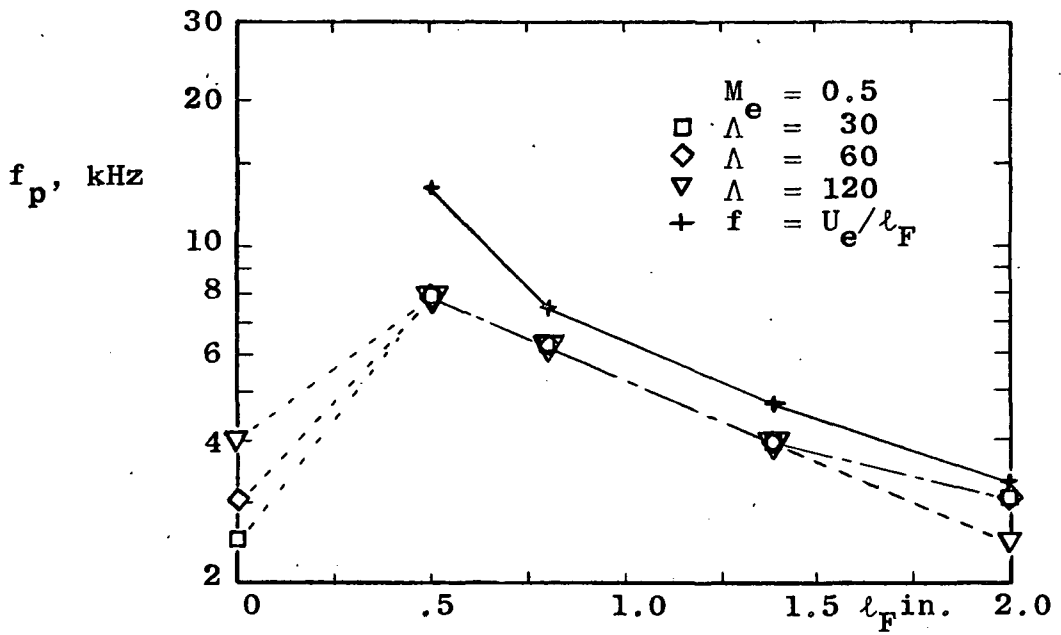
(a)   Peak Frequency Versus Dimensional Flap Length.
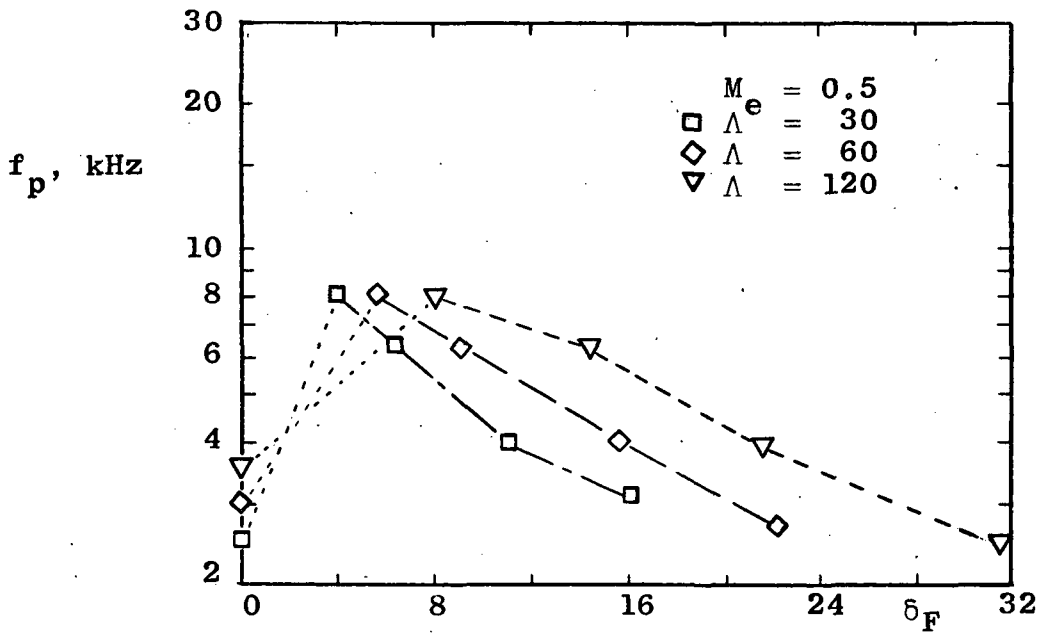
(b)   Peak Frequency Versus Dimensionless Flap Length.

Figure 19. Peak Frequency of Power Density Spectra
Versus Flap Length, $M_e = 0.5$.
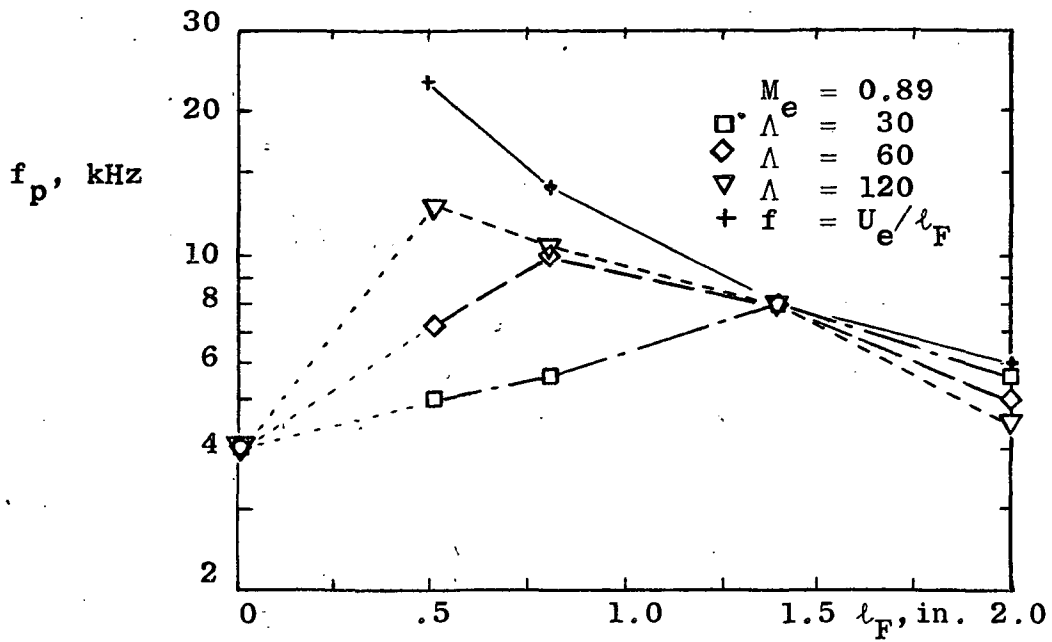
38

(a)   Peak Frequency Versus Dimensional Flap Length.
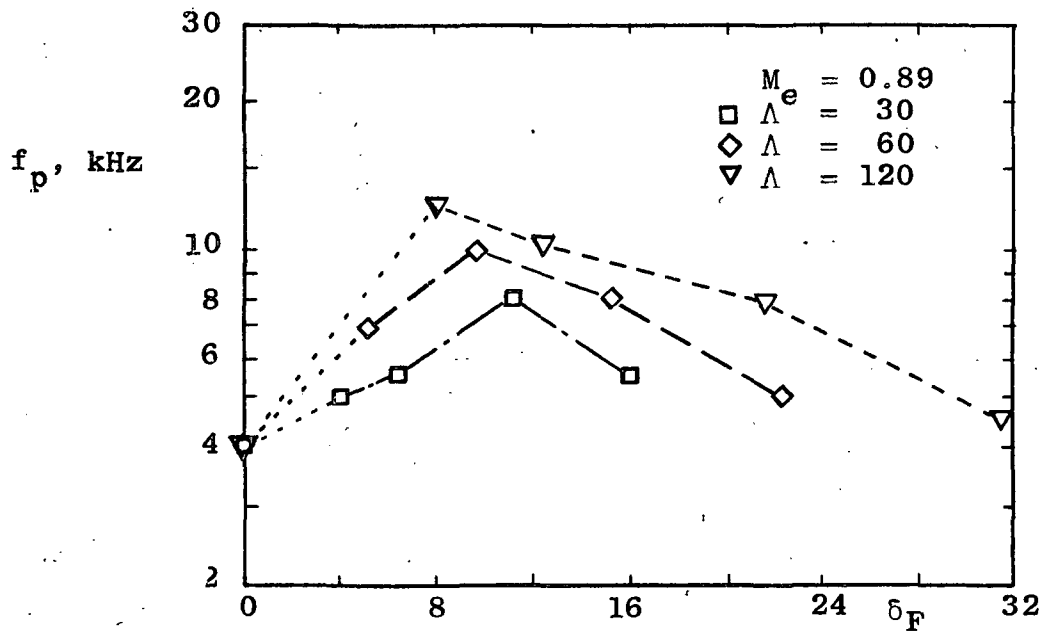
(b)   Peak Frequency Versus Dimensionless Flap Length.

Figure 20 .   Peak Frequency of Power Density Spectra
Versus Flap Length, M_e = 0.89.

abscissa, a certain pattern develops with peaks in the range $8 < \delta_F < 11$ (Figure 20). It seems, for higher subsonic Mach numbers, that the peak frequency increases with increasing flap length as long as the jet core extends over the trailing edge of the flap. As the core length depends on the nozzle height, the peak frequency depends also on the nozzle height and thus on the aspect ratio. If the flap length is larger than the core length, the peak frequency is again inversely proportional to the flap length and is independent on the nozzle height.

Summary

The influence of the Mach number on the overall sound power is discussed first. For higher subsonic Mach numbers (0.7 to 0.9) the overall sound power is proportional to

$$U_e^8 \qquad \text{for the circular nozzle}$$
$$U_e^8 \text{ to } U_e^7 \qquad \text{for the slot nozzles } (30 \leq \Lambda \leq 120)$$
$$U_e^6 \text{ to } U_e^5 \qquad \text{for jet flaps with } \Lambda = 60 \text{ and } 5.6 \leq \delta_F \leq 22.4$$

For low Mach numbers (0.3 to 0.5) the exponents are smaller by approximately 20% for all nozzles and jet flaps tested. The slopes are in agreement with those reported in (11) and (12). For low Mach numbers $P_{jet\,flap} > P_{slot\,nozzle} > P_{circular\,nozzle}$, but due to the power laws, the order of noisiness is reversed for higher Mach numbers. In Figures 6 (page 19) and 10 (page 25) this behavior can be observed,

although the highest Mach number of the tests is not large enough. The slot nozzles are not as noisy as the circular nozzle for $M_e > 0.45$ and the jet flaps are less noisy than the circular nozzle for $M_e > 0.85$ to 0.95, depending on the aspect ratio. If the data are extrapolated one may state that the jet flaps become less noisy than the slot nozzles around $M_e = 1$ or above.

The influence of the flap length, the aspect ratio and the exit velocity on the sound power and the peak frequency is best presented separately for jet flaps whose flaps are shorter than the potential core and those with flap lengths longer than the core. The reason is that a clear picture is only obtained for jet flaps with flaps longer than the core.

Summary for $\delta_F \gtrsim 10$

The total sound power is nearly independent of the flap length ($10 < \delta_F < 32$) and depends only for higher subsonic Mach numbers on the aspect ratio. The peak frequency is proportional to the exit velocity and inversely proportional to the flap length. It is independent of the aspect ratio ($30 \leq \Lambda \leq 120$).

Summary for $\delta_F \lesssim 10$

The total sound power increases with increasing flap length and increasing aspect ratio (Figure 8, page 22). The slopes are decreasing with increasing Mach number. The peak frequency behaves exactly as described for $\delta_F > 10$ as long as

41

the exit Mach number is smaller than, say, 0.8. For
M_e = 0.9 the peak frequency increases with increasing flap
length.

Discussion

Particular characteristics of the noise radiation from
jet flaps, which were observed in free-field tests and repor-
ted in the References (4), (5) and (8), were confirmed by
the results obtained in the reverberation chamber. Since in
all three references the jet flaps had flap lengths much
larger than the potential core, jet flaps with δ_F > 10 are
discussed first.

The first of these reported characteristics is the
increase in overall noise if a flap of moderate length
$(10 \lesssim \delta_F \lesssim 30)$ is added to a slot nozzle. This result is
shown in Figures 7, 8 and 11 (pages 21, 22 and 27). The
peak frequencies of the power density spectra are larger
for the jet flaps than for the slot nozzles, if $0.7 \lesssim M_e$
$\lesssim 0.9$. The question is whether the high frequency noise is
generated in the primary or in the secondary mixing region
(the inner boundary layer is not considered since it is be-
lieved that the two other regions of noise generation should
dominate because of their much larger volumes). According
to the reasoning of Grosche (8), the flap prevents the
mixing of the turbulent plane jet with the ambient air on
one side of the jet sheet, especially in the region near the

42

nozzle orifice which is commonly considered as the source of high frequency noise. Therefore, if the contents of high frequency noise increases, the most reasonable source of it is the secondary mixing region. If this is confirmed by the flow measurements, this has to be considered as a major drawback of jet flaps equipped with moderately long flaps, since noise generated in the secondary mixing region is radiating unobstructedly towards the ground.

The second of the reported characteristics is the decrease of overall noise of the jet flap compared to the slot nozzle, coupled with an increase of low frequency noise, if a long flap ($\delta_F \gtrsim 100$ approximately) is added. In order to confirm this result of the free-field tests by the results obtained in the reverberation chamber, both the test data of the overall sound power versus δ_F and the peak frequency of the power density spectra versus δ_F have to be extrapolated, since the longest flap tested was $\delta_F = 32$. In Figure 7 (page 21) the overall sound power at medium and higher subsonic Mach numbers is more or less constant for $12 \lesssim \delta_F \lesssim 32$. There is no indication in which direction the curves will turn if the flap length is increased. Maglieri and Hubbard (4) reported a reduction of overall sound power for $\delta_F = 190$ compared to the slot nozzle, whereas Grosche (8) reported a higher overall sound power compared to the slot nozzle for flaps with $\delta_F = 50$ and 100. Therefore, if the sound power decreases as is indicated by Reference (4), it decreases only very slowly with increasing δ_F.

43

The picture is clearer if the peak frequencies are considered. Figures 13 through 15 (pages 30, 32 and 33) and Figures 17 through 20 (pages 35, 37, 38 and 39) show that there is a consistent inverse proportionality between the peak frequency of the power density spectrum of the noise and the flap length (at constant exit velocity). There is no apparent reason why this inverse proportionality should not also hold for larger flap lengths. Therefore, this relationship between the peak frequency and the flap length, the aspect ratio having no or only a minor influence, seems to confirm that a major part of the radiated noise is generated in the secondary mixing region.

Next, consider the noise output of jet flaps with flap length $\delta_F \lesssim 10$. From the graph of the overall sound power versus the dimensional flap length ℓ_F (Figure 8, page 22), it is noticed that for a fixed Mach number the sound power increases with both the flap length and the aspect ratio (slot width). This is a strong indication for the presence of wall boundary layer noise, composed of quadrupole noise and dipole noise. Both of these noise sources are proportional to the flap length and width (in the x_3 direction) of the turbulent flow over the flap. Since the dipole noise dominates the quadrupole noise by a factor of $1/M^2$, the increase is largest for low Mach numbers and smallest for higher subsonic Mach numbers. The observed peaks of the overall sound power which occur only at small Mach numbers might be caused by strong dipole sources generated by the interaction between the unsteady motion of the potential core and the trailing edge of the flap.

44

Thus the additional overall sound power radiated due to the addition of a flap to a slot nozzle is composed of three types of noise: Quadrupole type wall boundary layer noise, dipole type boundary layer noise and quadrupole type noise of the secondary mixing region.

CHAPTER III

THE FLOW FIELD OF JET FLAPS

The objective of the flow measurements is to obtain

general information on the flow field of jet flaps, parti-

cularly on mean shear, turbulence intensity and turbulence

scale. This will lead to estimates of the acoustic source

strength distribution. Also it will enable estimates of the

relative source strength of the secondary mixing region to

be made.

I. SOME GENERAL CONSIDERATIONS AND INFORMATION

The Flow Field of a Slot Nozzle as a

Limiting Case of the Jet Flap

A limiting case of the jet flap is the plane turbulent

jet (flap length becomes zero). As the flap length increases

beyond the jet core length, it will gradually change the mean

and fluctuating velocity profiles of the primary mixing re-

gion. The dominating region of noise generation is the tur-

bulent flow with high turbulence intensity and large mean

shear, thus the central region of the mixing region. It will

be shown later that this part of the primary mixing region is

not influenced at all by any of the three flaps. Therefore

it is concluded, for the flap lengths under consideration here,

that theory and experimental data of the free turbulent mixing

region of the plane turbulent jet can be applied to the primary mixing region of the jet flap.

The plane turbulent jet was investigated by several researchers, among them Albertson, Dai, Jensen and Rose (14), Van der Hegge Zijnen (15), Mathieu and Synyach (16), Miller and Comings (17) and Liepmann and Laufer (18). The latter investigated the first regime of the plane turbulent half-jet. Theory and experimental data of the initial and transient region of the tangential plane turbulent wall jet would be directly applicable (neglecting eventual influences from the finite flap length), however, to the knowledge of the author, they are only available for the fully developed region.

As already outlined in Chapter I, the flow field of a slot nozzle is self-similar in the initial region as well as in the fully developed region. Since the initial region is of dominant importance for the generation of noise, the self-similarity was checked by measuring the mean and turbulent velocity profiles with a hot-wire anemometer. Figures 21 and 22 show these velocity profiles plotted against a non-dimensionalized lateral position. The mean velocity profiles are already similar for $x_1/h \geq 1$, whereas the turbulence velocity profiles become similar further downstream. One can deduce from the data that the velocity profiles become fully developed in the range $1 \leq x_1/h < 3$. Liepmann and Laufer (28) report fully developed velocity profiles for $x_1/h > 1.5$.

47
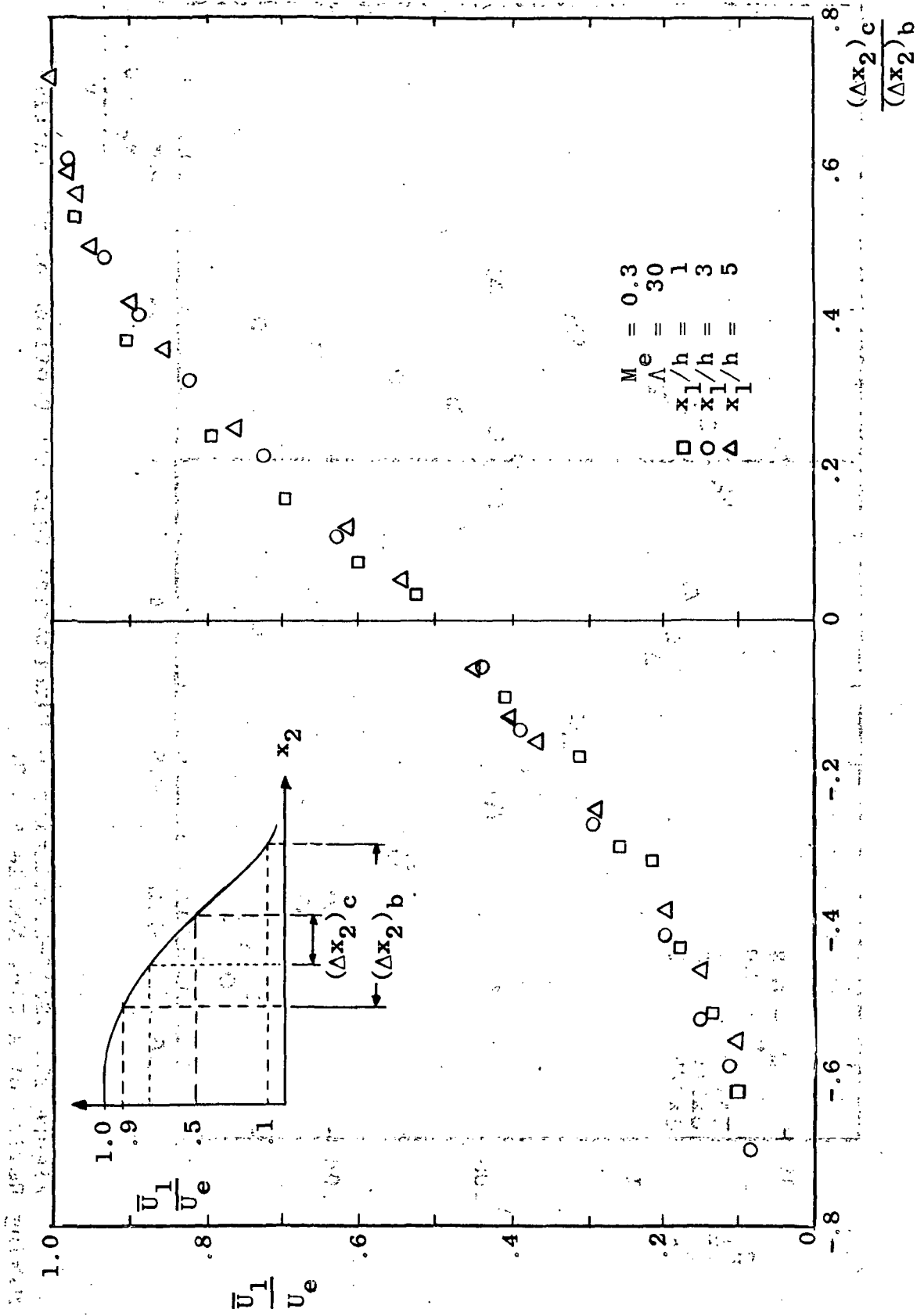
Figure 21. Self-Similarity of Mean Velocity Profiles of the Initial Mixing Region of a Slot Nozzle $\Lambda = 30$.
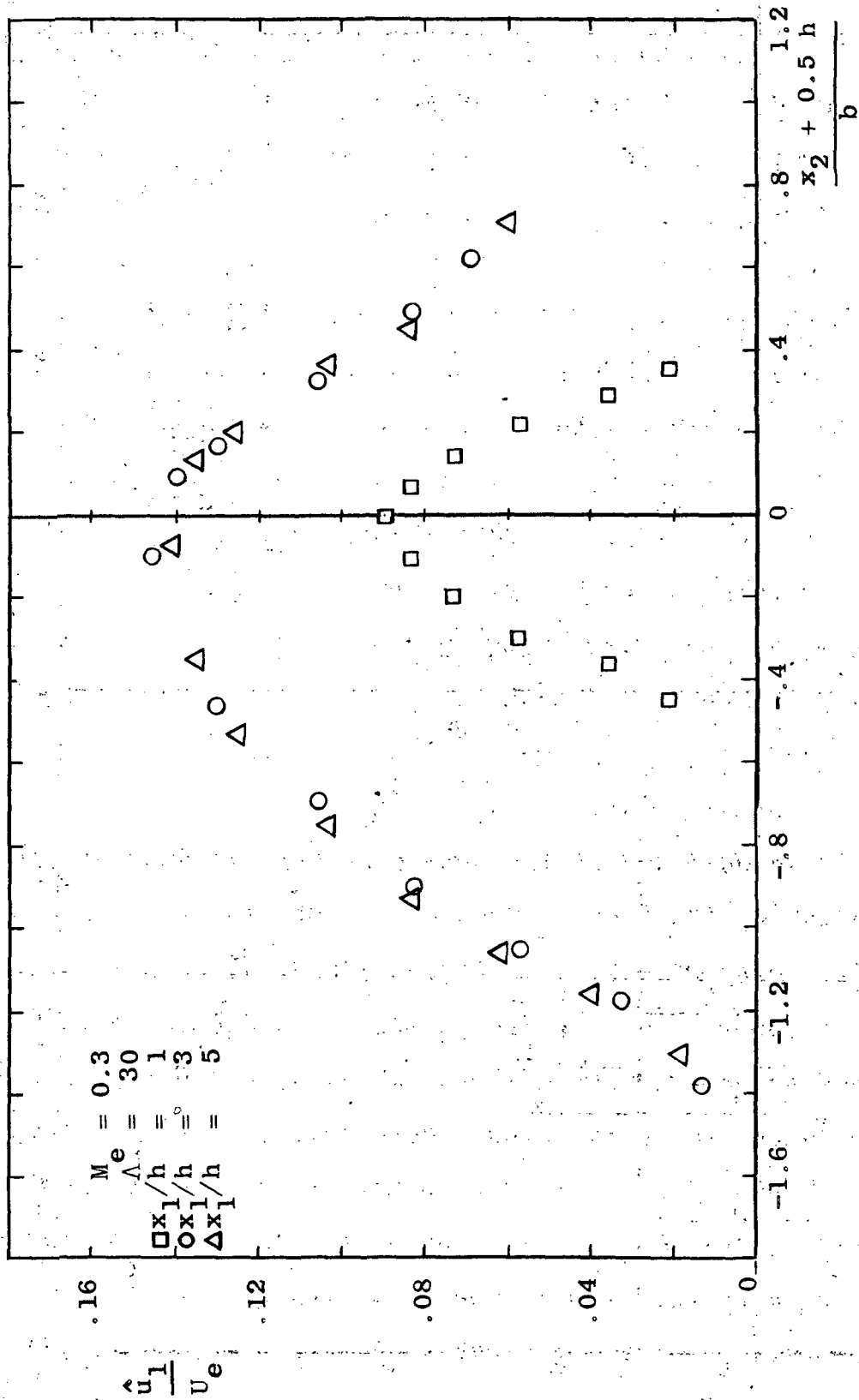
Figure 22. Self-Similarity of Fluctuating Velocity Profiles of the Initial Mixing Region of a Slot Nozzle $\Lambda = 30$

Information Obtained from Shadowgraph Pictures

Some general information on the flow field were obtained by shadowphotographs taken with a short duration spark as light source. The shadowgraphs show that the transition from laminar to turbulent mixing layer occurs very close to the nozzle exit. The transition point, measured on the circular reference nozzle, is located approximately at x_1/d = 0.2. The jet emerging from the slot nozzle (Λ = 60) undergoes transition somewhere before x_1/h = 0.5. Downstream of the transition point the primary mixing region with its high turbulence intensity develops, separated from the flap by the potential core and the inner boundary layer. In the case of the short flap, δ_F = 5.6, the potential core extends over the trailing edge of the flap. Behind the trailing edge the secondary mixing region originates. The shadowgraphs indicate a faster spread of the secondary mixing region as compared with the primary mixing region. The inner boundary layer is very thin and not visible on the picture.

In the case of a long flap (δ_F = 22.4), the core extends over less than half the flap length. The inner boundary layer becomes visible but is still so thin that no turbulent structure can be seen. Here, too, the secondary mixing region spreads faster than the primary mixing region.

II. HOT-WIRE MEASUREMENTS

The bulk of the data which will be reported are those obtained in the flow field of a jet flap with an aspect ratio $\Lambda = 60$ and flap length of $\delta_F = 5.6$, 8.95 and 15.4. Thus one flap is shorter than the potential core, one is of about the same length and one is much longer than the core. The exit velocity is usually 120 m/sec, corresponding to an exit Mach number of 0.35 and a Reynolds number of 1.75×10^4, based on the nozzle height. Since no measurements were attempted in the inner boundary layer, all reported data are those obtained in the primary or secondary mixing region. All data were measured by means of hot-wire anemometers and Figures 23 through 28 show a selection of typical mean and fluctuating velocity profiles. The major part of the results presented on the following pages was obtained from such velocity profiles. The instrumentation used for the measurements is described in Appendix C.

Two important features of the flow field of a jet flap are readily apparent from inspection of these profiles. First, the mean velocity and the turbulence intensity distributions in the primary mixing region are unaffected by the addition of any of the flaps. Second, very strong mean velocity gradients and high values of turbulence intensity occur in the secondary mixing region immediately behind the flap. This is shown quite clearly in Figures 23 and 24 and indicate a strong source of acoustic noise.

51
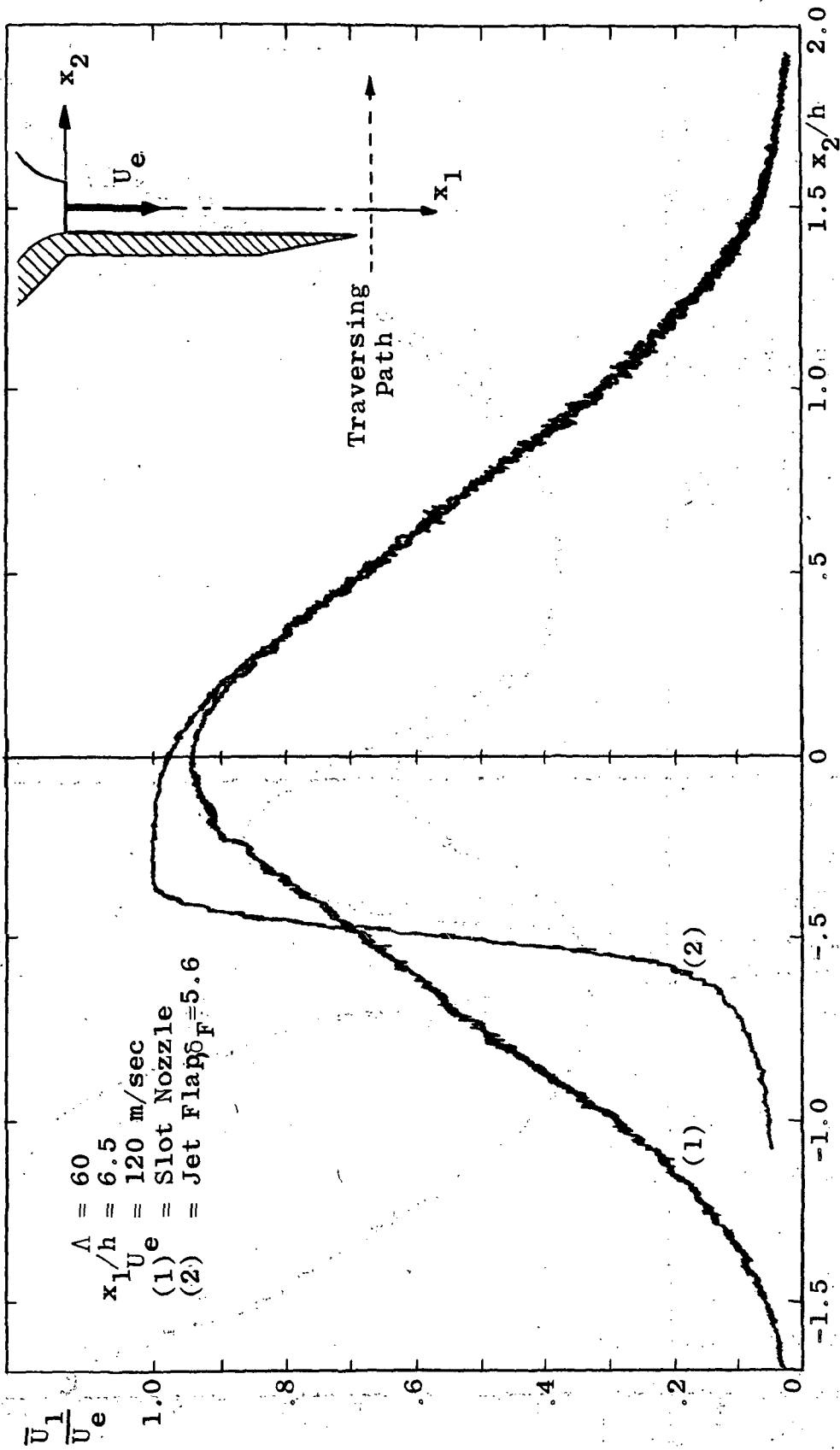
Figure 23. Mean Velocity Profiles of Slot Nozzle and Jet Flap at $x_1/h = 6.5$.

$$\frac{\bar{U}_1}{U_e}$$

$$\Lambda = 60$$
$$x_1/h = 6.5$$
$$U_e = 120 \text{ m/sec}$$
(1) = Slot Nozzle
(2) = Jet Flap $\delta_F = 5.6$

52
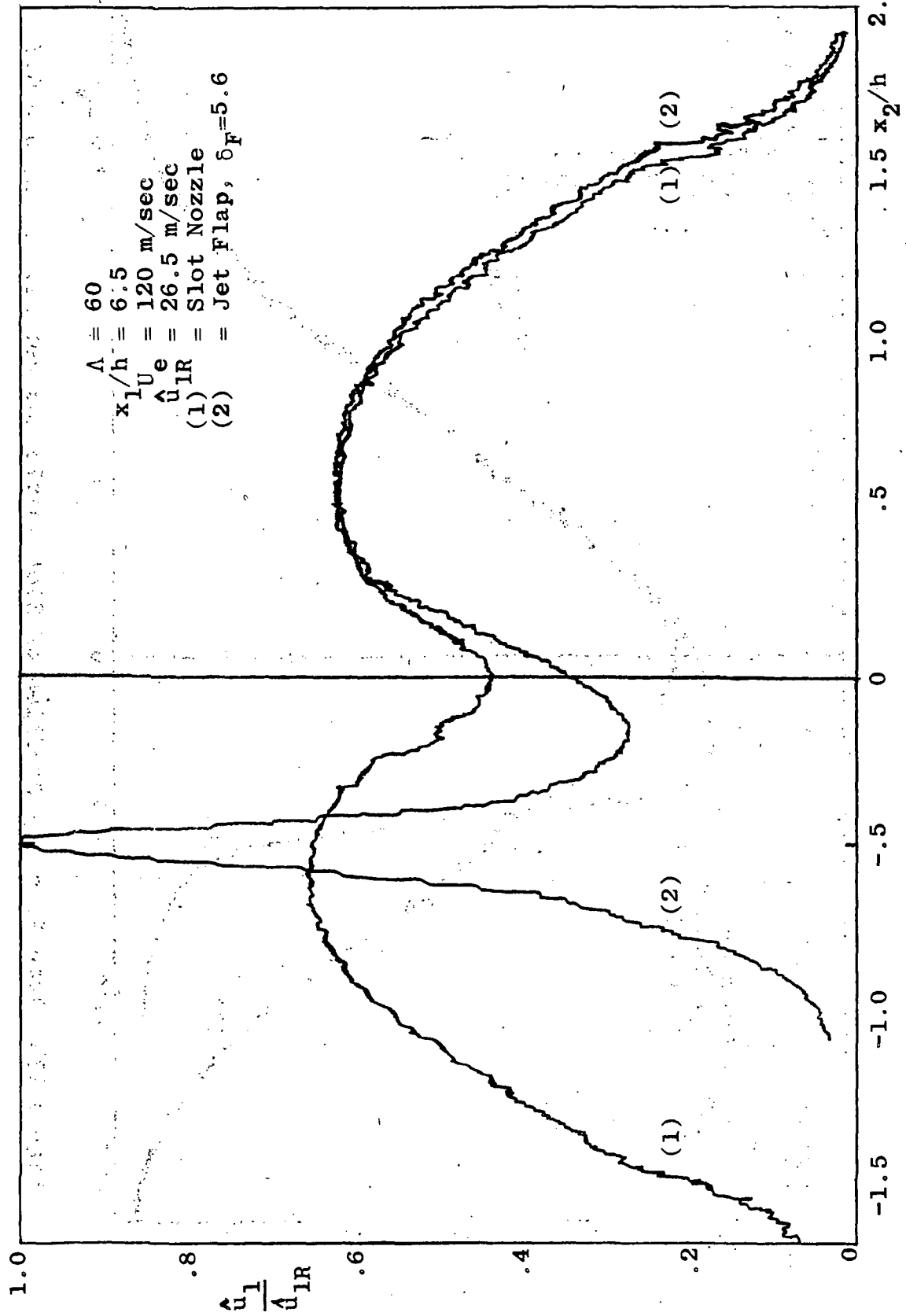
Figure 24. Turbulence Intensity Profiles of Slot Nozzle and Jet Flap at $x_1/h = 6.5$.

53
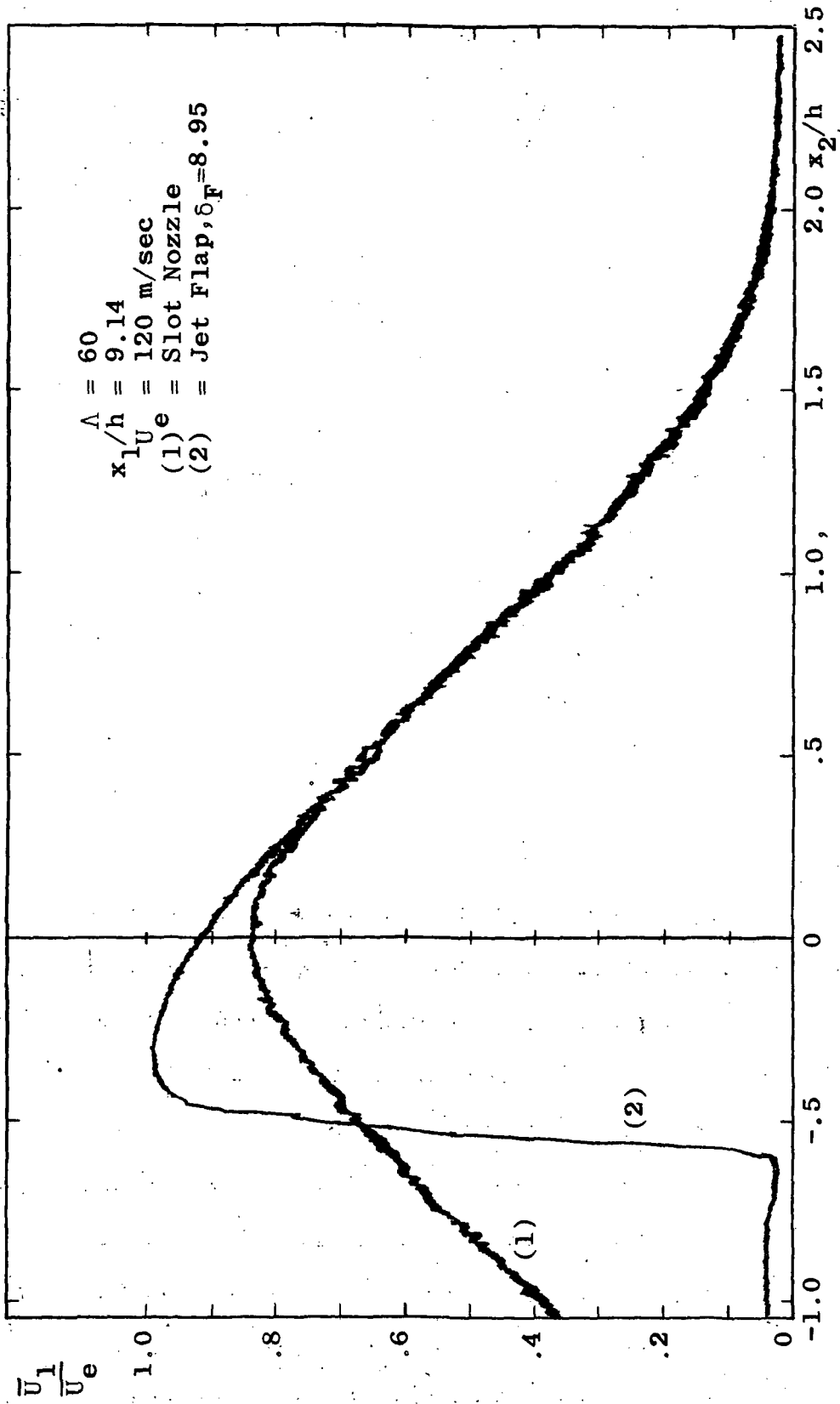
Figure 25. Mean Velocity Profiles of Slot Nozzle and Jet Flap at $x_1/h = 9.14$.

54
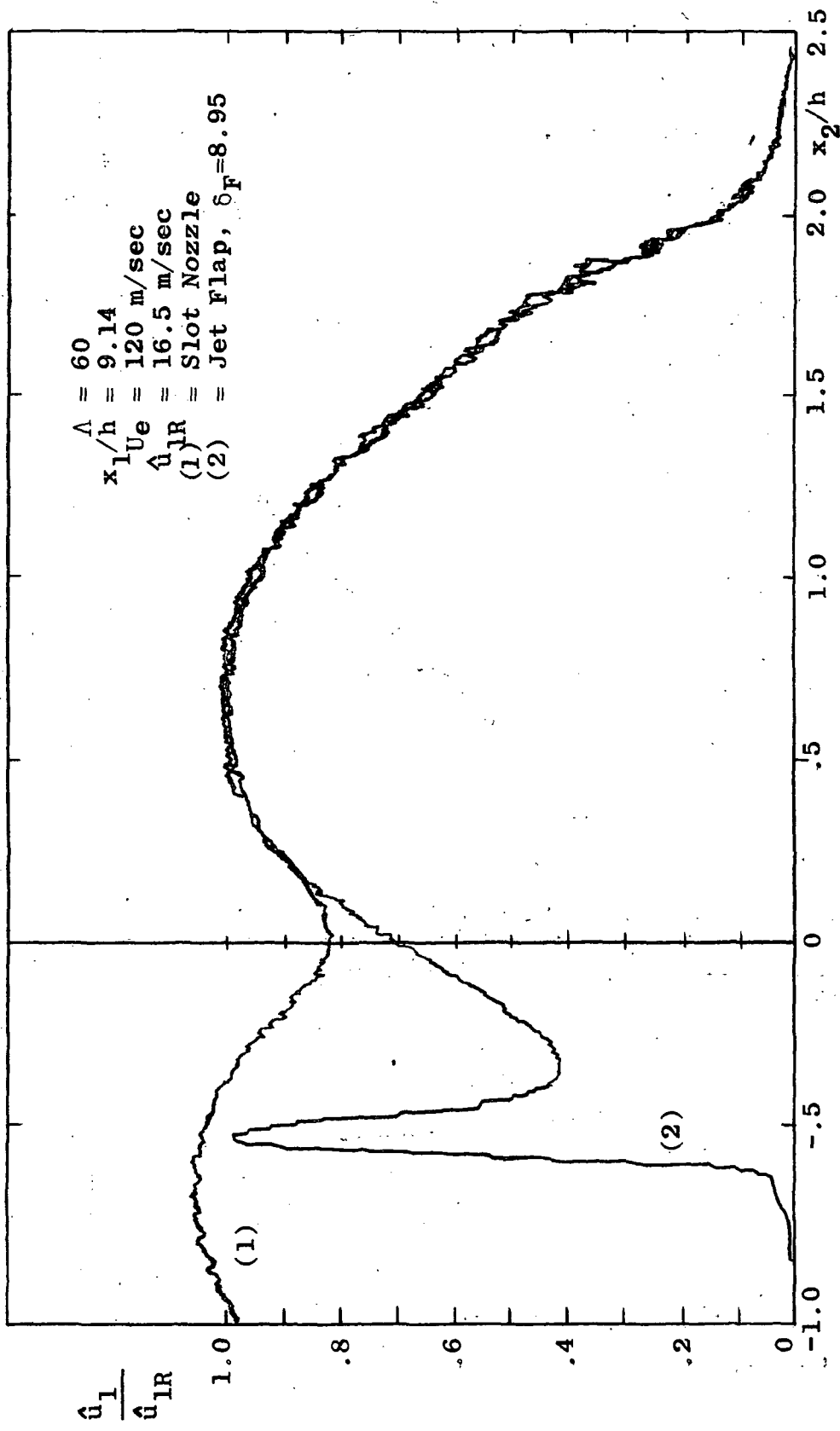
Figure 26. Turbulence Intensity Profiles of Slot Nozzle and Jet Flap at $x_1/h = 9.14$.

55
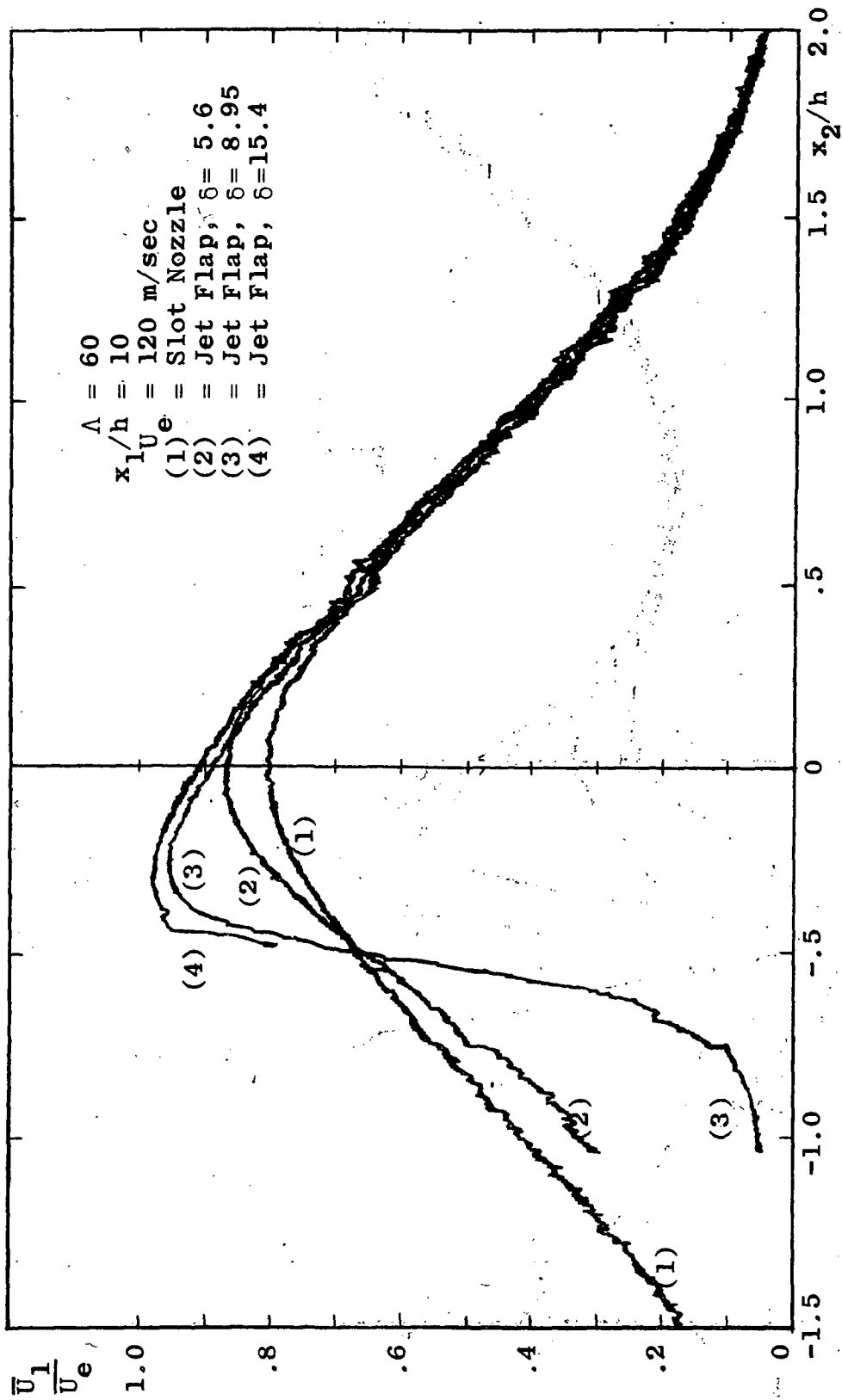
Figure 27. — Mean Velocity Profiles of Slot Nozzle and Jet Flaps at $x_1/h = 10$.

$$\frac{\bar{U}_1}{U_e}$$

$$\Lambda = 60$$
$$x_1/h = 10$$
$$U_e = 120 \text{ m/sec}$$
(1) = Slot Nozzle
(2) = Jet Flap, $\delta = 5.6$
(3) = Jet Flap, $\delta = 8.95$
(4) = Jet Flap, $\delta = 15.4$

x_2/h

56
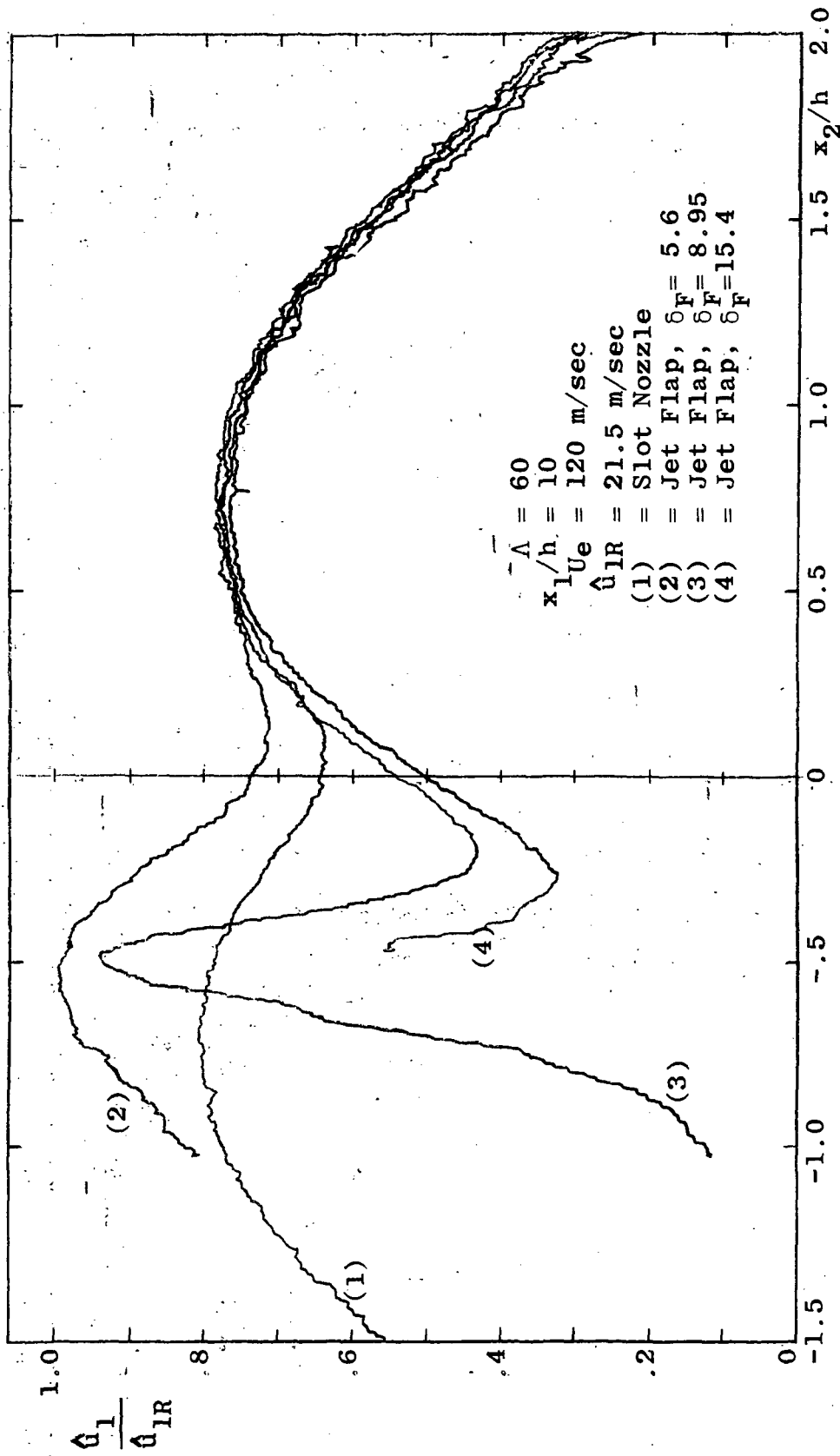
Figure 28. Turbulence Intensity Profiles of Slot Nozzle and Jet Flaps at $x_1/h = 10$.

57

Mean Velocity and Mean Shear

Figure 29 presents the axial mean velocity decay for the slot nozzle and the jet flaps. The downstream extension of the potential core is approximately $\delta_c = 4.75$ for the slot nozzle and $\delta_c = 6.5$, 9.4 and 10 for the jet flaps with $\delta_F = 5.6$, 8.95 and 15.4 respectively. Comparing the data of the slot nozzle with data compiled by Harsha (19), it is noticed that they agree within the usual margin of scatter. The theory predicts that the centerline mean velocity decreases with a slope of 1/2 for the fully developed turbulent plate jet. In Figure 29 this slope is reached at a downstream position of about $x_1/h = 15$.

The decay of the maximum mean velocity is faster for the jet flaps and it seems that the curves merge further downstream. That should be expected, since the influence of the relatively short flaps should level out at some downstream distance.

Figure 30 shows the maximum mean shear (lateral maximum mean velocity gradient), non-dimensionalized by the nozzle height and the exit velocity, versus the downstream position. The curve for the primary mixing region is well substantiated by data of different slot nozzles and jet flaps. Neither the flap length nor the aspect ratio appear to have any influence. The secondary mixing region exhibits large mean velocity gradients. They appear to decrease faster than those of the primary mixing region.

58
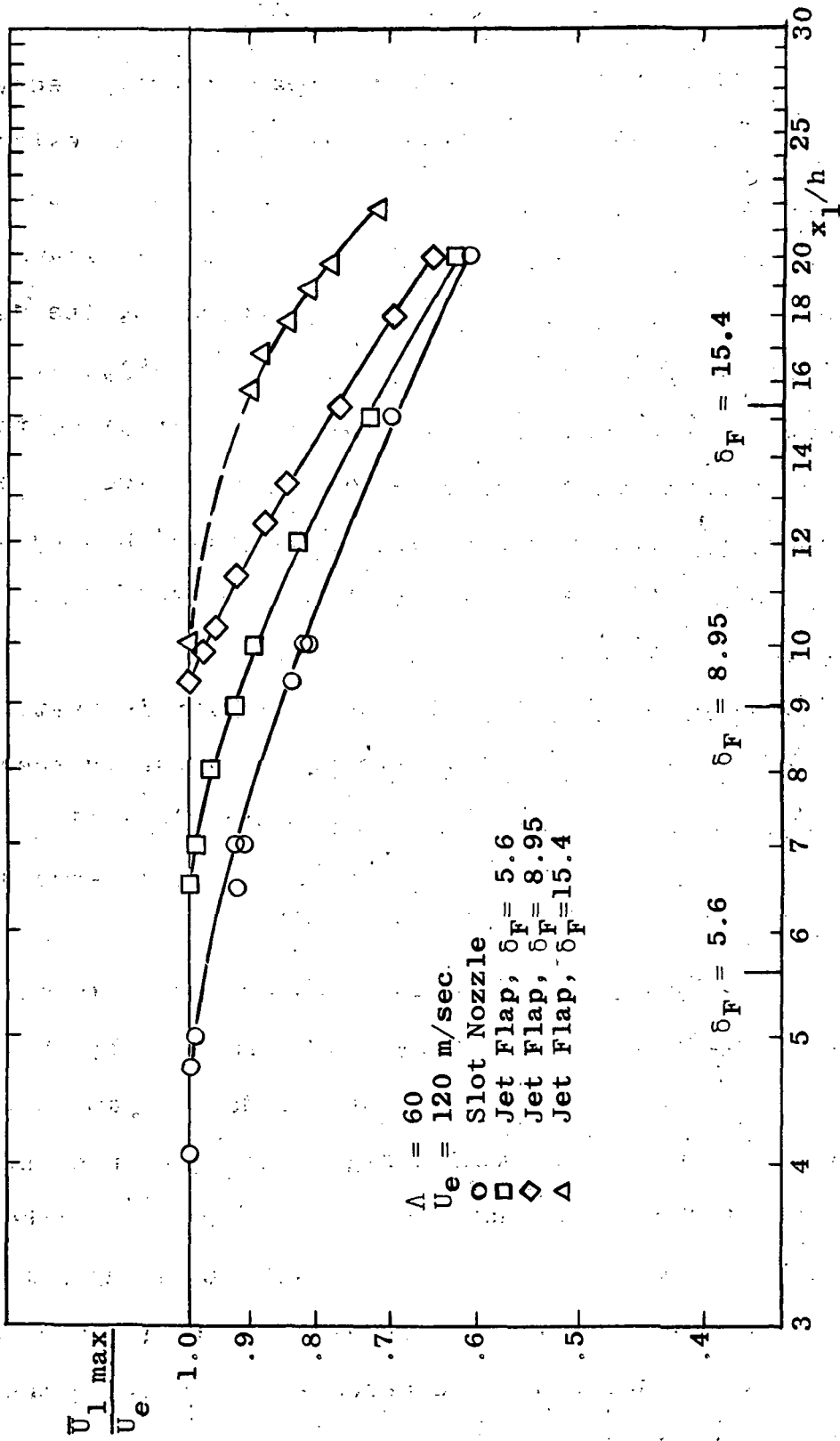
Figure 29. Mean Velocity Decay in Downstream Direction.

$\frac{U_{1 max}}{U_e}$

Λ = 60
U_e = 120 m/sec.
o   Slot Nozzle
□   Jet Flap, δ_F = 5.6
◇   Jet Flap, δ_F = 8.95
△   Jet Flap, δ_F = 15.4

δ_F = 5.6 δ_F = 8.95 δ_F = 15.4

x_1/h
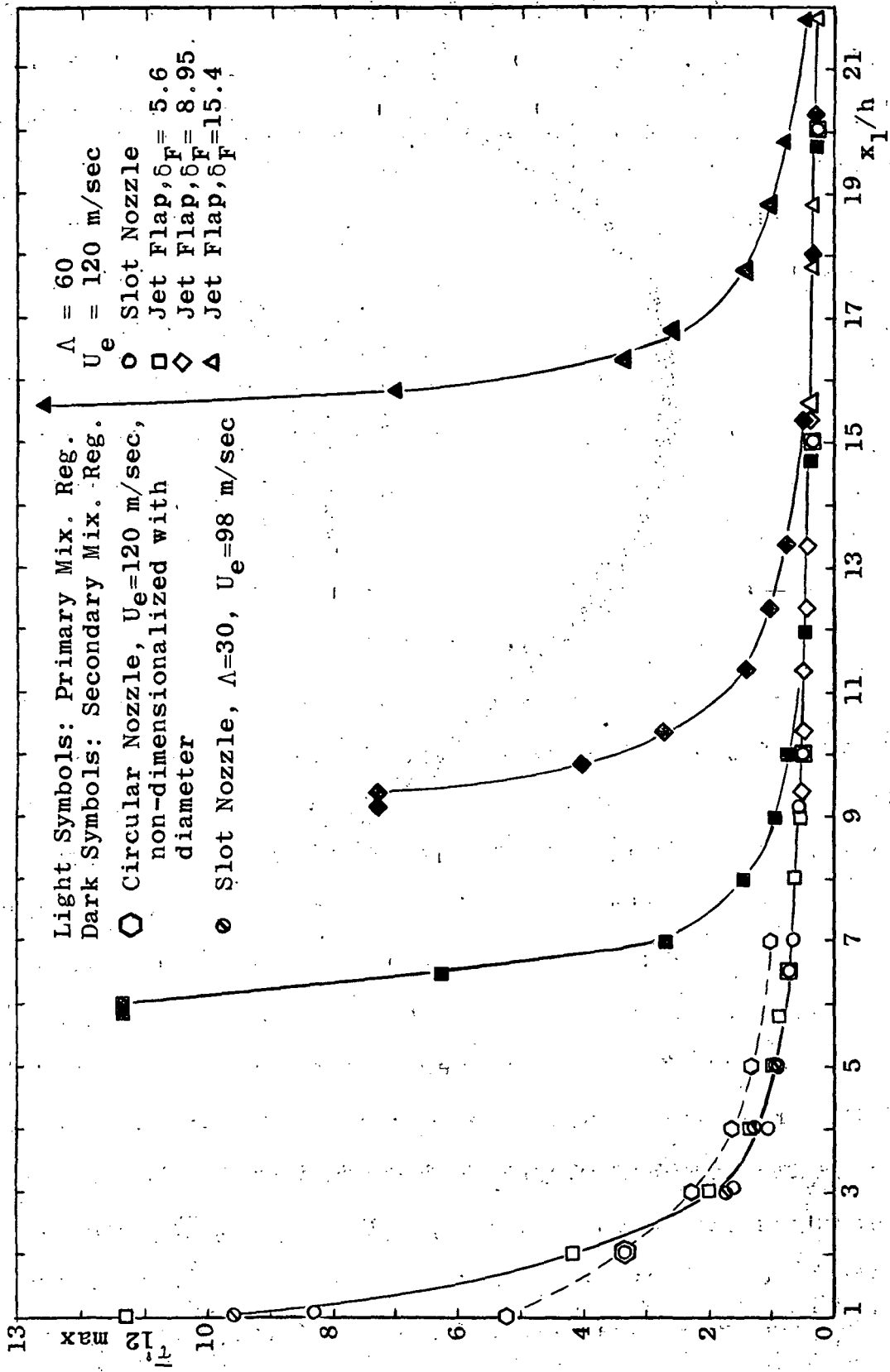
Figure 30. Dimensionless Mean Velocity Gradient Versus Downstream Position.

60

It was expected that the gradient just behind the trailing edge of the flap would decrease with increasing flap length. However, the inner boundary layer has a thin sublayer adjacent to the flap, whose mean velocity gradient is much larger than that of the major part of the inner boundary layer. For the shorter flaps the sublayer is still so thin that the major increase of speed occurs outside of it. For the long flap, however, the major increase in speed occurs in the sublayer and subsequently the maximum mean shear is very large. The same phenomenon was observed behind the trailing edge of a jet flap with an aspect ratio of 30 and a flap length of 16. The magnitude of the non-dimensionalized maximum mean velocity gradient was 14.

If the maximum mean velocity gradients of the secondary mixing region are plotted versus $(x_1 - \ell_F)/h$, the downstream position relative to the trailing edges, the curves coincide fairly well. The non-dimensional mean velocity gradient of the circular reference nozzle is also presented in Figure 30. Except near the nozzle exit, $x_1/d = 1$, the data agree well with those of the slot nozzle.

Figure 31 shows a somewhat arbitrarily defined width of the free mixing layer plotted versus the downstream position. The width presented is defined as the distance between the points having 10% and 90% of $\bar{U}_{1\ max}$. There are two reasons for not using the whole width of the free mixing layer, as it appears in the mean velocity profiles, besides the fact

61
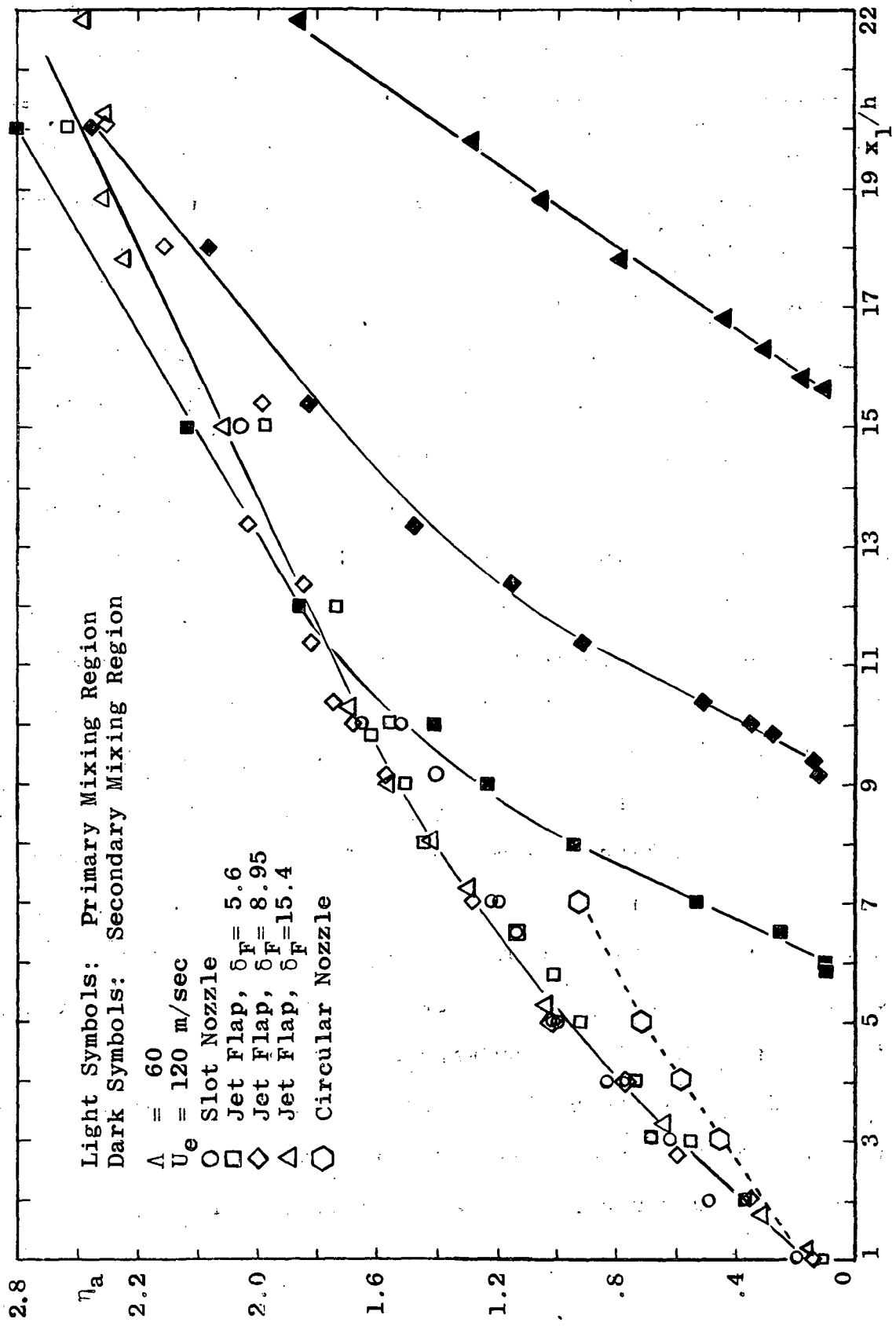
Figure 31. Width of Mixing Region, Obtained from Mean Velocity Profiles, Versus Downstream Position.

62

that it is very difficult to be determined accurately.
First the mean velocity plots do not represent the axial
velocity $\bar{U}_1$ in the low velocity region. They actually repre-
sent $\sqrt{\bar{U}_1{}^2 + \bar{U}_2{}^2}$ since the single hot-wire does not distin-
guish between $\bar{U}_1$ and $\bar{U}_2$. Miller and Comings (27) present
profiles of $\left(\bar{U}_1{}^2 + \bar{U}_2{}^2\right)^{1/2}$ and $\bar{U}_1$-profiles and the two curves
coincide everywhere except for $\bar{U}_1/U_e \leq 0.1$. Since the outer
edge of the jet is of no importance for the generation of
sound, the profiles given here are uncorrected. The second
reason is to present a width which approximately stands for
the width of constant mean shear. Therefore, the rounded
upper portion of the mean velocity graph is cut off.

In the first regime the width of the primary mixing
region increases linearly with increasing downstream position.
This appears to hold, with a smaller slope, also for the re-
gion of established flow. As the plane turbulent jet exhi-
bits self-preservation in both the first regime and the
region of established flow, the width should be proportional
to the downstream position. The width of the secondary mix-
ing region increases linearly, too, but much faster. Further
downstream the rate of increase becomes smaller and appears
to approach that of the primary mixing region.

If the width of the secondary mixing region is plotted
versus the downstream position relatively to the trailing
edges, the curves coincide fairly well (Figure 32).
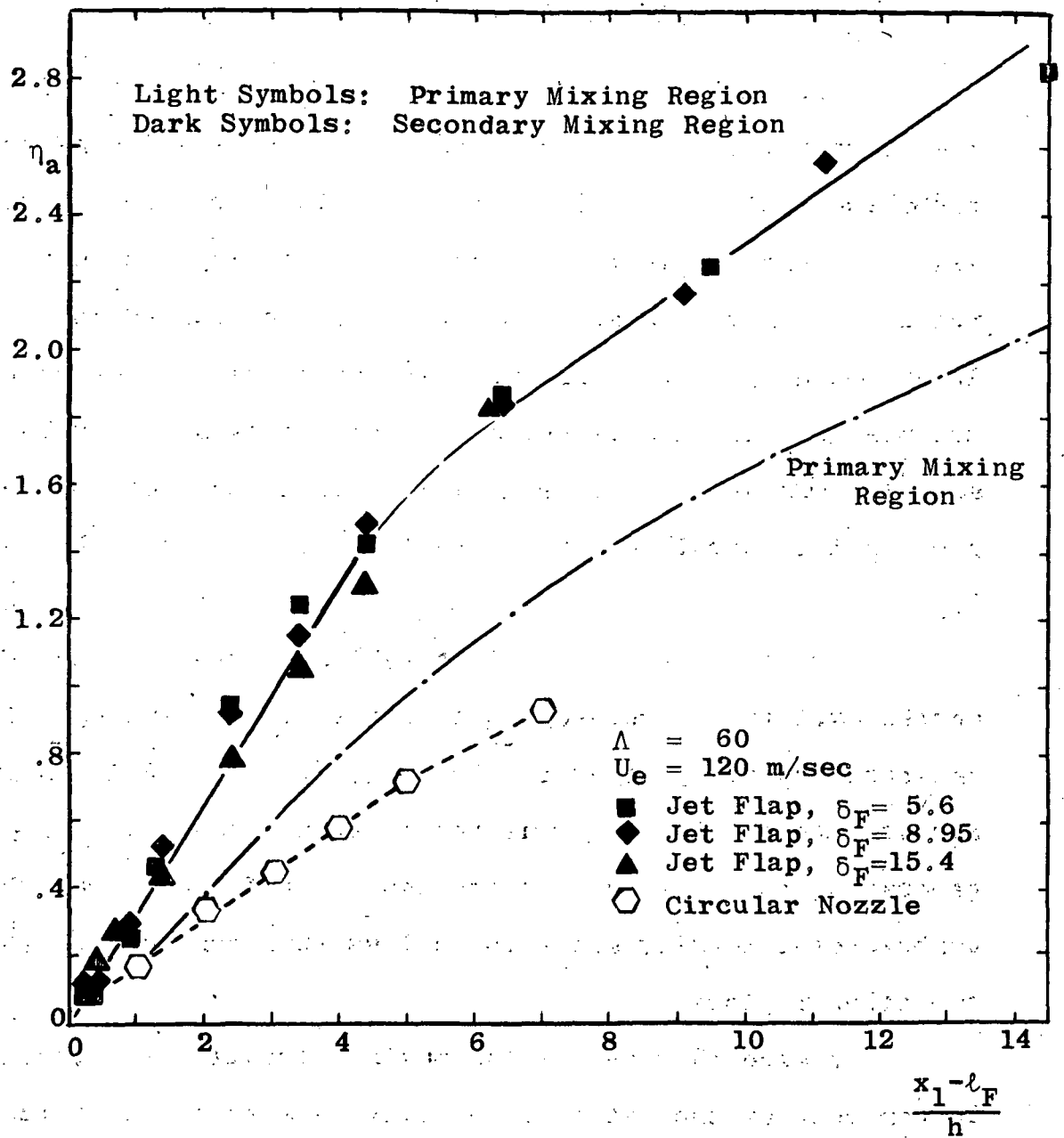
Figure 32. Width of Mixing Region, Obtained from
Mean Velocity Profiles, Versus Relative Downstream Position.

Turbulence Intensity

The turbulence intensity is defined as $I_1 = 100 \; \hat{u}_1/U_e$ (per cent), where $\hat{u}_1$ is the root-mean square value of the turbulence velocity in x_1-direction. The turbulence intensity was measured in the primary and secondary mixing region, but no systematic measurements have been performed in the inner boundary layer. However, in the course of measuring the mean and turbulence velocity profiles by sweeping the hot-wire across the jet, some information was obtained concerning the turbulence intensity level in the inner boundary layer.

As early as one nozzle height downstream of the nozzle exit the turbulence intensity at the outer edge of the inner boundary layer is about 2%, at $x_1/h = 3$ it is 5%, and at $x_1/h = 5$, 8.5%. Thus the inner boundary layer is generating noise as well as the two other regions, but the turbulence intensity seems to be less than observed in the two other regions.

Figure 33 presents the maximum turbulence intensity in per cent of the jet exit velocity as a function of the downstream position. The turbulence intensity of the primary mixing region increases rapidly within a short distance of about two nozzle heights and remains fairly constant over the following twenty nozzle heights. The data seem to indicate that the flap length has a small effect on the intensity in the primary mixing region. However, the tests were performed

in which great care was taken to let the hot-wire probe traverse in the same cross-section and from the same starting point. Then, the well-rounded peak of the intensity profiles of the primary mixing region (Figures 24 and 26, pages 53 and 55) were not altered by adding a flap to the slot nozzle. It is therefore concluded that the flap length has no influence on the turbulence intensity in the primary mixing region.

The turbulence intensity of the secondary mixing region is distinguished by its remarkably high levels. Since the mean shear is considered to be the generator of turbulence, a relationship between them was expected such that the turbulence is high if the mean shear is high. Comparing Figure 30 (page 60) and Figure 33, it is noticed that this relationship holds only for the two shorter flaps, but not for the longest. The longest flap has the highest mean shear and yet the lowest maximum turbulence intensity. It should also be noted that the turbulence intensity levels are generally much higher in the secondary mixing region than in the primary mixing region, although the mean shears are approximately equal in magnitude a short distance beyond the end of the flap.

The growth of the width of the mixing region, measured at one-half of the maximum turbulence intensity, is presented in Figure 34. Again, the width of the secondary mixing region increases faster than the width of the primary mixing region. Coles (5), comparing experimental data of slot and circular nozzles, arrived at the same conclusion.

66

Light Symbols: Primary Mixing Region
Dark Symbols: Secondary Mixing Region

◇ Circular Nozzle, d=20 mm, U_e=120 m/sec
⬡⊕ Circular Nozzle, Reference [34]
○ Slot Nozzle
□ Jet Flap, δ_F= 5.6
◇ Jet Flap, δ_F= 8.95 Λ = 60, U_e = 120 m/sec
△ Jet Flap, δ_F=15.4
◐ Wall Jet, Reference [28]
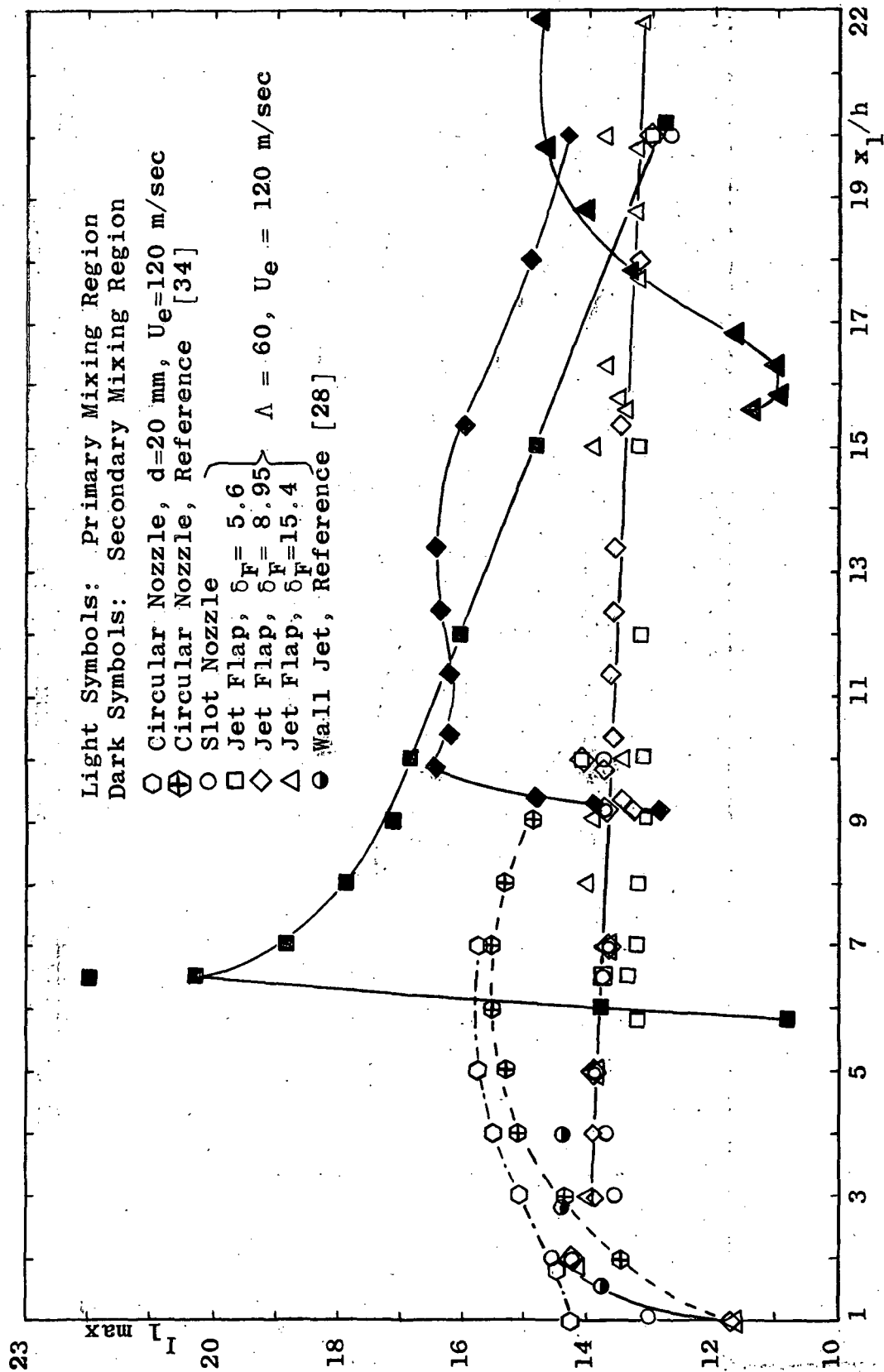
Figure 33.   Maximum Turbulence Intensity Versus Downstream Position.

67
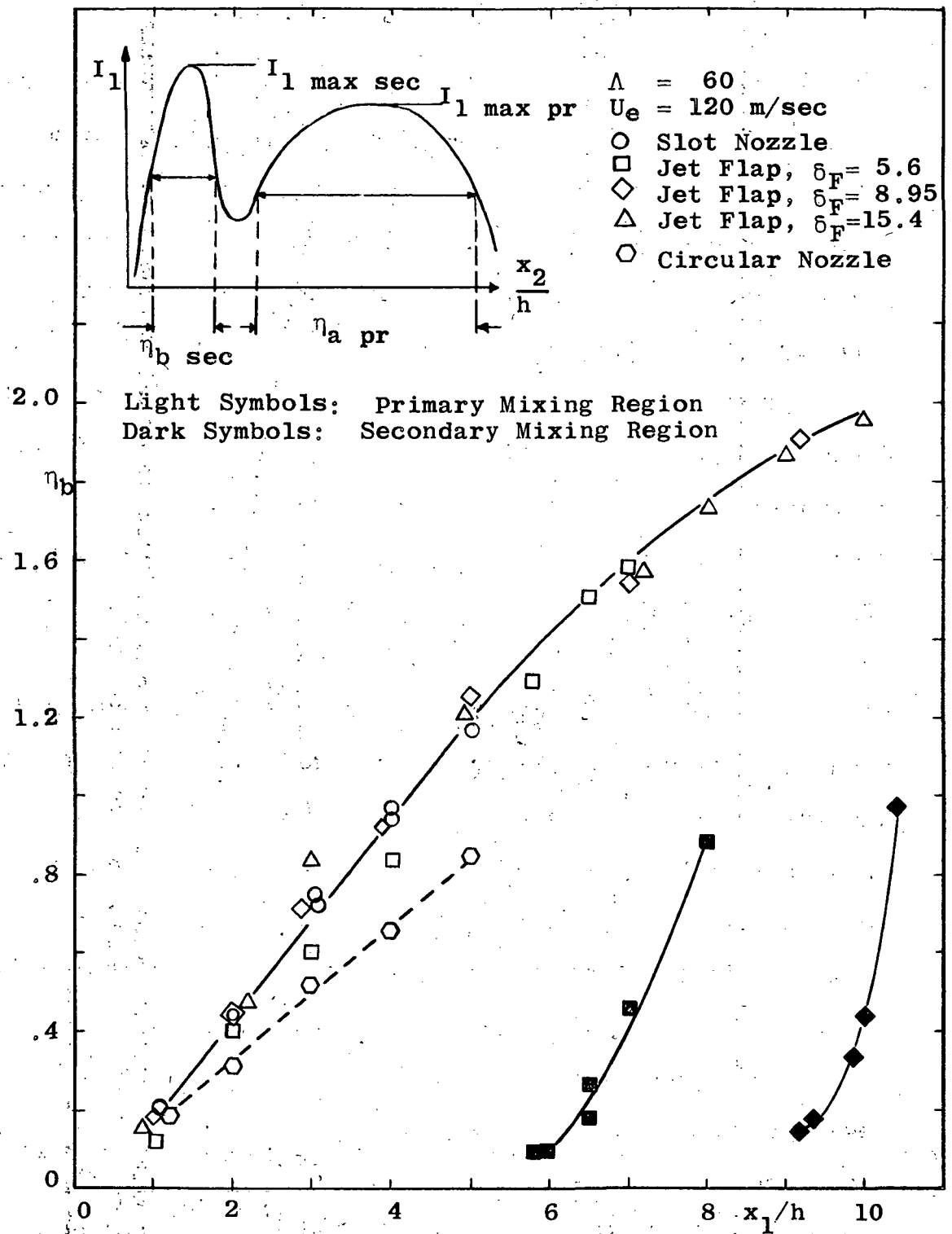
Figure 34. Width of Mixing Region, Obtained from
Turbulence Intensity Profiles, Versus Downstream Position.

The spectra of the hot-wire signal exhibit the same general shape as those of the sound pressures measured in the reverberation chamber. The energy is well-distributed over the whole spectrum, resulting in broad, bell-shaped peaks. From the 1/3 octave spectra the power density spectra were calculated and their spectrum peak frequency, measured at the maximum turbulence intensity, is plotted versus the downstream position in Figure 35. In the primary mixing region the peak frequency decreases monotonically with increasing downstream position and appears to be independent of the flap length. Tests were made leaving the hot-wire probe stationary at the maximum turbulence intensity in the flow field of a slot nozzle at different downstream positions. Different flaps were then added to the slot nozzle and the frequency spectrum for each one obtained. Since the frequency spectrum did not change at all, it is concluded that the spectrum peak frequencies obtained in different tests in the primary mixing region should all coincide with one curve.

The spectrum peak frequencies of the secondary mixing region display some interesting characteristics. First the peak frequency decreases with increasing flap length, or, in other words, the longer the flap the lower the characteristic frequency of the velocity fluctuations in the secondary mixing region. Secondly, for the two shorter flaps the peak of
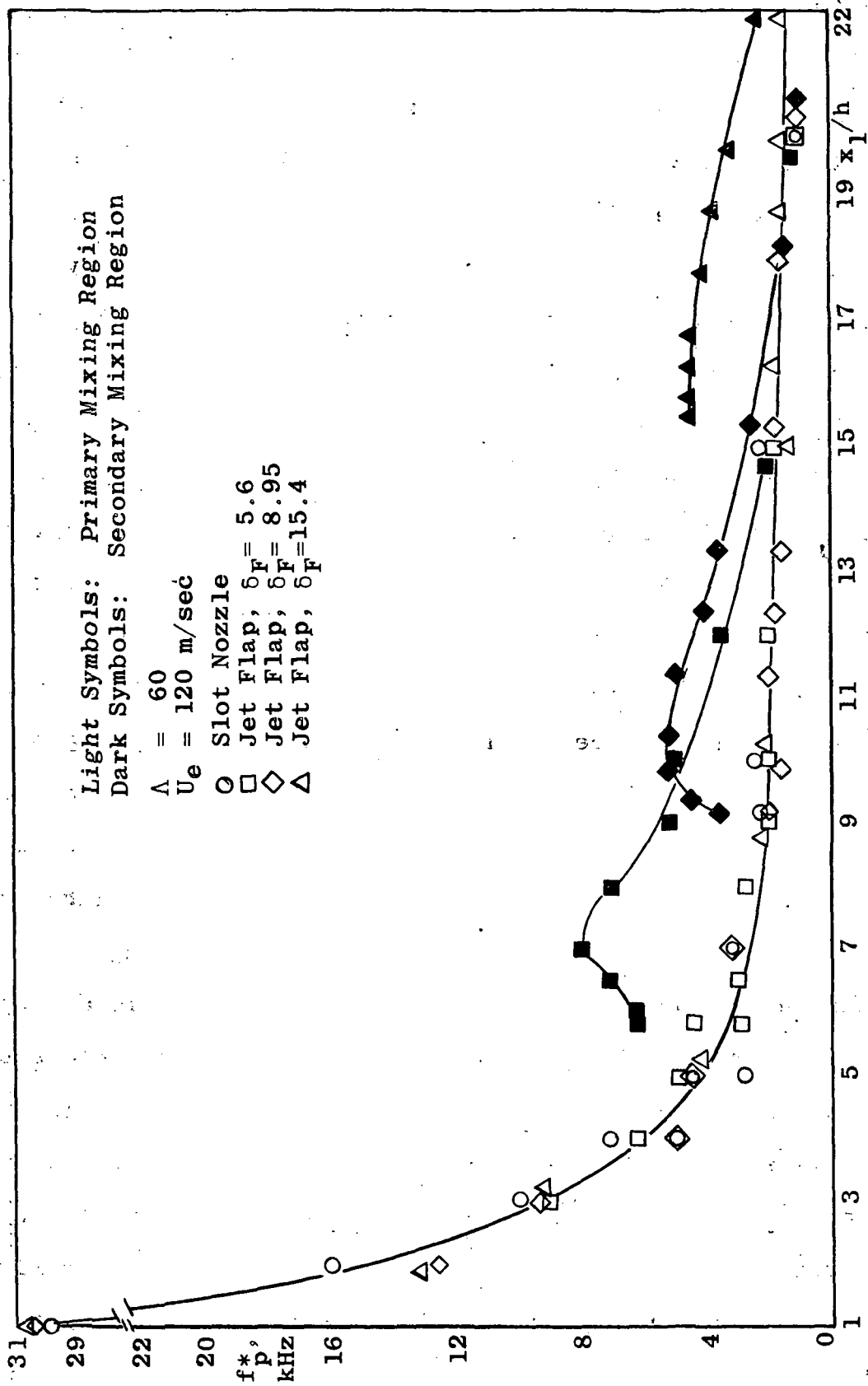
Figure 35. Peak Frequency of Power Density Spectra of Fluctuating Velocity Versus Downstream Position.

70

the curves does not occur directly behind the trailing edge
of the flap at the beginning of the shear layer. Instead,
the peak frequency first increases directly behind the
trailing edge and starts to decrease at some position further
downstream. The rate of decrease is faster than that of the
primary mixing region, and the curves of the secondary mixing
region merge with the curve of the primary mixing region suffi-
ciently for downstream.

The turbulence intensity profiles, shown in Figures 24,
26 and 28 (pages 53, 55 and 57) are broad-band profiles. If
the signal of the laterally traversing hot-wire is sent through
a set of filters, narrow-band turbulence intensity profiles are
obtained. Figures 36 and 37 show graphs of this kind for the
jet flap Λ 60 and δ_F = 8.95, obtained with filter sets of
1% bandwidth. Figure 36 shows the primary mixing region at
x_1/h = 1, Figure 37 the secondary mixing region at the same
downstream distance relative to the trailing edge (the down-
stream position of the primary mixing region in Figure 37 is
x_1/h = 10). Both figures show that no major change of the
distribution occurs if the turbulence intensity is decomposed
into different frequency bands. In Figure 36 the peaks of the
narrow-band turbulence intensity spectra are all at about the
same lateral position, whereas Figure 37 shows that the peaks
move away from the center of the jet with decreasing center
frequency. The same effect should be present also in Figure 36,
but it becomes blurred due to the narrowness of the mixing
region.

71

Figure 36. Narrow Band Turbulence Intensity Profiles of Jet Flap $\Lambda = 60$, $\delta_F = 8.95$ at $x_1/h = 1$.
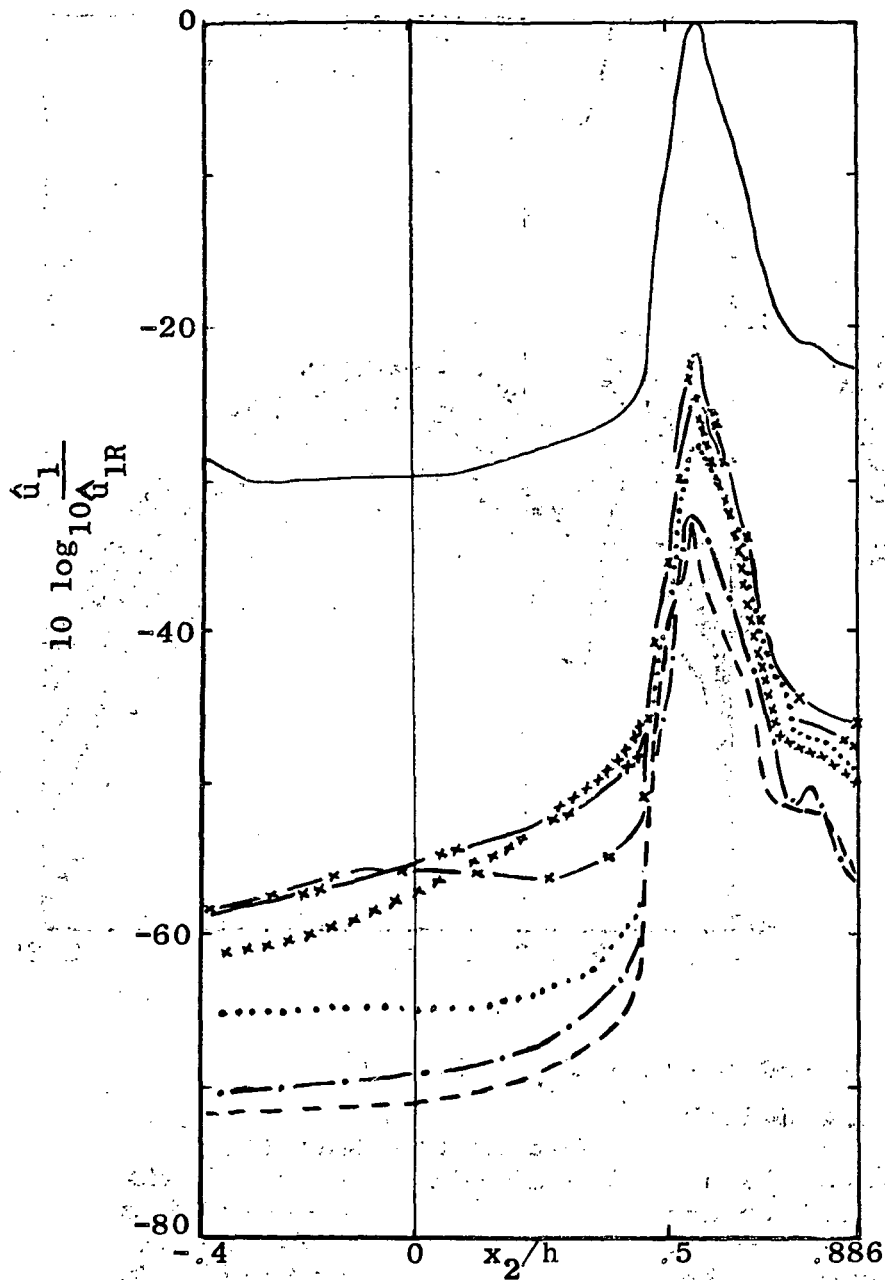
$U_e = 120$ m/sec, $\hat{u}_{1R} = 14$ m/sec
1% Bandwidth

Center Frequencies

——— Linear .1 - 20 kHz   ...... 5 kHz
– – – .5 kHz   —x— 10 kHz
—·— 1.0 kHz   —xx— 15 kHz
—··— 2.0 kHz   xxxx 20 kHz

Figure 37. Narrow Band Turbulence Intensity Profiles of Jet Flap $\Lambda = 60$, $\delta_F = 8.95$ at $x_1/h = 10$.
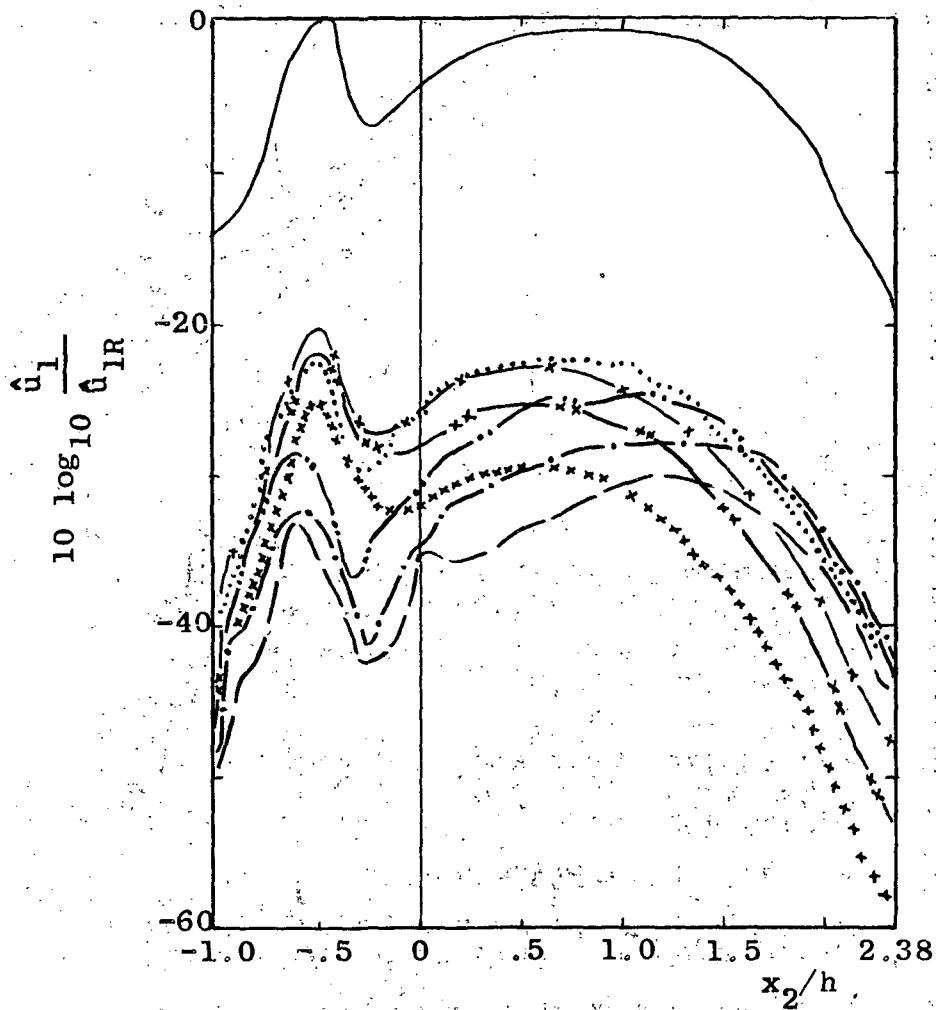
$U_e = 120$ m/sec, $\hat{u}_{1R} = 17$ m/sec

1% Bandwidth

Center Frequencies

——— Linear .1 - 20 kHz ······ 5 kHz
– – – .5 kHz —×— 10 kHz
—·— 1.0 kHz —×x— 15 kHz
—··— 2.0 kHz ×××××20 kHz

Lateral Scale of Turbulence

The definition of the lateral scale of turbulence is

$$L_{x_2} = \int_0^\infty \frac{\overline{u_1\,(x_2)\,u_1\,(x_2 + \Delta\,x_2)}}{u_1\,(x_2)\,.\,u_1\,(x_2 + \Delta\,x_2)}\,dx_2$$

In experimental practice the upper limit is usually the first zero of the integrand. This scale of turbulence is usually associated with the dimension of the largest local eddies. The lateral correlation coefficient

$$g\,(x_2) = \frac{\overline{u_1\,(x_2)\,u_1\,(x_2 + \Delta\,x_2)}}{u_1\,(x_2)\,u_1\,(x_2 + \Delta\cdot x_2)}$$

was measured for the circular reference nozzle, the slot nozzle and the three jet flap configurations, for the latter only in the secondary mixing region. The area under the correlation curve was then determined by graphical integration using the first zero as upper integration limit.

The lateral scale of turbulence, non-dimensionalized by either the nozzle height or the diameter, and plotted against the downstream position, is shown in Figure 38. As the points of the secondary mixing region seem to collapse on one curve, L_{x_2} was also plotted in Figure 39 against the downstream distance relative to the trailing edges. This figure contains also data of the lateral scale of turbulence of a circular nozzle measured by Laurence (20). His data agree very well with the data obtained here for the circular reference nozzle.

74
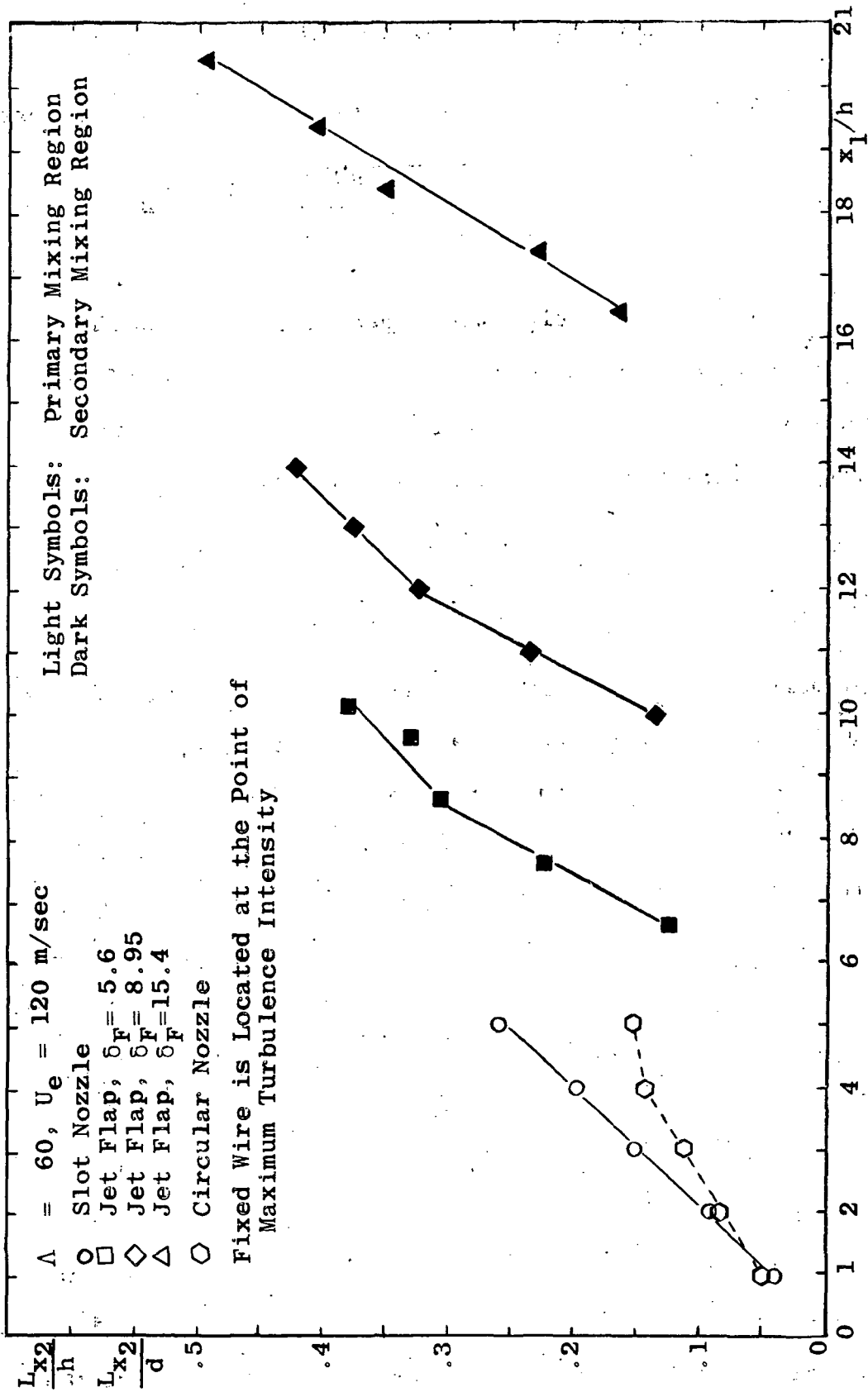
Figure 38. Dimensionless Lateral Scale of Turbulence of Circular Nozzle, Slot Nozzle and Jet Flaps Versus Downstream Position.
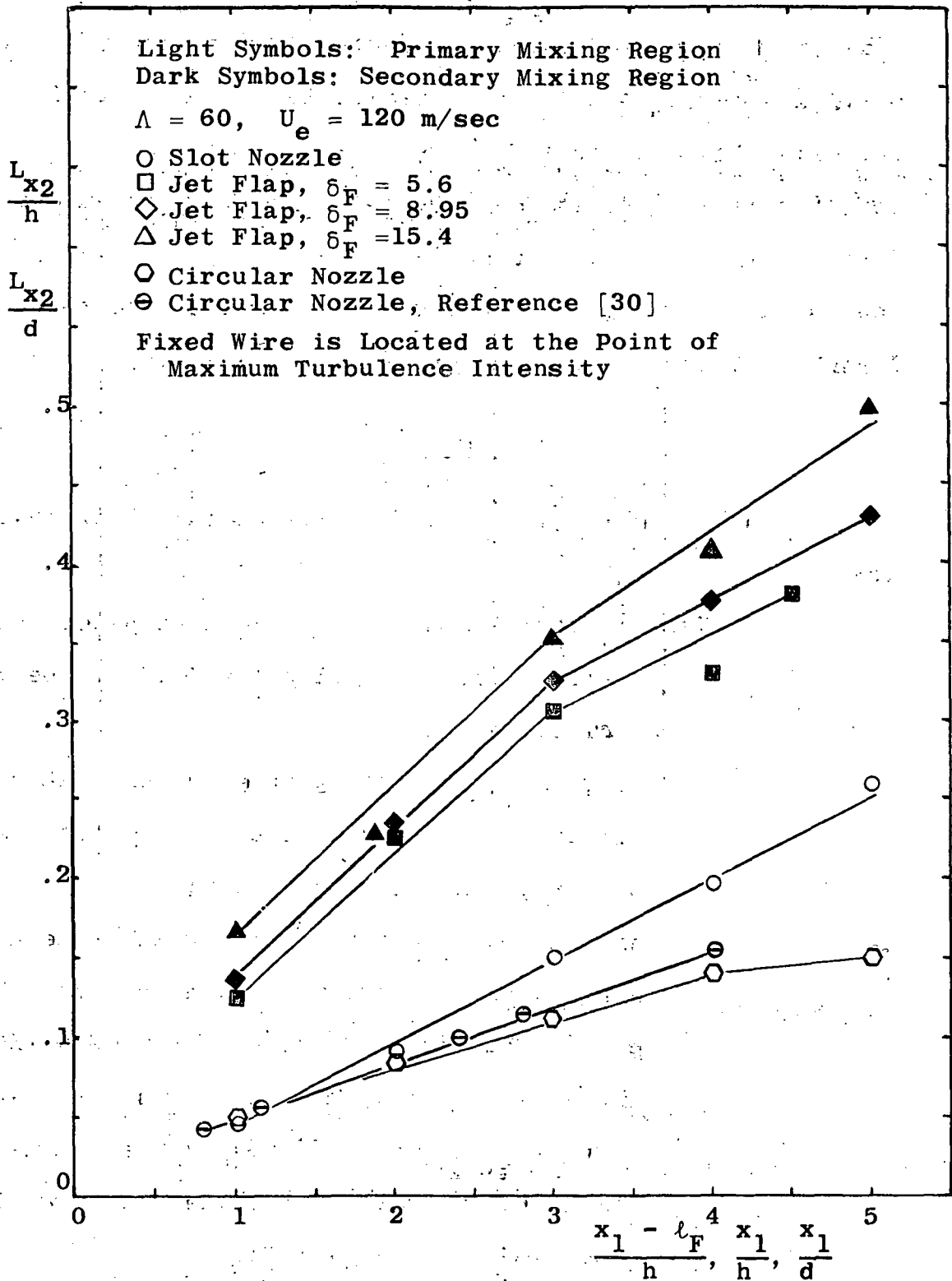
Figure 39. Dimensionless Lateral Scale of Turbulence of Circular Nozzle, Slot Nozzle and Jet Flaps Versus Downstream Position, Relative to ℓ_F/h.

76

The scale of the slot nozzle has a larger slope than that of the circular nozzle, whereas the slope of the lateral scale in the secondary mixing region is considerably larger. There is also a clear influence of the flap length in the way that the lateral scale is directly proportional to the flap length. This is understandable since the lateral scale just behind the trailing edge should be proportional to the boundary layer thickness at the trailing edge of the flap.

Summary

There are two important results of the flow field measurements.

1. Very intense turbulent mixing takes place behind the trailing edge of a flap ($\delta_F \leq 16$). The mixing is characterized by

    a. large mean velocity gradients comparable in magnitude to those of the development stage of the primary mixing region;

    b. high turbulence intensities which exceed those observed in the primary mixing region. The peak turbulence intensity decreases with increasing flap length. The intensity level stays well above the level of the primary mixing region for approximately ten nozzle heights ($\delta_F = 5.6$ and 9);

c. lateral scales of turbulence which are larger
    than those in the primary mixing region at the
    same downstream position relative to the
    trailing edge or nozzle exit respectively.
    The lateral scale of turbulence just behind
    the trailing edge is proportional to the flap
    length;

d. more rapid spread of the turbulent mixing
    region;

e. maximum peak frequencies of the fluctuating
    velocity component which are in the mid-
    frequency range and inversely proportional
    to the flap length.

2. The noise radiated by the primary mixing region is
    practically uninfluenced by a flap ($\delta_F \lesssim 16$).
    This conclusion is drawn from the experimental
    evidence that the central region of the primary
    mixing region in the range $0 < \frac{x_1}{h} \lesssim 10$ (which is
    associated with the bulk of the noise emitted)
    remains practically unchanged in its

    a. mean velocity profile;

    b. mean velocity gradient;

    c. turbulence intensity profile;

    d. power density spectrum (which implies spectrum
        peak frequency).

The fact that the core length increases up to nearly
twice its size in the flow field of a slot nozzle does there-
fore not lead to an increase of the radiated sound power.

CHAPTER IV

ESTIMATE OF THE ACOUSTIC SOURCE STRENGTH DISTRIBUTION

In order to estimate the acoustic source strength distribution within the primary and the secondary mixing region, certain assumptions and simplifications were made:

1. The self-noise was neglected. Lilley (6) showed that in the initial region more than 80% of the noise is due to shear amplified turbulence. The contribution of the self-noise increases gradually and becomes equal to the shear noise contribution in the fully developed flow region. However, since the bulk of the noise is generated within the first six to eight nozzle heights, the self-noise is of less importance. It seems therefore justified to base this estimate on the contribution of the shear noise alone. It was shown by Lilley that the acoustic source intensity of shear amplified turbulence is given by

$$I\ (x_1,\ x_2) = C \left[\frac{\partial \bar{u}_1}{\partial x_2} \right]^6 \overline{u_1^2}\ L^5_{x_1} \qquad (4.1)$$

where L_{x_1} is the longitudinal scale of turbulence and C is a constant of proportionality.

2. As discussed in Chapter III, the primary mixing region is practically uninfluenced by the presence of a flap $(\delta_F \lesssim 16)$. The source strength distribution is calculated for one mixing region of the

slot nozzle and is considered to be the same

for the primary mixing regions of the jet

flaps, irrespective of minor changes near the

x_1-axis.

3. Lilley (6) derived Equation 4.1 assuming homo-

geneous isotropic turbulence. With this assump-

tion, the longitudinal scale of turbulence is

just twice the lateral scale of turbulence. There-

fore it is of no importance which one is used in

Equation 4.1. However, since the longitudinal

scale was not measured in the course of the

experiments, the lateral scale will be used here.

In Appendix D test data for the longitudinal

scale, obtained by Laurence (14), and test data

of the lateral scale of turbulence are compared.

Expressing the acoustic source term of the shear noise,

Equation 4.1, in dimensionless form gives

$$I^* = \frac{I\,h}{U_e^8} = \left(\frac{h}{U_e} \cdot \frac{\partial \bar{U}_1}{\partial x_2}\right)^6 \left(\frac{\hat{u}_1}{U_e}\right)^2 \left(\frac{L_{x_2}}{h}\right)^5 \qquad (4.2)$$

Thus the non-dimensional source term I* consists of the non-

dimensional mean shear, the turbulence intensity and the non-

dimensional scale of turbulence and can be computed from the

results of the data obtained from the measurements described

in Chapter III. The results of this computation is displayed in

Figures 40-43 for both the primary and secondary mixing regions.

80
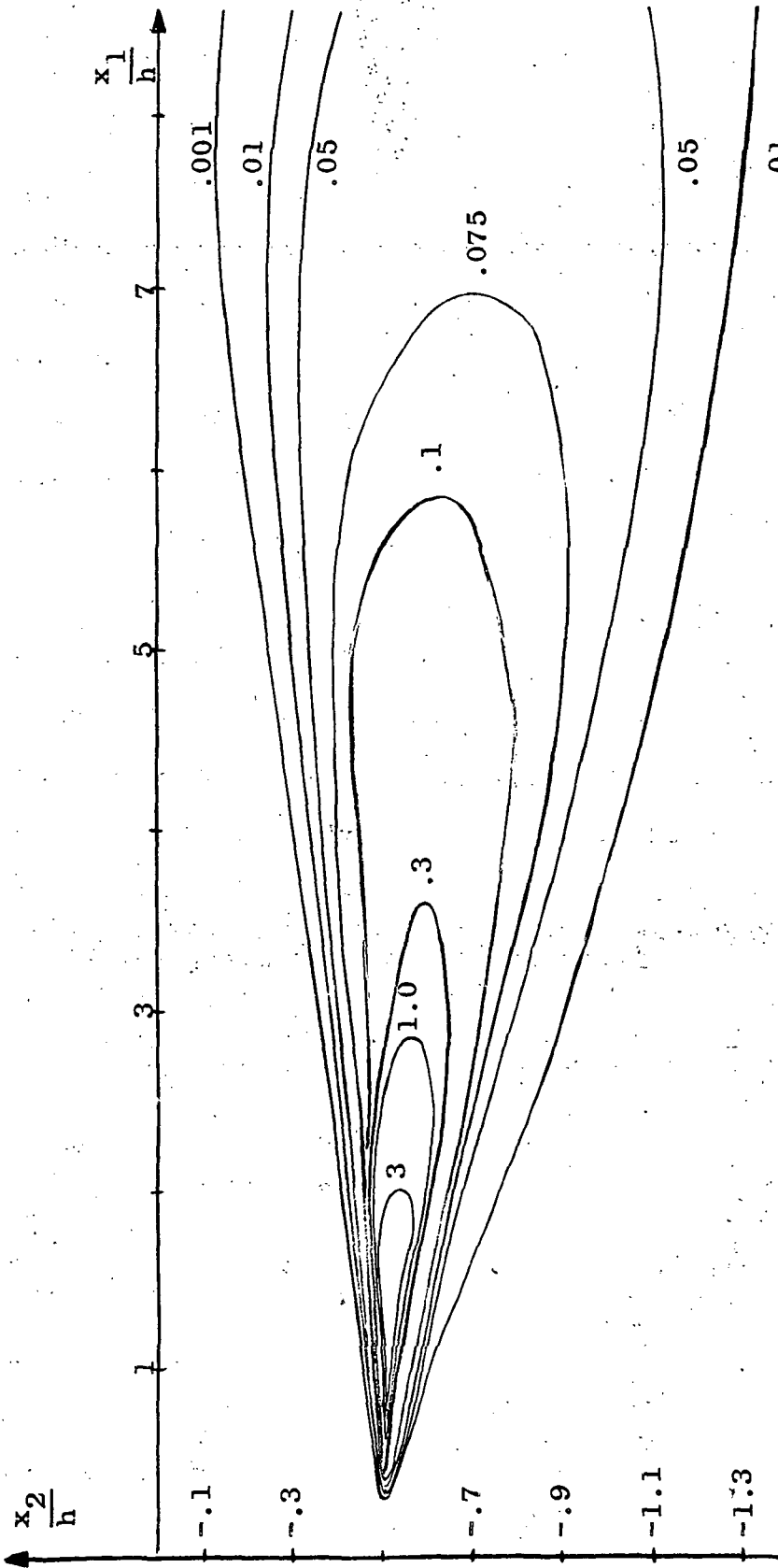
Figure 40. Acoustic Source Strength Distribution for Slot Nozzle $\Lambda = 60$ Versus Downstream Position.
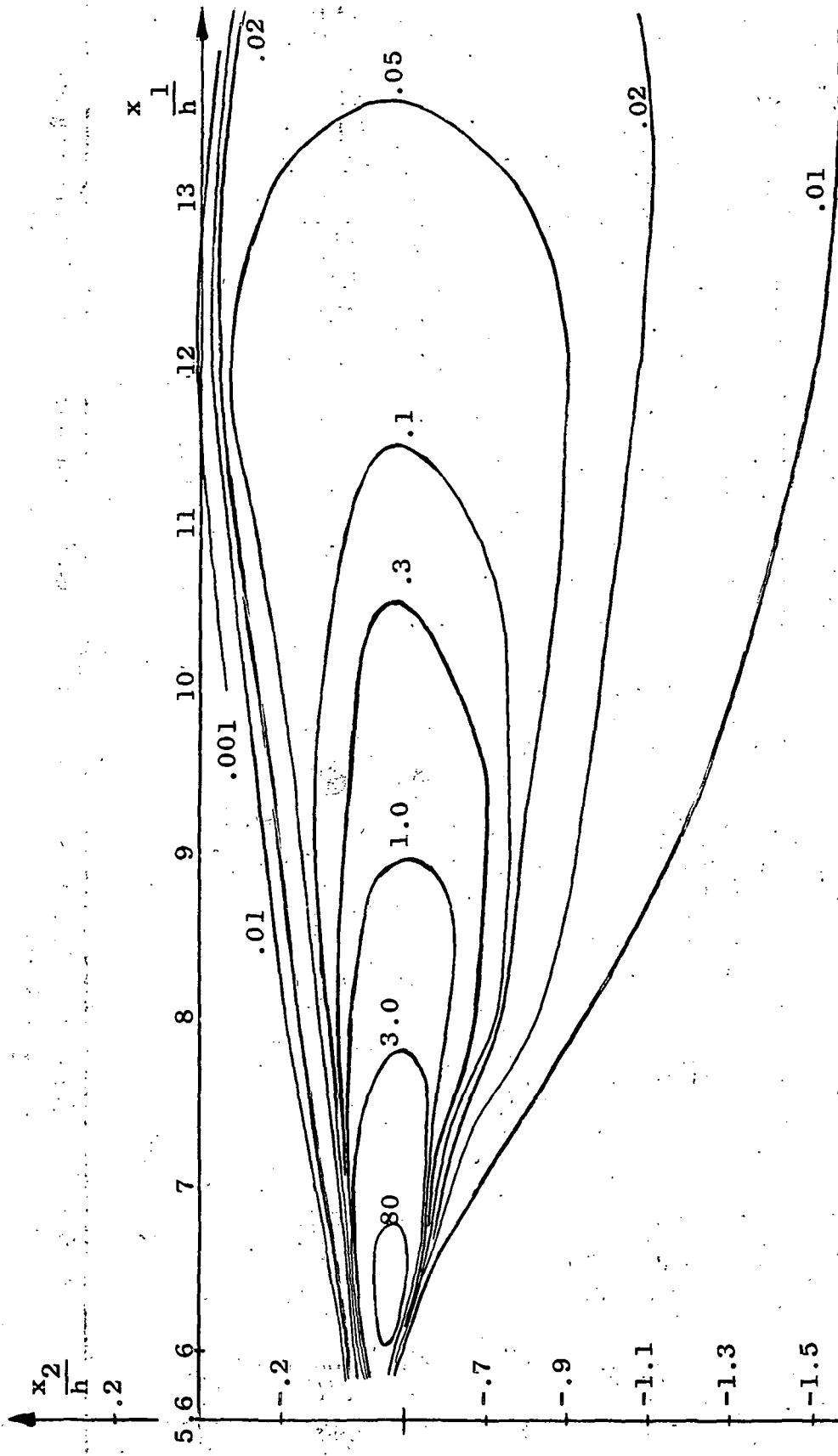
Figure 41. Acoustic Source Strength Distribution in Secondary Mixing Region for Jet Flap $\Lambda = 60$, $\delta_F = 5.6$.
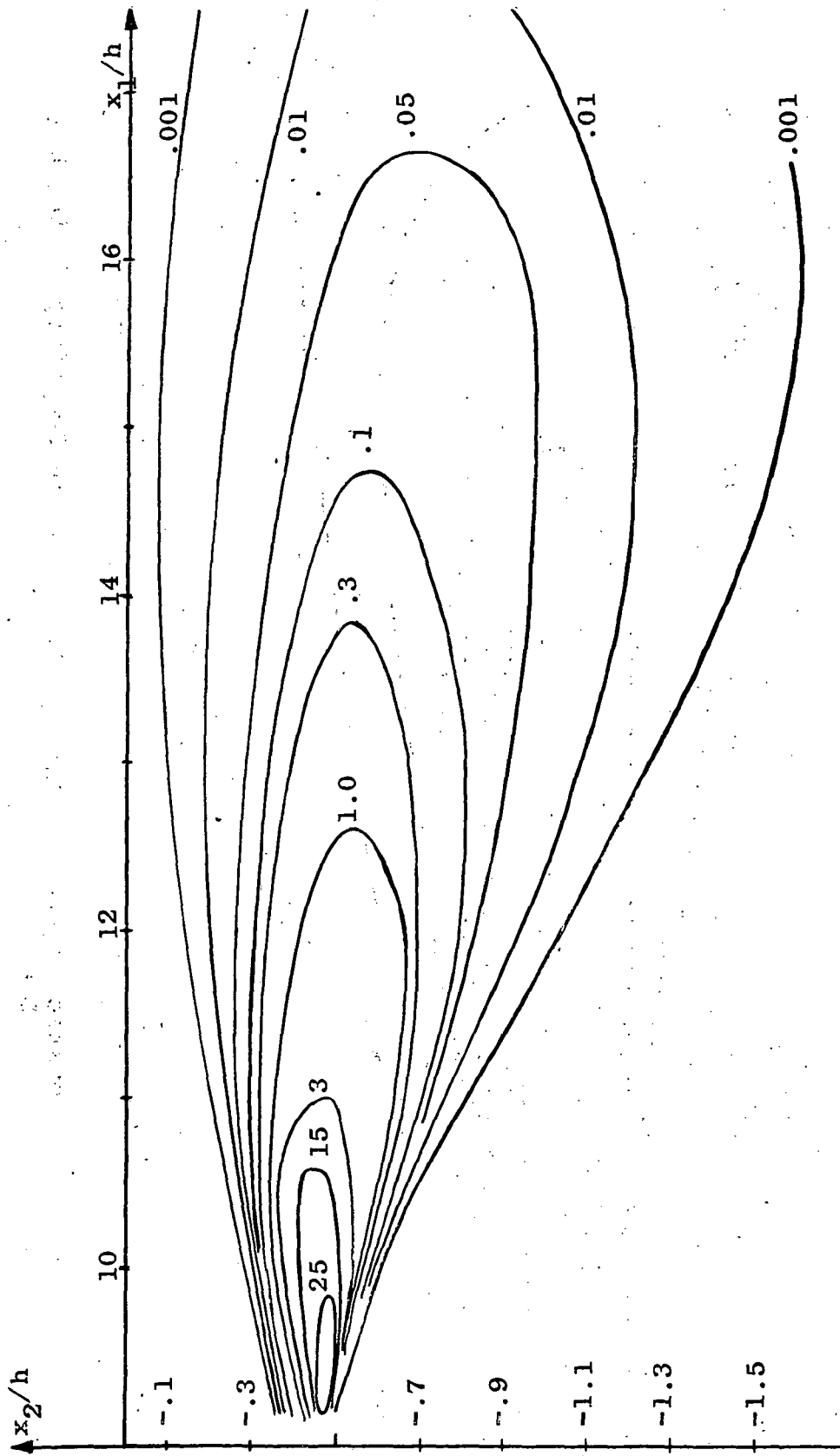
Figure 42. Acoustic Source Strength Distribution in Secondary Mixing Region for Jet Flap $\Lambda = 60$, $\delta_F = 8.95$.

83
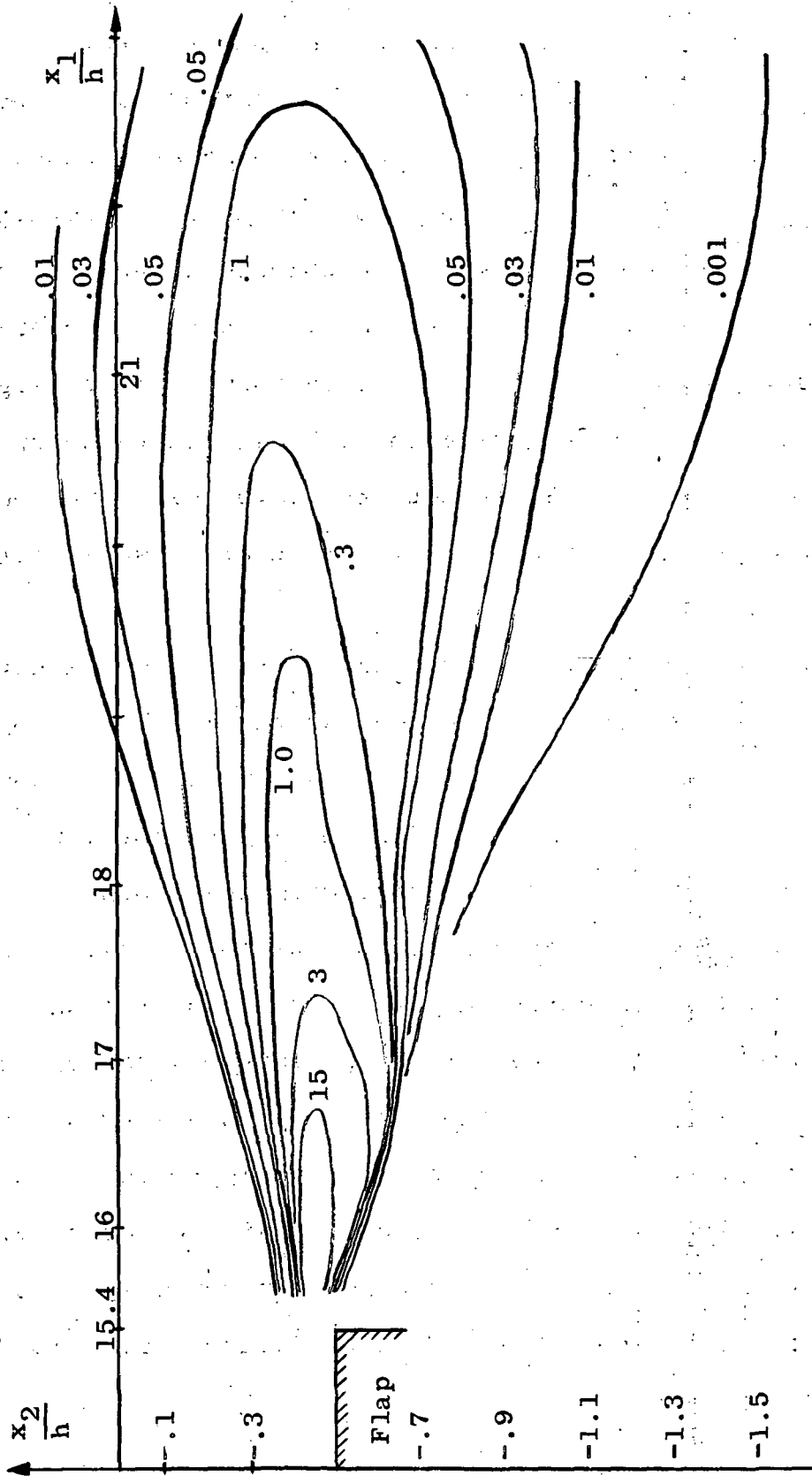
Figure 43. Acoustic Source Strength Distribution in Secondary Mixing Region for Jet Flap $\Lambda = 60$, $\delta_F = 15.4$.

The figures show that the high intensity regions of both mixing zones are fairly small. A comparison with Figure 30 (page 60) indicates that they extend mainly over the region of approximately constant mean shear. Close to the exit of the slot nozzle the acoustic source strength decreases due to the decrease of turbulence intensity and turbulence scale and reaches zero at the point of transition. The acoustic source strength of the secondary mixing region does not have such a "starting point." It can be described as an extension of the inner boundary layer since the equal source strength lines are a continuation of those within the inner boundary layer.

Within the first approximately six nozzle heights downstream of the trailing edge or the nozzle exit, comparable equal source strength lines enclose a larger volume of the turbulent flow in the secondary mixing region than in the primary one. As Equation 4.1 represents the acoustic sound power per unit volume of turbulent flow, this means higher overall sound power output. Further downstream the equal source strength lines of the primary mixing region encircle the larger flow volume, however, the source strength itself has already decreased very much. Approximate integration of the intensity distribution reveals that the secondary mixing region has at least twice the sound power output as the primary mixing region for the flow conditions given in Figures 41-43.

CHAPTER V

CONCLUSIONS AND RECOMMENDATIONS

The overall sound power and the spectrum of the noise of a jet emerging from a slot nozzle over an attached flap (jet flap) were investigated in an experimental survey. The aspect ratios of the slot nozzles were 30, 60 and 120; the non-dimensional flap length varied in the range $4 \leq \delta_F \leq 31.4$;

the flap deflection was zero degrees; and the nozzle exit Mach number was varied between 0.28 and 0.9. All nozzles had the same exit area.

The major conclusions resulting from these investigations are:

1. The overall sound power of a jet flap at higher subsonic Mach numbers increases with the fifth or sixth power of the nozzle exit velocity.

2. The overall sound power of jet flaps increases with increasing flap length, but only up to $\delta_F \stackrel{\circ}{=} 8$, and remains fairly constant thereafter. The increase is proportional to the "wetted area," i.e. the area of the flap in contact with the turbulent flow. This effect occurs at all jet exit velocities but is more pronounced at low Mach numbers.

3. The dominant frequency range of the noise radiated by a jet flap is proportional to the exit velocity, inversely proportional to the flap length,

and independent of the aspect ratio. A different

behavior was only observed for flaps with flap

lengths $\delta_F \lesssim 8$ at an exit Mach number of 0.9.

Furthermore, flow field properties of a jet emerging

from a slot nozzle over a flap attached to the nozzle (jet

flap) were measured. The aspect ratio of the slot was 60;

the non-dimensional flap lengths were $\delta_F = 5.6$, 9 and 15.4;

the flap deflection zero degrees; and the nozzle exit Mach

number 0.35.

The major conclusions reached from these measurements

are:

1. Very intense turbulent mixing takes place in the
   jet flow behind the nozzle orifice, and behind
   the trailing edge of the flaps.

2. An estimate of the acoustic source strength
   distribution of the shear-noise indicates that
   the secondary mixing region generates at least
   twice as much noise as the primary mixing region.

3. In the secondary mixing region the dominant
   frequencies are in the range from 8 to 4 KHz
   and decrease with increasing flap length.

4. The flow field properties in the central region of
   the primary mixing region remain practically un-
   affected by the presence of a flap, at least up
   to $x_1/h = 10$. (The central region is that part of
   the mixing region that has approximately constant
   mean shear and contains the maximum of the turbulence
   intensity.)

Considering both acoustic measurements and the flow field measurements made in this study as well as information obtained from published results of other investigations, several additional general conclusions can be made about the noise generated by jet flaps.

1. Adding a flap to a slot nozzle increases the over-all radiated sound power. The difference between the sound power radiated from a slot nozzle and a jet flap increases up to a flap length $\delta_F = 8$ and thereafter is approximately constant for $8 \leq \delta_F \leq 100$. The total increase is largest for small exit Mach numbers. According to Reference (4) extremely long flaps ($\delta_F = 200$) have less overall radiated sound power than the pure slot nozzle.

2. At higher subsonic Mach numbers ($M_e \gtrsim 0.7$) the jet flap radiates as much overall sound power as a circular nozzle of the same exit area.

3. As the central region of the primary mixing region is uninfluenced by the flap, the total noise radiated from this region is generated mainly within the first 6 to 8 nozzle heights from the exit and is independent of the presence of a flap.

4. A flap prevents the development of a free turbulent mixing layer on one side of the slot nozzle. However, a free turbulent mixing layer will develop behind the trailing edge of the flap instead. This secondary mixing region generates at least as much noise as the first one would have generated.

88

5. The spectrum peak frequency of the radiated overall noise from a jet flap appears to be predominantly determined by the frequencies of the turbulent velocity fluctuations in the region just behind the trailing edge.

6. A part of the radiated noise is wall boundary layer noise. This is concluded from the dependence of the overall sound power on the wetted area of the flap. The difference in proportionality of the overall sound power on the nozzle exit velocity, $P_{slot\ nozzle} \sim U_e^7$ to U_e^8 compared to $P_{jet\ flap} \sim U_e^5$ to U_e^6, suggests furthermore that the additional wall boundary layer noise is mainly dipole noise. Both Grosche (11) and Hayden (12) reported strong dipole noise sources in the flow field of a jet flap.

Therefore, jet flaps except those with extremely long flaps, can be expected to be more noisy than pure slot nozzles. Sizable reductions of the overall radiated sound power will only be accomplished, if the noise generation in the secondary mixing region can be suppressed to a large extent. However, even if the radiated sound power is large, the jet flap can be acoustically advantageous due to the directivity of its sound radiation. Since the directivity depends to a large extent on the effectiveness of the flap as an acoustic reflector, the secondary mixing region is again of primary importance.

As long as this region radiates a sizable portion of the overall sound power, the directivity pattern of the jet flap will not differ very much from the directivity pattern of a slot nozzle. Therefore, since any reduction of its noise generation will not only reduce the overall radiated power, but improve at the same time the directivity pattern of the jet flap.

A device which might have some potential in this respect is the "Coanda-Surface" (Figure 44). The principle is that the curved flap surface with the jet attached will increase the width of the free mixing region more rapidly than a straight flap. Consequently the mean velocities and the mean shear will decrease at an increased rate which in turn results in smaller mean shear and turbulence intensity in the secondary mixing region. Although this is known from related investigations, the quantitative effects will have to be investigated.
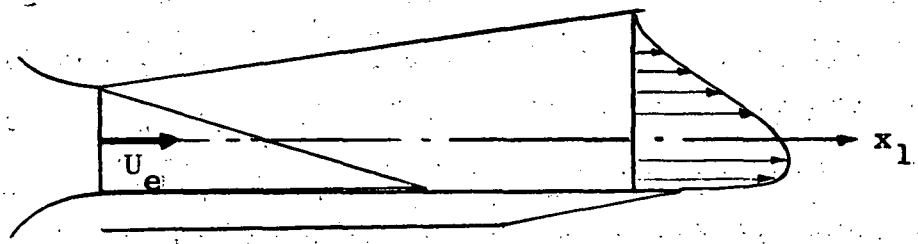
(a) Jet Flap Tested in this Study.
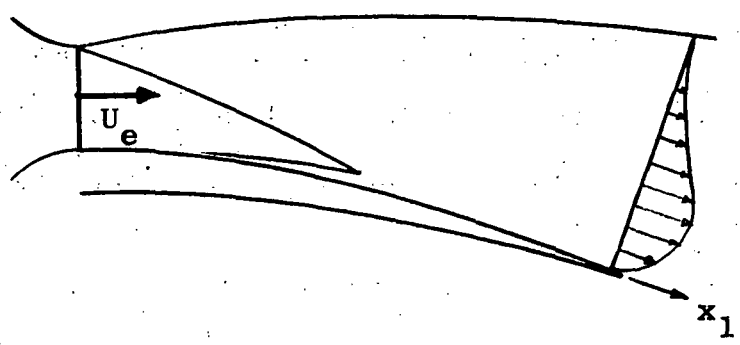
(b) Coanda Surface.

Figure 44. Coanda Surface Versus Jet Flap with Plane Flap.

LIST OF REFERENCES

1. Siddon, T. E. "Jet Noise Research - Progress and Prognosis," Inter-Noise 72 Proceedings, International Conference on Noise Control Engineering, Washington, D. C. October 1972.

2. Dorsch, R. G., E. A. Kresja and W. A. Olsen. "Blown Flap Noise Research," American Institute of Aeronautics and Astronautics, Paper No. 71-745, June 1971.

3. Ciepluch, C. C. "Design Trends for Noise Control for Aircraft Power Plants - The NASA Quiet Engine," Inter-Noise 72 Proceedings, International Conference on Noise Control Engineering, Washington, D. C. October 1972.

4. Maglieri, D. J. and H. H. Hubbard. "Preliminary Measurements of the Noise Characteristics of some Jet-Augmented Flap Configurations," National Aeronautics and Space Administration Memorandum 12-4-58L, January 1959.

5. Coles, W. D. "Jet-Engine Exhaust Noise from Slot Nozzles," National Aeronautics and Space Administration Technical Note D-60, Lewis Research Center, September 1959.

6. Lilley, G. M. "On the Noise from Air Jets," Aeronautical Research Council No. 20376, September 1958.

7. Lighthill, M. J. "On Sound Generated Aerodynamically - I. General Theory," Proceedings of the Royal Society of London, Series A, Volume 211, May 1952.

8. Grosche, F. R. "Zur Schallerzeugung durch einen turbulenten Luftstrahl uber einer endlich grossen ebenen Platte," Mitteilungen aus dem Max-Planck-Institut für Strömungsforschung und der Aerodynamischen Versuchsanstalt, Selbstverlag Max-Planck-Institut für Strömungsforschung und Aerodynamische Versuchsanstalt, Göttingen, Nr. 45, 1969.

9. Hayden, R. E. "Sound Generation by Turbulent Wall Jet Flow over a Trailing Edge," Master's Thesis, Purdue University, August 1969.

10. Powell, A. "On the Aerodynamic Noise of a Rigid Flat Plate Moving at Zero Incidence," Journal of the Acoustical Society of America, Volume 31, No. 12, December 1959.

11. Harper, W. L. "An Experimental Study of Noise Produced by Jet-Flap Type Nozzles," Master's Thesis, The University of Tennessee Space Institute, Tullahoma, Tennessee, March 1971.

12. Gruschka, H. D. "On Noise from Jet Flaps and Slotted Jets," National Aeronautics and Space Administration, Paper presented at a meeting on Aeronautical Fluid Mechanics, Washington, D. C., June 1971.

13. Gruschka, H. D. and G. O. Schrecker. "Aeroacoustic Characteristics of Jet-Flap Type Exhausts," American Institute of Aeronautics and Astronautics Paper No. 72-130, January 1972.

14. Albertson, D. L., Y. B. Dai, R. A. Jensen and H. Rose. "Diffusion in Submerged Jets," Transactions of the American Society of Civil Engineers, Volume 115, Paper No. 2409, December 1950.

15. Van der Hegge Zijnen, B. G. "Measurement of the Velocity Distribution in a Plane Turbulent Jet of Air," Applied Scientific Research, Section A, Volume 7, No. 4, April 1958.

16. Sunyach, M. and J. Mathieu. "Zone de mélange d'un jet plan - Fluctuations induites dans le cône a potentiel-intermittence," International Journal of Heat and Mass Transfer, Volume 12, Part 1, October 1957.

17. Miller, D. R. and E. W. Comings. "Statistic Pressure Distribution in the Free Turbulent Jet," Journal of Fluid Mechanics, Volume 3, Part 1, October 1957.

18. Liepmann, H. W. and J. Laufer. "Investigation of Free Turbulent Mixing," National Advisory Committee for Aeronautics, Technical Note 1257, August 1949.

19. Harsha, T. P. "Free Turbulent Mixing: A Critical Evaluation of Theory and Experiment," Ph.D. Dissertation, The University of Tennessee Space Institute, Tullahoma, Tennessee; December 1970.

20. Laurence, J. C. "Intensity, Scale and Spectra of Turbulence in Mixing Region of Free Subsonic Jet," National Advisory Committee for Aeronautics, Report 1292, April 1956.

21. Brüel & Kjaer Instruments, Inc. "Audio Frequency Spectrometer Type 2112," Instructions and Applications, Copenhagen, Denmark, July 1967.

22. Bendat, J. S. and A. G. Piersol. "Random Data: Analysis and Measurement Procedures," New York: Wiley-Interscience, 1971.

23. Hinze, J. O. "Turbulence," New York: McGraw-Hill Book Company, Inc., 1959.

24. Davies, P. O. A. L., M. J. Barratt and M. J. Fisher. "Turbulence in the Mixing Region of a Round Jet," Journal of Fluid Mechanics, Volume 15, March 1963.

APPENDIX A

ACOUSTIC MEASUREMENTS: TEST SET-UP AND TEST FACILITY

Air Supply System

A schematic of the air supply system is shown in Figure 45, a sketch of the plenum chamber in Figure 46. Using one-dimensional isentropic flow relations, the conditions in the exit area are fully determined if the total pressure and the total temperature in the plenum chamber are measured and the pressure in the reverberation chamber is known. The latter is determined by measuring the barometric pressure and the pressure difference between the barometric and the reverberation chamber pressure.

Nozzles and Flaps

Only convergent nozzles with a constant exit area of $314.15 \ mm^2$ were used. Except for the slot height h and the slot width w the three slot nozzles are all alike. The flaps which were attached to the nozzles, differed only in the flap length ℓ_F. Figure 47 shows a schematic of a slot nozzle with an attached flap. In this study slot nozzles and flaps of the following dimensions have been used:

1. Nozzles

   Slot Nozzle $\Lambda = 30$:   h =   3.2 mm

   w =   95.8 mm
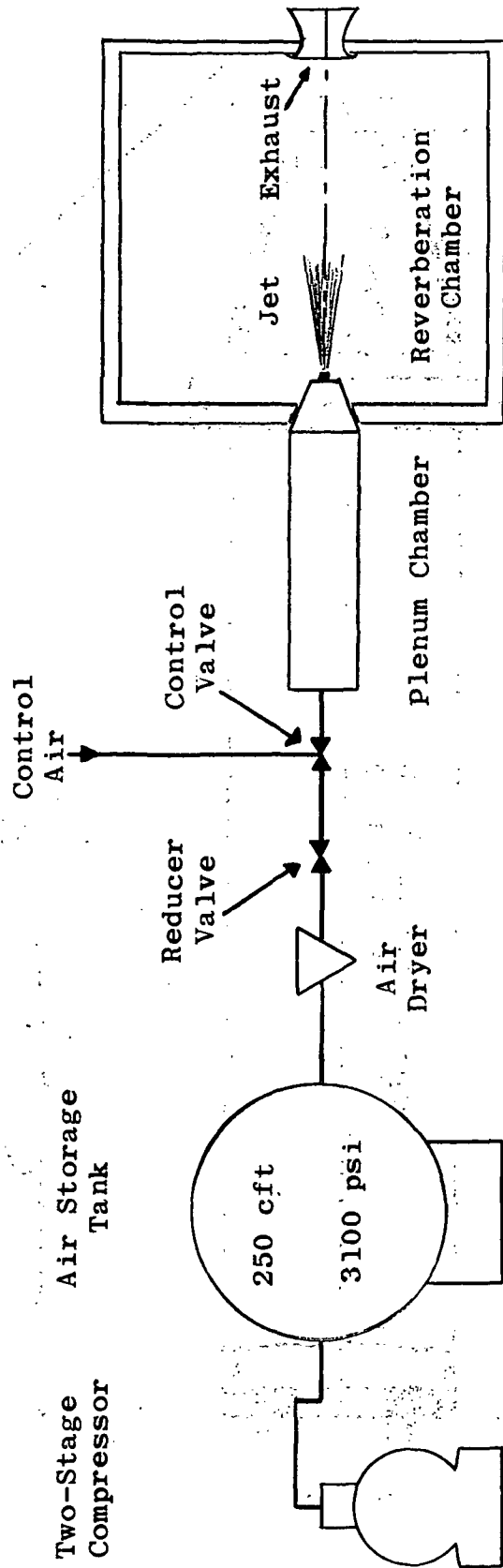
Figure 45. Schematic of the Air Supply System.

Figure 46. Schematic of Plenum Chamber.

Flange for Nozzle Attachment
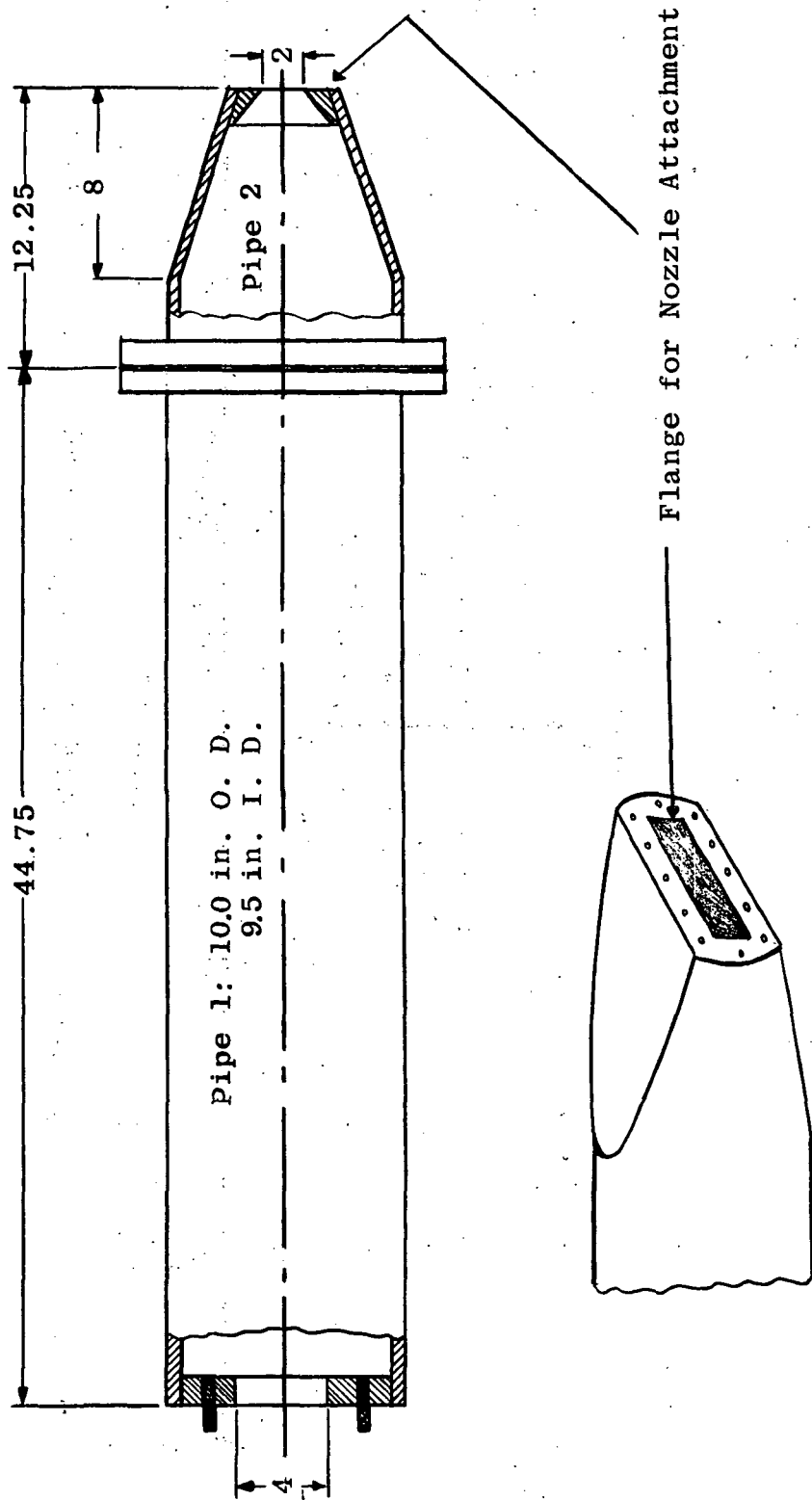
All Dimensions in Inches

Pipe 1: 10.0 in. O. D.
9.5 in. I. D.

Pipe 2

44.75

12.25

8

2

4

97
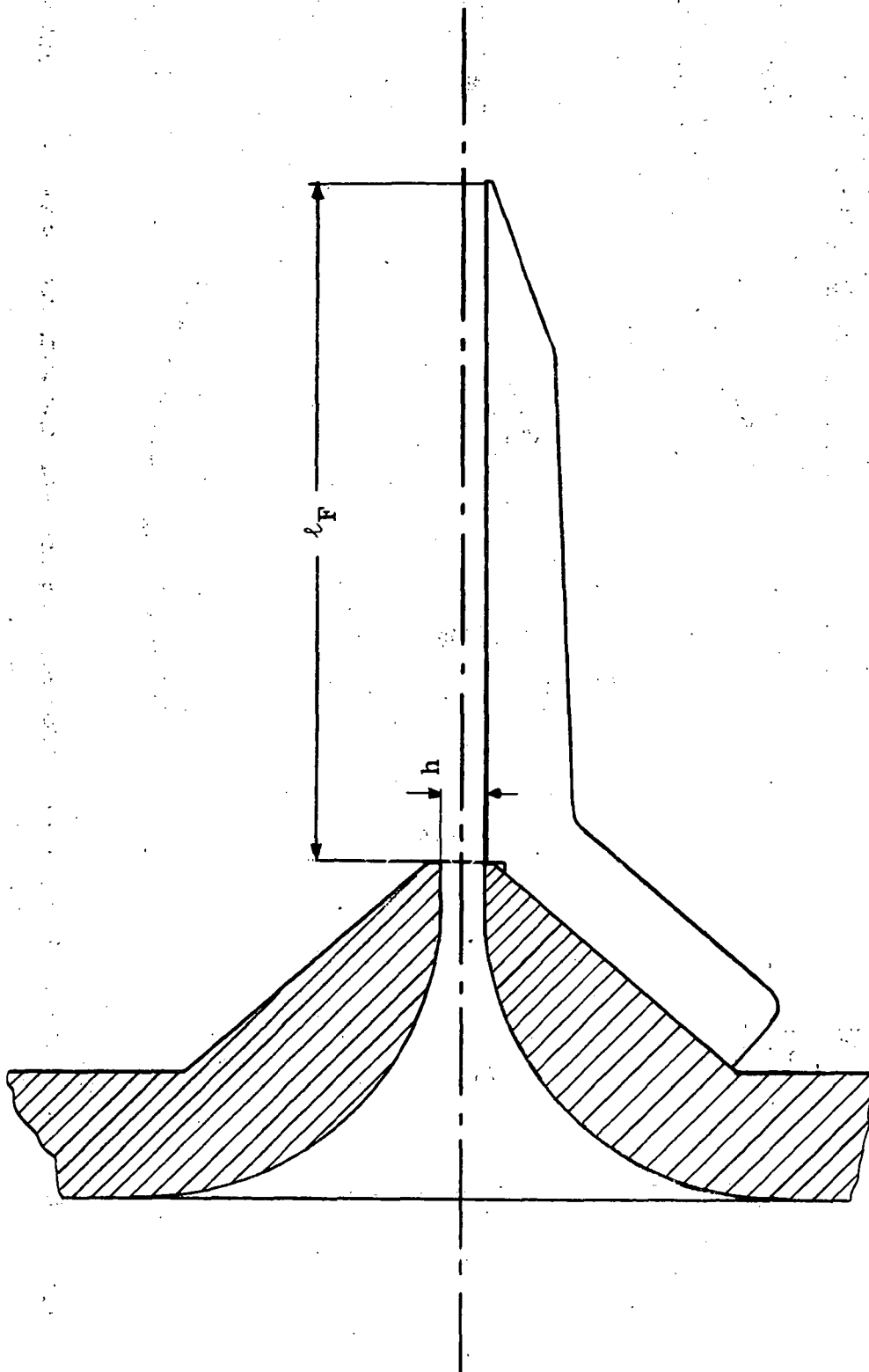
Figure 47. Schematic of a Cross-Section of a Slot Nozzle with an Attached Flap.

Slot Nozzle $\Lambda = 60$:   h =   2.27 mm

                                     w = 136.4   mm

Slot Nozzle $\Lambda = 120$:   h =   1.61 mm

                                     w = 193.5   mm

Circular Reference Nozzle: d =   20.0   mm

2. Flaps

    (i) ℓ_F = 0.5   in. = 12.7 mm

    (ii) ℓ_F = 0.8   in. = 20.35 mm

    (iii) ℓ_F = 1.38 in. = 35.0 mm

    (iiii) ℓ_F = 2.0   in. = 50.8 mm

    All flaps were 10 inches wide and had an angle of

    deflection of $0°$.

Reverberation Chamber

There are two types of well-defined acoustical envi-
ronments, the acoustically free field and the diffuse field.
The free field is a field without any sound reflecting
obstacles. A microphone placed into it would measure the
sound pressure of the free progressive waves originated at
the sound source. If there are any sound reflecting objects
in the acoustic field, it measures, however, a combination
of the pressure due to the original waves and the reflected
waves.

The acoustically diffuse field is a field where a
great number of reflected waves, from all directions, com-
bine in such a way that the average sound energy density is
uniform everywhere in the field. Such a field exists, at

least approximately, in the reverberation chamber. The directivity of the noise source is not detectable any more. However, the diffuseness of the field allows a relatively easy estimate of the sound power because the sound energy density in the room is directly related to the difference between the sound energy absorbed by the room walls. Since this absorption depends on the frequency, a weighting function, the reverberation time, is needed. The reverberation time is defined as the time required for the average sound pressure level, originally in steady state, to decrease 60 dB after the source has stopped to radiate sound. Knowing the volume of the reverberation room and the reverberation time as a function of the frequency, the overall radiated sound power as well as the narrow band sound power levels can be determined (11). The reverberation room, used for these tests, was described in (11). It is sufficient to say here that its lower limiting frequency, which is inversely proportional to the volume of the chamber, is 0.5 KHz.

Instrumentation

The instrumentation consisted of the microphone, a microphone amplifier, the audio frequency spectrometer and a level recorder. The chain of the signal processing is shown in Figure 48.

```
                                  Condensor
                                  Microphone
                                  Brüel & Kjaer
                                  Type 4136
                                  (without grid)

                 ┌──────────────┐
                 │ 1/3 Octave   │
                 │ Audio        │                  ┌──────────────┐
                 │ Frequency    │                  │ Level        │
  ┌────────────┐ │ Analyser     │                  │ Recorder     │
  │ Microphone │ │ Brüel & Kjaer│                  │ Brüel & Kjaer│
  │ Amplifier  │ │ Type 2112    │                  │ Type 2305    │
  └────────────┘ └──────────────┘                  └──────────────┘
```
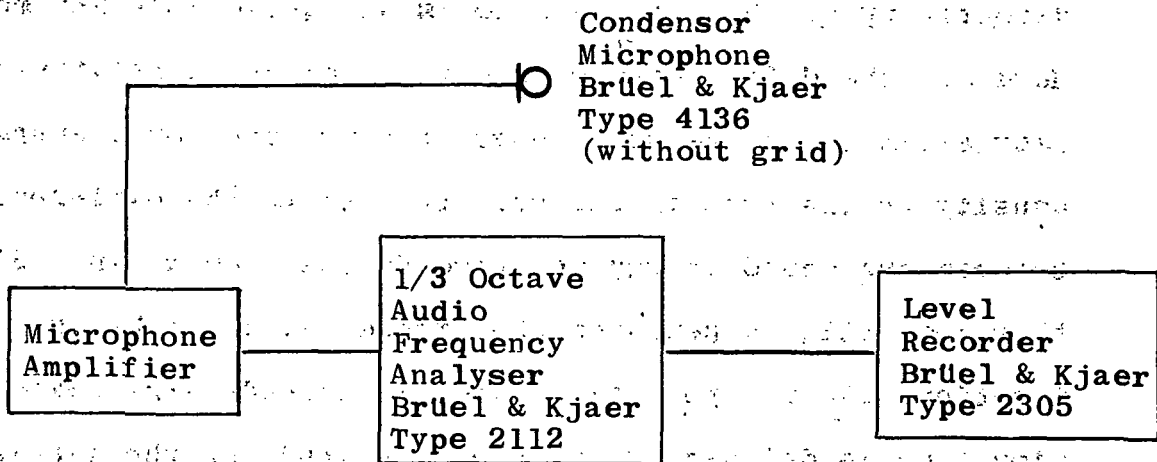
Figure 48. Instrumentation for Acoustic Tests.

The signal is limited to $22 < f < 45,000$ Hz and is
analyzed in the audio frequency spectrometer by 1/3 or
1-octave band-pass filters. For these measurements the
1/3-octave filters were always employed.

In order to obtain the absolute sound pressure level
values (with reference to $2 \times 10^{-4} \mu bar$), spectrometer and
level recorder were calibrated before each test (21) .

The microphone was selected such that its frequency
response tends to cancel out the effect of absorption of
the sound by air (Figures 49 and 50).

101

Figure 49. Attenuation of Sound by Air.

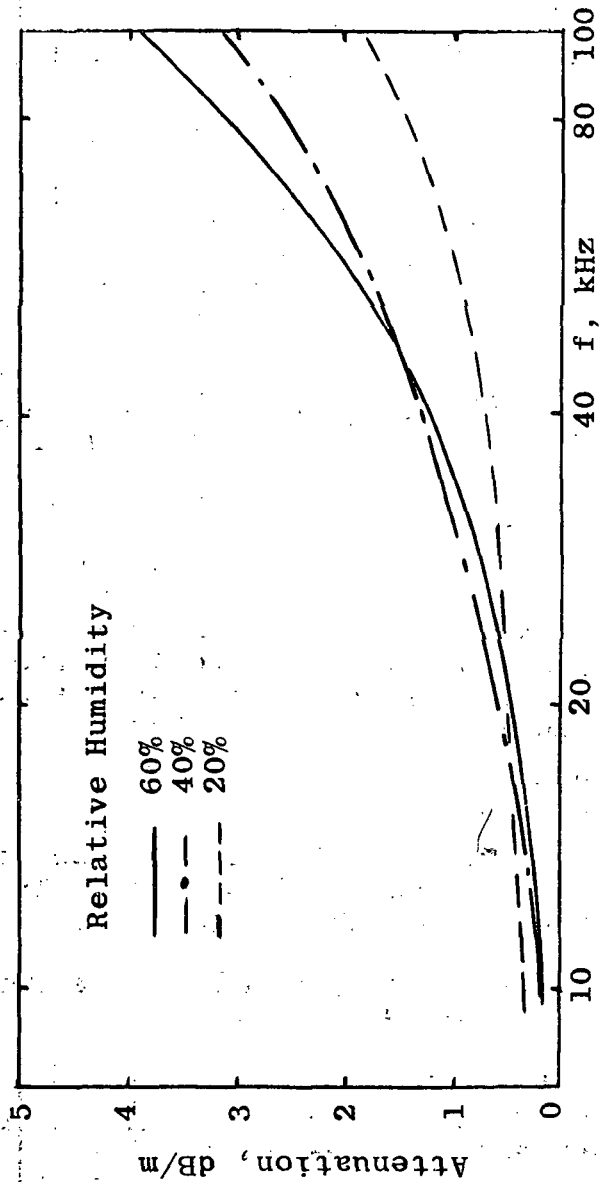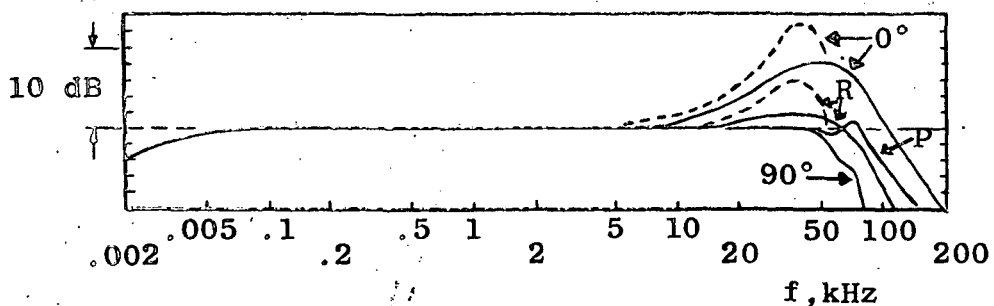Source: Grosche, F.-R. "Zur Schallerzeugung durch einen turbulenten Luftstrahl über einer endlich grossen ebenen Platte." Mitteilungen aus dem Max-Planck-Institut für Strömungsforschung und der Aerodynamischen Versuchsanstalt, Selbstverlag Max-Planck-Institut für Strömungsforschung und Aerodynamische Versuchsanstalt, Göttingen, Nr. 45, 1969.

90° = Free-Field Response at 90° (Grazing Incidence)
 0° = Free-Field Response at 0° (Normal Incidence)
 R = Random Incidence Response (Diffuse Field)
 P = Pressure Response

Full Line: Without Grid
Dashed Line: With Grid

     In this Study, the Microphone was Used without Grid
in a Diffuse Field (Reverberation Chamber). The Response
is thus Given by the Solid R-Curve.

     Figure 50. Frequency Response of the Condensor
Microphone, Brüel & Kjaer, Type 4136.

     Source: Brüel & Kjaer Instruments, Inc., "Audio
Frequency Spectrometer Type 2112," Instructions and
Applications, Copenhagen, Denmark, July 1967.

APPENDIX B

ESTIMATE OF THE POWER SPECTRAL DENSITY

A power spectral density estimate is given (22) by

$$G_x (f_c) = \frac{\overline{x^2} (f_c, \Delta f)}{\Delta f}$$

where $\overline{x^2}$ is the mean square of the instantaneous signal and f_c is the center frequency of the bandwidth Δf.

The Audio Frequency Analyzer measures the sound pressure level in a bandwidth of 1/3 octave with respect to a reference pressure and reads it out in decibels:

$$n (f_c, \Delta f) = 20 \log_{10} \frac{\sqrt{\overline{p^2}}}{p_R}$$

where $\overline{p^2}$ is the mean square value of the instantaneous sound pressure and p_R is an arbitrary reference pressure. Commonly the pressure of 2×10^{-4} μbar is used as reference pressure. The power spectral density is estimated from the sound pressure level $n (f_c, \Delta f)$ as follows:

$$\overline{p^2} = p_R^2 \times 10^{n/10}$$

$$G (f_c) = \frac{\overline{p^2}}{\Delta f} = \frac{\overline{p_R^2}}{\Delta f} 10^{n/10}$$

$$\frac{f_R \, G (f_c)}{p_R^2} = \frac{f_R}{\Delta f} 10^{n/10}$$

where f_R is an arbitrary reference frequency

$$10 \log_{10} \frac{f_R \, G(f_c)}{p_R^2} = n(f_c, \Delta f) - \log_{10} \frac{\Delta f}{f_R} \qquad dB$$

Reference [31] suggests a correction of $- 0.4$ dB for the "effective bandwidth," which is larger than 1/3 octave. Thus the equation for estimating the non-dimensional power spectral density becomes

$$10 \log_{10} \frac{f_R \, G(f_c)}{p_R^2} = n(f_c, \Delta f) - (0.4 + \log_{10} \frac{\Delta f}{f_R}) \qquad dB$$

A power density spectrogram represents accordingly

$$10 \log_{10} \frac{f_R \, G(f_c)}{p_R^2} \text{ versus } f_c$$
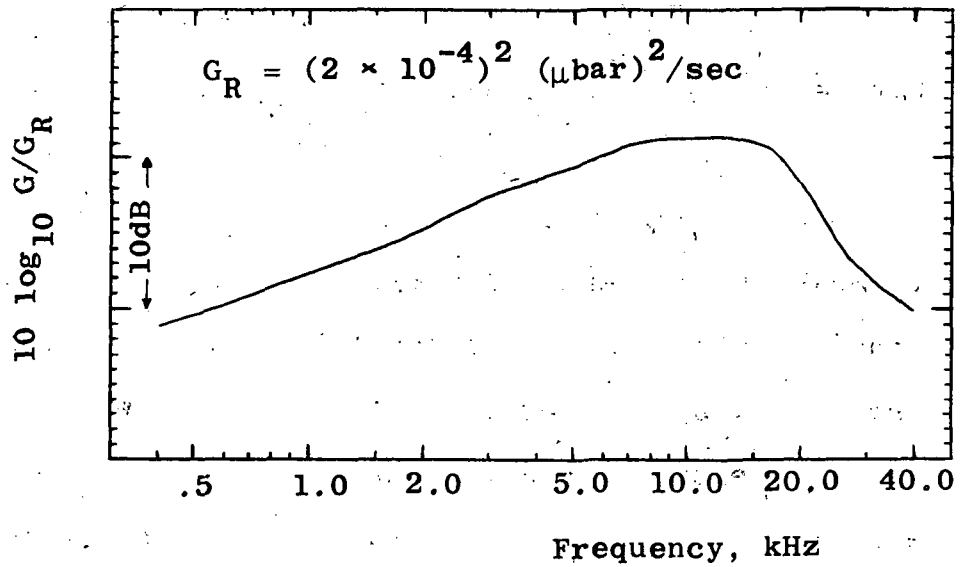
A typical power density spectrum is shown in Figure 51.

Figure 51. Typical Power Density Spectrum.

APPENDIX C

FLOW MEASUREMENTS: INSTRUMENTATION AND PROCEDURE

Hot-Wire Anemometer Measurements

The air supply system, the nozzles and the flaps are the same as described in Appendix A. The jet emanates again into the reverberation chamber, but the function of the chamber is now limited to provide shelter to both the jet and the hot-wire probes against weather conditions. The jet is located far enough from any wall to insure its unobstructed development. The pressure in the chamber is equal to the barometric pressure since its large door is kept open during the tests.

The instrumental set-up, shown in Figure 52, was used to measure the mean velocity, turbulence intensity, turbulence spectra and the autocorrelograms. In order to measure these flow properties the hot-wire probe was placed, mounted to a traversing mechanism, into the flow field such that the wire was parallel to the x_3-axis of the coordinate system and traversed[14] in a plane parallel to the nozzle exit plane (Figure 53). This results in plots of the mean velocity and turbulence intensity versus x_2 for fixed x_1 and x_3. x_3 is of no importance as long as the flow field is two-dimensional.

---

[14] The wire is not moved continuously, but stepwise through the flow.

Figure 52. Instrumentation Set-Up for Flow Measurements.

(a) General Set-Up of the Hot-Wire Instrumentation
(Mean Velocity and Turbulence Intensity Profiles, 1/3 Octave
Turbulence Velocity Spectrograms, Autocorrelograms).

(b) Set-Up for the Determination of Space
Correlograms.

## Instruments Numbered in Figure 53 (a) and (b)

1. Constant Temperature Anemometer, Type 55D01, DISA, Elektronik A/S
2. Linearizer, Type 55D10, DISA
3. Auxiliary Unit, Type 55D25, DISA
4. Sweep Drive Unit, Type 52B01, DISA
5. Digital DC Voltmeter, Type 55D30, DISA
6. True RMS-Voltmeter, Type 55D35 Mark II, DISA
7. X-Y-Recorder, Model 135, Moseley Co.
8. Single Beam Oscilloscope, Type 515A, Tektronix
9. Dual Beam Oscilloscope, Type 502A, Tektronix
10. Audio Frequency Spectrometer, Type 2112, Brüel & Kjaer
11. Level Recorder, Type 2305, Brüel & Kjaer
12. Analog Correlator, Type 9410, Honeywell
13. Loop-Tape Recorder, Frequency Modulated, Type LAR 7490, Honeywell
14. Stepper Motor, Type 52C01, DISA
15. Hot-Wire Probe, DISA (various kinds were used)
16. High-Pass Filter
17. Constant Temperature Anemometer, Model 1010A, Thermo-System Inc.
18. Linearizer, Model 1005B, Thermo-System Inc.
19. Analog Correlator, Type 55D70, DISA
20. RMS-Voltmeter, Type 3400A, Hewlett-Packard
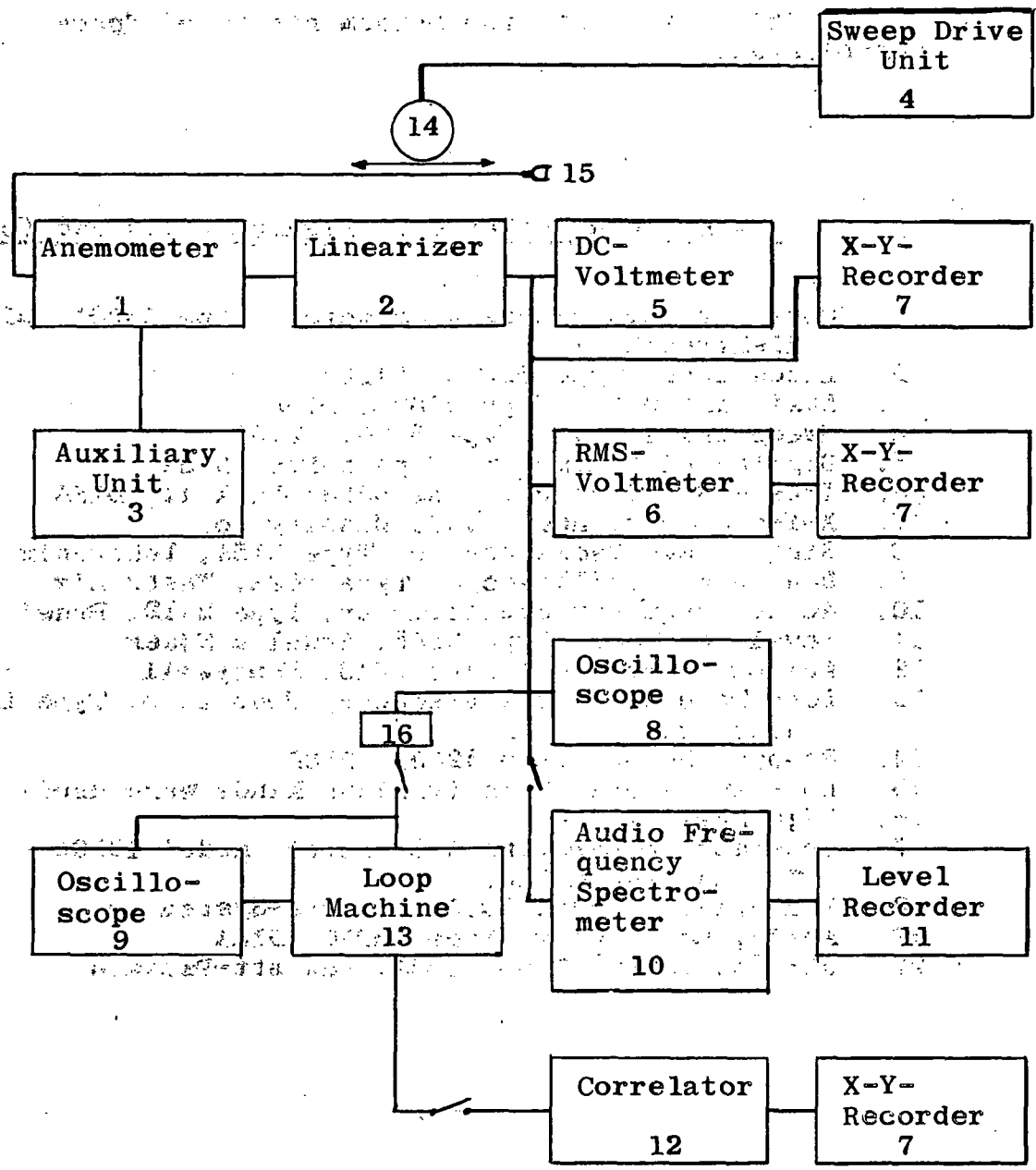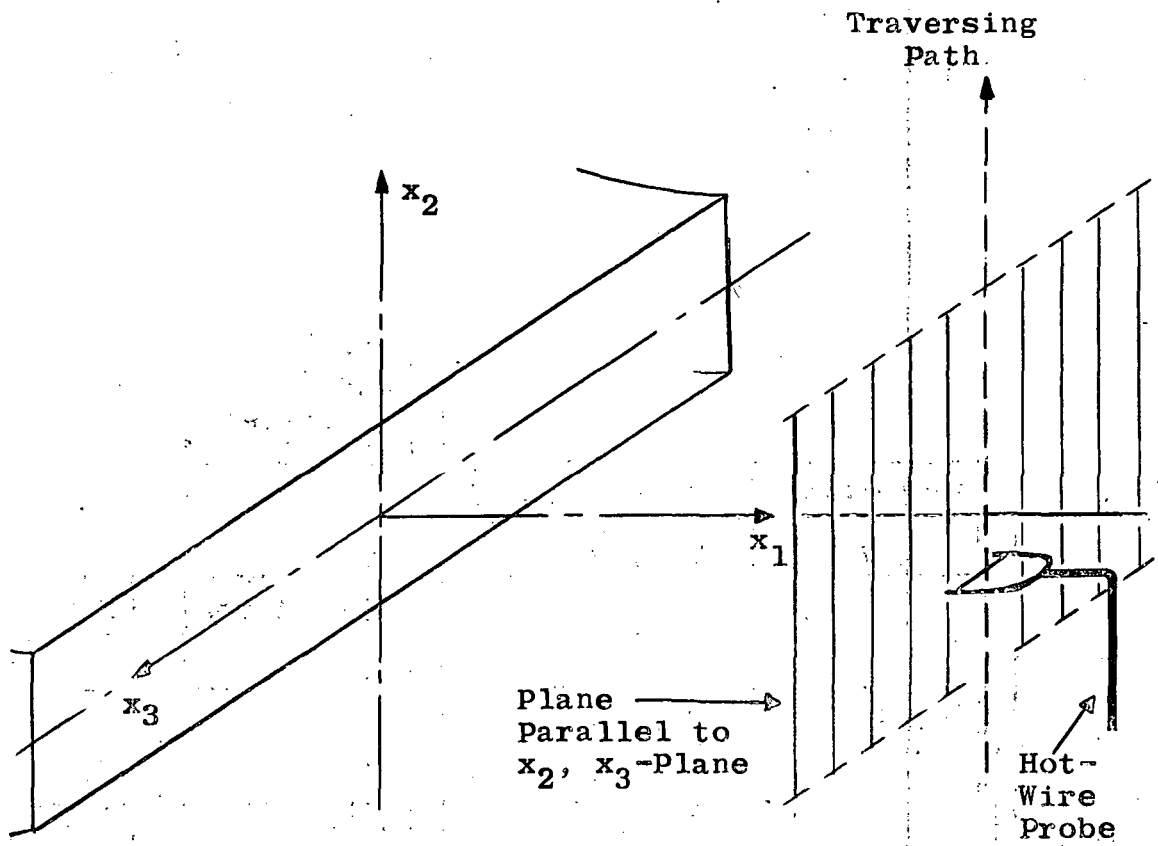
(a)
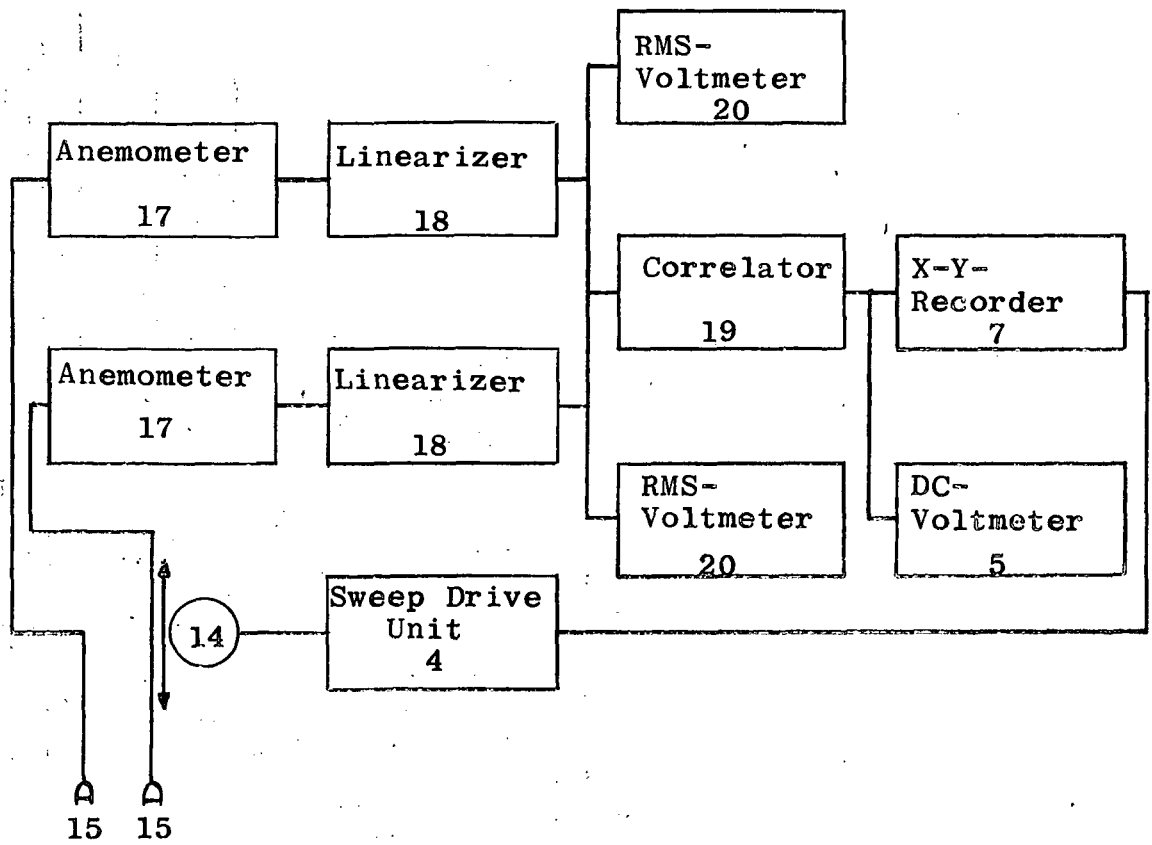
Figure 52.

(b)

Figure 52. (continued)

Figure 53. Orientation of the Hot-Wire.

During the measurements x_3 was usually approximately zero.
In order to obtain turbulence spectra the sweep is stopped
at selected points and the signal of the hot-wire is analyzed
in the 1/3-octave bandwidth audio frequency spectrometer. A
power spectral density estimate is then obtained from the
spectra as described in Appendix B. All power density
spectra whose peak frequencies f_p^* are plotted in Figure 36
(page 72) were obtained at the points of maximum turbulence
intensity of both mixing regions at different downstream
positions. Similarly the autocorrelograms were obtained for
certain points of the flow field. Because the measurement
of a correlation curve takes a considerable amount of time
in which the flow field has to remain in a steady state, the
signal was played on a tape loop. The autocorrelation curve
was then obtained from the stored signal.

A different set-up was used for the measurements of
the lateral space correlation function (Figure 52, pages 109
to 110). Both hot-wires were positioned as described above
and shown in Figure 53. One wire remained in a fixed posi-
tion, whereas the other wire moved in x_2-direction. The
resulting plot is the lateral space correlation coefficient
versus Δx_2 for the point in the flow determined by the
fixed wire. The lateral scale of turbulence was then ob-
tained by graphical integration. A critical quantity to be
determined during the measurements was the initial distance
between the two hot-wires. The plot of the lateral space
correlation function versus Δx_2 has to be extrapolated over

112

the initial distance before the graphical integration can be performed. The smaller Δx_2 of the first zero, the more accuracy is needed in determining the initial gap. Since no optical device was available to measure this distance with sufficient accuracy, it had to be estimated by comparing it to gaps of known width. This method did not provide the necessary accuracy near the nozzle exit, where the scale of turbulence is very small.

Two-Dimensionality of the Flow Field

From the experimental point of view, a two-dimensional flow does not exist due to the necessity of limiting the slot width w. However, it can be approximated by using slots of high aspect ratios. According to Van der Hegge Zijnen (15) the three-dimensional end effects of a slot nozzle are limiting the two-dimensional flow to downstream distances of approximately 2 w (in the plane of symmetry perpendicular to the nozzle exit area), or, expressing it non-dimensionally, 2Λ. As the measurements were conducted in the flow field of slot nozzles with aspect ratios of $\Lambda = 30$ and 60 at downstream positions $x_1/h < 22$, the condition of two-dimensionality was always satisfied.

Turbulence is naturally three-dimensional. However, within the two-dimensional flow region, it is homogeneous in x_3-direction, which means that the structure of turbulence does not change in that direction.

113

Measurement of Flow Properties

In a Point of the Flow Field

The hot-wire can be pictured as a cylinder, measuring 0.005 mm in diameter and 1.2 mm in length. If it is orientated parallel to the x_3-axis as shown in Figure 53 (page 111), the length is unimportant. Since the diameter of the wire is extremely small compared to the height of the slot (2.27 mm for the slot nozzle with $\Lambda = 60$, the data can be considered as those of a point in a flow field.

The length is of importance, however, if the wire is not correctly orientated parallel to the x_3-axis. Two kinds of errors can occur: First, the wire is located in the x_2, x_3-plane but forms an angle β with the x_3-axis. Secondly, the wire remains in the x_1, x_3-plane but forms an angle γ with the x_3-axis. Because the gradients within the flow field are much larger in x_2-direction than in x_1-direction, the influence of γ can be neglected against the influence of β. If $\beta \leq 5°$, the effective diameter becomes already 0.1 mm or 1/20 of the height of the slot approximately. Therefore, particularly near the orifice, the correct orientation of the wire is important.

Similar are the difficulties if the longitudinal velocity correlation function is to be measured at a point of the flow field. The two wires have to be oriented as shown in Figure 53 (page 111). Both have to be located in the same plane parallel to the x_1, x_3-plane such that one is exactly

114

downstream of the other. Difficulties arise when one wire is in the wake of the other. Therefore, they have to be displaced by a Δx_2. Due to the small size of the nozzles any displacement in x_2-direction close to the nozzle exit results in a substantial error. The correlation coefficient which should be unity for $\Delta x_1 = 0$ will decrease considerably due to $\Delta x_2 \neq 0$. Furthermore it is extremely difficult to keep the moving hot-wire in the plane parallel to the x_1, x_3-plane, into which it was initially placed. This introduces an additional error that may be large due to the small nozzle height. Finally the measurements suffer from the same difficulty of determining the initial distance as already described.

The last mentioned source of error is the only important one in obtaining the lateral space correlation function. Even if sizable deviations from the traversing path occur, the errors will be small due to the small gradients in x_1-direction.

It can be stated generally that deviations which involve changes in x_2-direction, will introduce large errors, those in x_1-direction small errors and those in x_3-direction no errors at all. As errors in the orientation of the probe and traversing path are inevitable, their relative effect will be inversely proportional to the nozzle height.

A single hot-wire is sensitive to velocities perpendicular to its axis and more or less insensitive to velocities parallel to its axis. If the wire is orientated as shown in Figure 53 (page 111), the velocities which influence the signal of the hot-wire are $\overline{U}_1$, $\overline{U}_2$, u_1 and u_2 (the latter are here the instantaneous values of the fluctuating velocity components). The total error due to the u_2-component is approximately given by

$$100 \ (\overline{U}_1 + \hat{u}_1) \ [\sqrt{1 + \frac{\overline{u_2^2}}{(\overline{U}_1 + \overline{u_1^2})^2}} \ - 1] \qquad \text{per cent}$$

whereas the influence of the $\hat{u}_2$-component on the mean velocity only is approximately given in Reference (23) as

$$100 \ \overline{U}_1 \ (1 - \frac{1}{4} \frac{\overline{u_1^2}}{\overline{U}_1^2} + \frac{1}{2} \frac{\overline{u_2^2}}{\overline{U}_1^2}) \qquad \text{per cent}$$

If the turbulence intensity (with respect to the local mean velocity) increases over 20%, the errors become quite large. They can be avoided by using so-called "X"-probes, which consist of two separated wires which form an "X." The two signals allow the determination of both $\hat{u}_1$ and $\hat{u}_2$ if the probe is orientated such that the plane of the "X" is parallel to the x_1, x_2-plane.

Due to the small size of the nozzles, this orienta-
tion would result in signals of both wires which represent
an average[15] velocity without any relationship to the velo-
cities in certain points. The influence of $\bar{U}_2$ is only of
importance at the outer edge of the free mixing region. As
the central region of the mixing regions is here of particu-
lar interest, $\bar{U}_2$ is neglected.

_____

[15]Averaged over Δx_2 = wire length $/ \sqrt{2}$.

APPENDIX D

LONGITUDINAL AND LATERAL SCALES OF TURBULENCE

For the axisymmetric jet both the longitudinal[16] and the lateral[17] scales of turbulence have been measured by Laurence (20), Davies, Barratt and Fisher (24) and others.

Laurence reported that the longitudinal and lateral scales of turbulence are nearly independent of the Mach and Reynolds number and, in the central region of the mixing zone, vary proportionally with the distance from the nozzle. The lateral scale is more or less constant within a cross-section, whereas the longitudinal scale varies by approximately 20% in the central region of the turbulent mixing region. The longitudinal scale is larger than the lateral scale by a factor of the order of 1.5 to 2.5.

Coles 5 based his analysis of the overall radiated sound power of jets from circular and slot nozzles on similarities of fundamental mixing-zone structure. One of these

---

[16]The longitudinal scale of turbulence is defined as

$$L_{x_1} = \int_0^\infty \frac{\overline{u_1(x_1)\, u_1(x_1 + \Delta x_1)}}{\sqrt{\overline{u_1^2(x_1)}}\,\sqrt{\overline{u_1^2(x_1 + \Delta x_1)}}}\, dx_1$$

[17]The lateral scale of turbulence is defined as

$$L_{x_2} = \int_0^\infty \frac{\overline{u_1(x_2)\, u_1(x_2 + \Delta x_2)}}{\sqrt{\overline{u_1^2(x_2)}}\,\sqrt{\overline{u_1^2(x_2 + \Delta x_2)}}}\, dx_2$$

is the similarity between the scales of turbulence. The dimensional scales of the slot nozzle are much smaller than those of the circular nozzle (with the same exit area) due to the smaller characteristic length. Non-dimensionalized by the characteristic length they should become equal if similarity exists.

Figure 54 presents data of non-dimensionalized scales of turbulence in the primary mixing region obtained either from literature or in the course of the experiments. The data of the lateral scale of turbulence were obtained by correlating the signals of two hot-wires. Although two-wire measurements are also the most straightforward method to determine the longitudinal scale, it was here[18] determined from single-wire measurements. From the autocorrelograms of the single hot-wire signal the longitudinal scale was obtained utilizing Taylor's Hypothesis (Reference 23).

If a conclusion may be reached on the basis of the limited data available, the non-dimensional scale of turbulence of the slot nozzle is slightly larger than that of the circular nozzle. The lateral scale, however, is considerably larger than that of the circular nozzle. This is consistent with the larger lateral spread of the turbulence mixing region of a slot nozzle (Figure 32, page 64).

Equation (4.1.), which is an expression for the overall radiated sound power generated by turbulence interacting

---

[18]The reason is outlined in Appendix C.
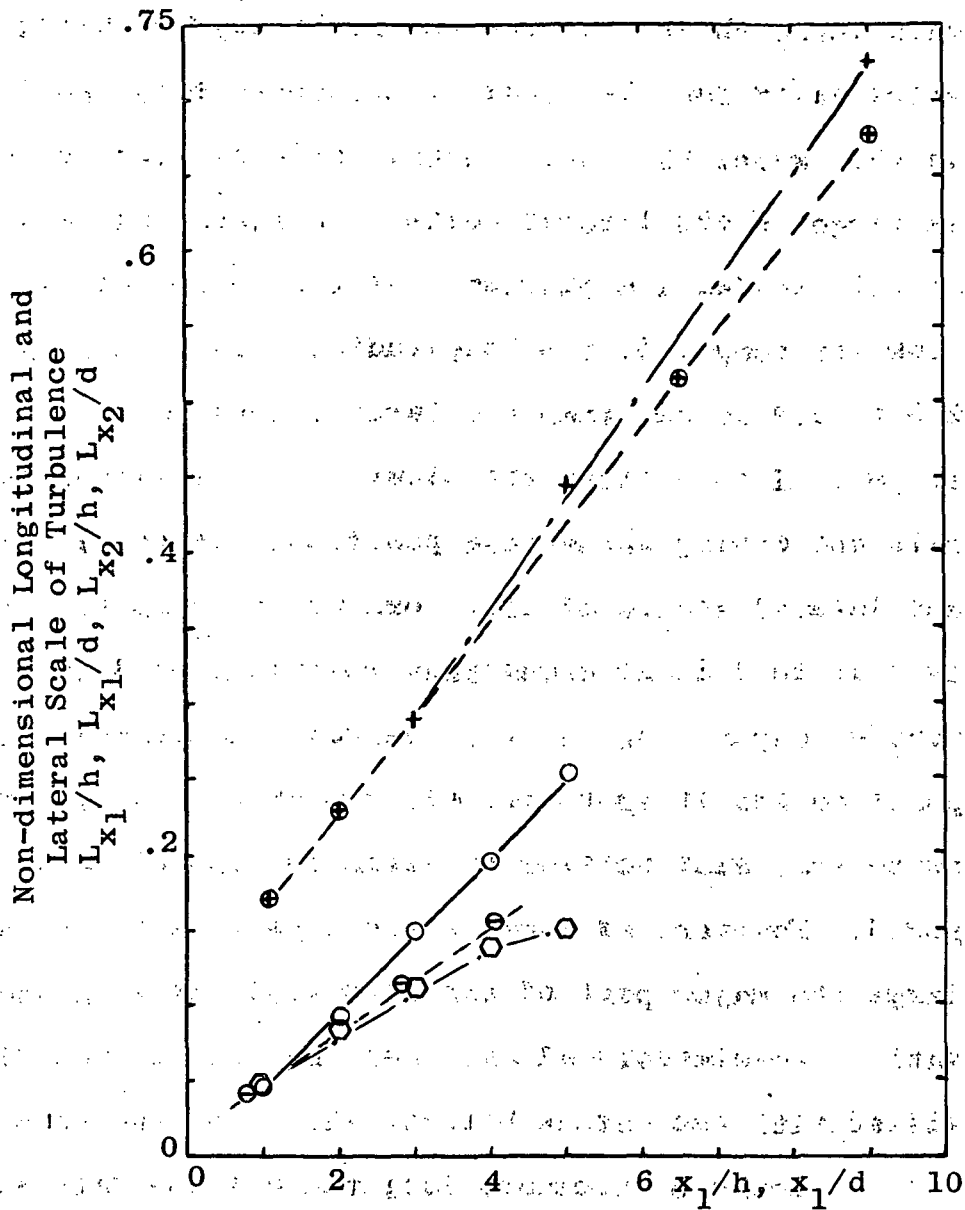
Lateral Scale:
- O Slot Nozzle, Λ = 60
- O Circular Nozzle
- ⊖ Circular Nozzle Reference (20)

Longitudinal Scale:
- + Slot Nozzle, Λ = 60 (Single Wire Measurements, using Taylor's Hypothesis)
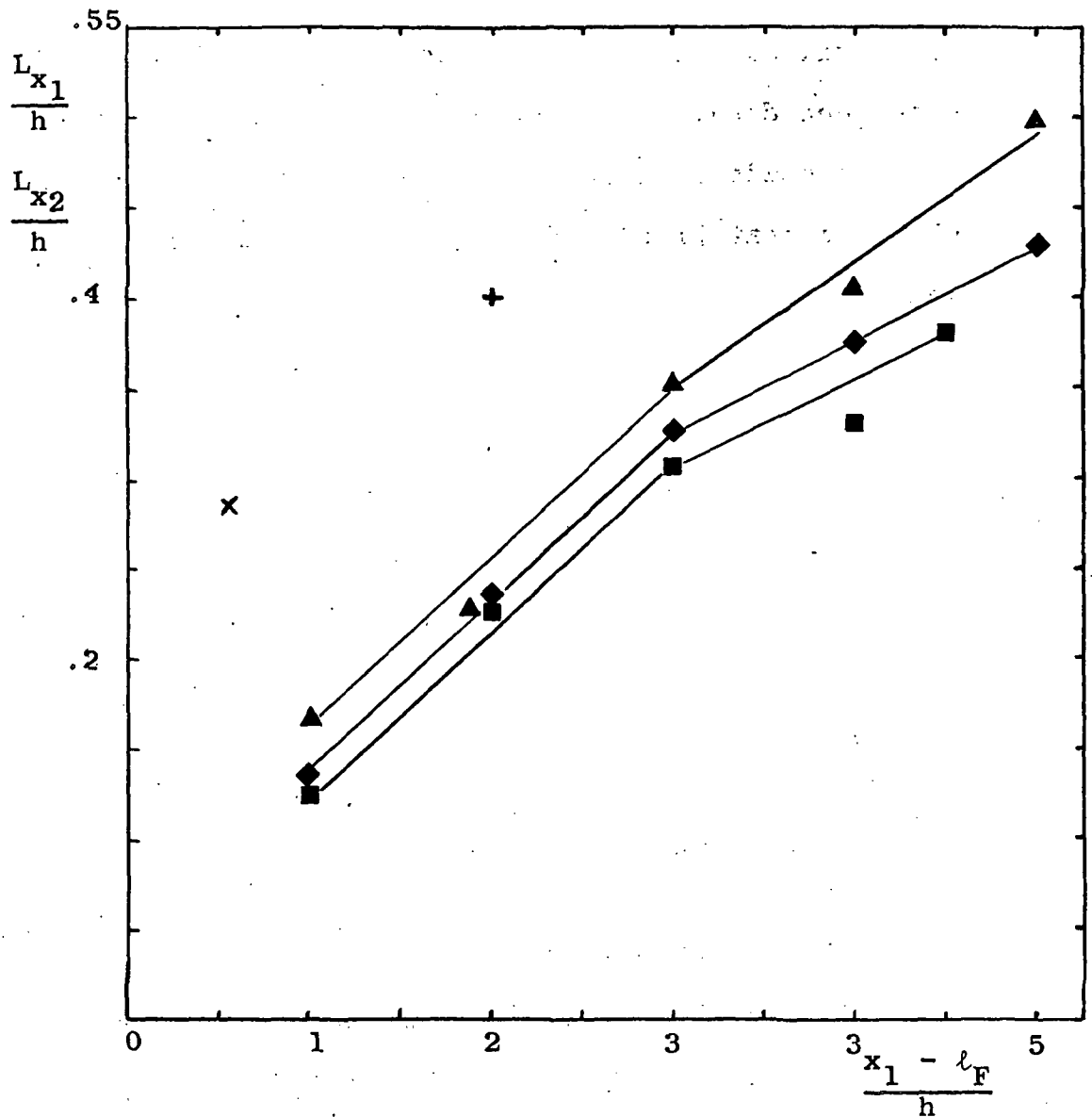- ⊕ Circular Nozzle, Reference (20)

Fixed Wire is Located at the Point of Maximum Turbulence Intensity

Figure 54. Comparison Between Longitudinal and Lateral Scales of Turbulence of Circular Nozzle and Slot Nozzles.

with large shear, was derived by Lilley (6) using relation-
ships valid for the model of homogeneous isotropic turbulence.
In this model the longitudinal scale of turbulence is twice
as large as the lateral scale. In Figure 54, measured data
of both scales are plotted. If the scales of circular noz-
zles are compared, the longitudinal scale is by a factor of
2.3 to 3.4 larger than the lateral scale at downstream posi-
tions of 1 to 5 times the diameter. The factor increases
with decreasing downstream position. If the longitudinal
and lateral scales of slot nozzles are compared, the factor
is 1.75 to 1.85 at downstream positions of 3 to 5 times the
nozzle height. Again it increases with decreasing downstream
position and is approximately 3.2 at $x_1/h = 1$. It should be
noted that slot nozzles of different aspect ratio were com-
pared. However, as long as the aspect ratio is sufficiently
large the major part of the flow field is with good approxi-
mation two-dimensional and then the scales, non-dimension-
alized with the nozzle height, should be the same.

Figure 55 presents longitudinal and lateral scales
of turbulence measured in the secondary mixing region of
various jet flaps. Although only two data points are
available for the longitudinal scale, they indicate that the
factor between the longitudinal and the lateral scale is in
the same range as in the primary mixing region.

Thus, this comparison as well as the results reported
by Laurence (20) show that the relationship between the

Lateral Scale (Two-Wire Measurements):

- ■ $\delta_F = 5.6$
- ◆ $\delta_F = 9.0$ $\Lambda = 60$, $U_e = 120$ m/sec
- ▲ $\delta_F = 15.4$

Fixed Wire is Located at the Point of Maximum
  Turbulence Intensity

Longitudinal Scale (Single Wire Measurement, Using
  Taylor's Hypothesis):

- + $\delta_F = 4.0$
- × $\delta_F = 15.9$ $\Lambda = 30$, $U_e = 98$ m/sec

Figure 55.   Comparison Between Longitudinal and
Lateral Scales of Turbulence in the Secondary Mixing Region
of Jet Flaps.

longitudinal and lateral scale of turbulence depends on the space coordinates. However, the factor by which the longitudinal scale is larger than the lateral, is still fairly close to that predicted by the homogeneous isotropic turbulence model.

"The aeronautical and space activities of the United States shall be conducted so as to contribute . . . to the expansion of human knowledge of phenomena in the atmosphere and space. The Administration shall provide for the widest practicable and appropriate dissemination of information concerning its activities and the results thereof."
—NATIONAL AERONAUTICS AND SPACE ACT OF 1958

NASA SCIENTIFIC AND TECHNICAL PUBLICATIONS

TECHNICAL REPORTS: Scientific and technical information considered important, complete, and a lasting contribution to existing knowledge.

TECHNICAL NOTES: Information less broad in scope but nevertheless of importance as a contribution to existing knowledge.

TECHNICAL MEMORANDUMS: Information receiving limited distribution because of preliminary data, security classification, or other reasons. Also includes conference proceedings with either limited or unlimited distribution.

CONTRACTOR REPORTS: Scientific and technical information generated under a NASA contract or grant and considered an important contribution to existing knowledge.

TECHNICAL TRANSLATIONS: Information published in a foreign language considered to merit NASA distribution in English.

SPECIAL PUBLICATIONS: Information derived from or of value to NASA activities. Publications include final reports of major projects, monographs, data compilations, handbooks, sourcebooks, and special bibliographies.

TECHNOLOGY UTILIZATION PUBLICATIONS: Information on technology used by NASA that may be of particular interest in commercial and other non-aerospace applications. Publications include Tech Briefs, Technology Utilization Reports and Technology Surveys.

Details on the availability of these publications may be obtained from:

SCIENTIFIC AND TECHNICAL INFORMATION OFFICE

NATIONAL AERONAUTICS AND SPACE ADMINISTRATION

Washington, D.C. 20546